Louisiana Tech University
Louisiana Tech Digital Commons

Summer 2009

Applications of electricity in the rehabilitation and health monitoring of concrete structures

Saiprasad Vaidya
Louisiana Tech University

Follow this and additional works at: https://digitalcommons.latech.edu/dissertations

Part of the Civil Engineering Commons, and the Electrical and Computer Engineering Commons

APPLICATIONS OF ELECTRICITY IN THE REHABILITATION AND HEALTH MONITORING OF CONCRETE STRUCTURES

by

Saiprasad Vaidya B.S.

A Dissertation Presented in Partial Fulfillment
of the Requirements for the Degree
Doctor of Philosophy

COLLEGE OF ENGINEERING AND SCIENCE
LOUISIANA TECH UNIVERSITY

August 2009

UMI Number: 3374697

INFORMATION TO USERS

The quality of this reproduction is dependent upon the quality of the copy submitted. Broken or indistinct print, colored or poor quality illustrations and photographs, print bleed-through, substandard margins, and improper alignment can adversely affect reproduction.

In the unlikely event that the author did not send a complete manuscript and there are missing pages, these will be noted. Also, if unauthorized copyright material had to be removed, a note will indicate the deletion.

UMI®

LOUISIANA TECH UNIVERSITY

THE GRADUATE SCHOOL

June 12, 2009
_____
Date

We hereby recommend that the dissertation prepared under our supervision

by____ Saiprasad Vaidya _____

entitled_____

Applications of Electricity in the Rehabilitation and

Health Monitoring of Concrete Structures

_____

_____

be accepted in partial fulfillment of the requirements for the Degree of

Doctor of Philosophy

_____
Supervisor of Dissertation Research

_____
Head of Department

Civil Engineering
_____
Department

Recommendation concurred in:

_____

_____

_____   Advisory Committee

_____

Approved:

_____
Director of Graduate Studies

Approved:

_____
Dean of the Graduate School

_____
Dean of the College

ABSTRACT

The dissertation research work presented herein consists of two separate findings: one investigates a potential new coating technique that could be used to rehabilitate deteriorated concrete sewer pipes, and the other researches inducing electrical conductivity into geopolymer concrete to serve as smart material by being able to sense stress changes. Both applications utilize electricity to enhance the performance and/or functionality of hardened cementitious materials.

Microbiologically induced corrosion (MIC) in concrete wastewater conveyance systems is a leading deterioration mechanism in such structures. This work focuses on breaking the MIC cycle by preventing colonization of the bacteria responsible for converting hydrogen sulfide to sulfuric acid. Electrokinetics was used to drive an antimicrobial agent (cuprous oxide) into the porous wall surface of a pre-cast concrete pipe. An electric potential difference applied between the steel reinforcement embedded in the concrete and a copper electrode placed in the coating solution provides the driving force to the copper ions. Atomic absorption tests performed on the coated specimens were used to determine the percentage of cuprous oxide that penetrated the porous surface and migrated into the hardened concrete matrix. A pilot study conducted on three mock pipe specimens demonstrated that the process is effective on partially corroded and non-corroded pipes. Test data also revealed that the amount of copper that migrated into the concrete matrix is time dependent. Based on the preliminary test

results, a treatment procedure was designed and implemented on a 15" diameter commercial pre-cast concrete pipe. The data suggest that the method could be reemployed to "immunize" new and partially deteriorated steel reinforced concrete pipes against MIC.

Geopolymer concrete is finding a growing number of niche applications in the field of civil engineering due to its high compressive strength, strength gain rate, fire resistance, maintenance of structural properties in elevated temperature environments, chemical stability in highly acid environments, and relatively low cost and environmental benefits. Electrically conductive geopolymer could serve as a new smart material that could monitor its own health. Typically, health monitoring in structures is done by assessing their state of stress. One such method involves monitoring electrical resistance variations as an indirect indication of the stress variations in the structure. Carbon fibers were added to a fresh geopolymer mix to enhance its electrical conductivity. AC-impedance spectroscopy analysis was performed on sample specimens to obtain their electrical resistance. Results from the preliminary phases demonstrated that geopolymer exhibits superior performance to OPC–made concrete as a conductor of electrical current. Conductive geopolymer concrete specimens containing an optimum percentage of carbon fibers were dynamically loaded to observe the changes in electrical resistance. Data obtained from the dynamic test suggests that conductive geopolymer could serve as a smart material.

APPROVAL FOR SCHOLARLY DISSEMINATION

The author grants to the Prescott Memorial Library of Louisiana Tech University the right to reproduce, by appropriate methods, upon request, any or all portions of this Dissertation. It is understood that "proper request" consists of the agreement, on the part of the requesting party, that said reproduction is for his personal use and that subsequent reproduction will not occur without written approval of the author of this Dissertation. Further, any portions of the Dissertation used in books, papers, and other works must be appropriately referenced to this Dissertation.

Finally, the author of this Dissertation reserves the right to publish freely, in the literature, at any time, any or all portions of this Dissertation.

Author _____

Date _____07 - 27 - 2009_____

TABLE OF CONTENTS

LIST OF TABLES

LIST OF FIGURES

ACKNOWLEDGEMENTS

CHAPTER 1

INTRODUCTION

1.1 General Introduction

Currently, ordinary Portland Cement Concrete is the prime choice as a construction material, with approximately one ton of concrete produced per capita annually. Portland cement, a main ingredient in making concrete, is also a contributor to the global green house effect because in order to produce one ton of Portland cement, 1.5 tons of raw material is required giving out approximately one ton of carbon dioxide (CO_2). It is estimated that cement production by itself contributes to about 7% of the total greenhouse gases that are being emitted into the earth's atmosphere [1].

Concrete suffers from several additional drawbacks including a relatively slow strength gain rate, susceptibility to acid and sulfate attacks, and shrinkage. Enhancing the sustainability of our urban society requires extending the useful life of current infrastructure systems as well as extending the design life of new ones. There is also a need for smart materials which provide a continuous feedback of their stress state in a manner that can be monitored on a regular basis.

The following dissertation work is divided into two parts: the first part concerns with an advanced rehabilitation technique that could be used to mitigate biogenic sulfuric acid corrosion in concrete sewer pipes. The second part describes a technique in which a

1

new type of cementitious material (geopolymer) is electrically altered to serve as self health monitoring system in infrastructure.

1.2 Part I

1.2.1 Introduction

Microbiologically induced corrosion (MIC) of concrete sewer pipes is one of the most common types of deterioration encountered in such structures. It is also known as bacterial corrosion, biogenic sulfuric acid corrosion and hydrogen sulfide corrosion. According to a study done by EPA, annual damage to wastewater collection and storage systems associated with MIC are on the order of several billion dollars [2]. The estimated cost to rehabilitate more than 10% of the wastewater collection system in Los Angeles county that suffers from MIC is about $852 million, and in Germany it is $142 billion per year to restore damaged sewer collection systems. Damage done by MIC in Flanders (Belgium) is estimated to be $7 million per year, representing 10% of the total cost of expenditure on wastewater collection systems. This cost shows the importance of mitigating MIC which otherwise can lead to significant expenditure [3].

Sulfuric acid corrosion of concrete is not new; it has been studied for more than half a century since its discovery in 1945. A number of studies demonstrated that the underlying corrosion of cementitious matrix is the result of metabolic activity of thiobacilli bacteria [4, 5, 6, & 7]. The leading cause for sulfuric acid corrosion in concrete sewers is the generation and presence of hydrogen sulfide (H_2S). Hydrogen sulfide is produced by sulfate reducing bacteria (SRB) *Desulfovibrio desulfuricans* that grow inside a slime layer on the pipe wall under the water line. Inside the slime layer SRB converts elemental sulfates in the wastewater to sulfides which react with dissolved

hydrogen to form H_2S. The produced H_2S escapes into the sewer atmosphere where it is converted into sulfuric acid by sulfide oxidizing bacteria *(Thiobacillus thiooxidans)* which resides on the sewer wall above the water line. The sulfuric acid produced attacks the concrete pipe matrix via dissolution and expansion. Methods for mitigating MIC in concrete sewer pipes range from adding chemicals to the wastewater to spray on coating of the pipe interior. The latter, while cost effective, lacks a mechanical anchorage to the concrete substrate and, thus, has a very limited service life. This work is an attempt to address the problem of transporting and securing the anti-bacterial coating on to the concrete substrate by forming a mechanical interlock between the coating material and the substrate.

1.2.2 Objective and Scope

The objective of this research (Part I) is to develop an innovative methodology for protecting degraded concrete sewer pipes against microbiologically induced corrosion. In the present work, electric potential difference is used as driving force to transport heavy metal oxide (copper oxide) particles into the surface of concrete. The benefits of coating a pipe with heavy metal oxides were demonstrated by Hewayde et al. [8]. The proposed technique allows the coating material to form a mechanical interlock with the substrate of the pipe as a mean of overcoming drawbacks such as poor adhesion, flaking and shrinkage of the coating material encountered in current spray-on processes.

1.3 <u>Part II</u>

1.3.1 <u>Introduction</u>

Geopolymer is cementitious material that does not require the presence of ordinary Portland cement (OPC). Similarly to ordinary Portland cement concrete, geopolymer also has a source material and a liquid phase. Instead of cement, however, materials with high percentages of Silica (Si) and alumina (Al) can be used as a source material in geopolymer and water is replaced with alkaline liquids. Since no water is used in making geopolymers, they are also known as alkali activated alumino-silicate binders. Source materials include metakaolin, kaolinite, clays and mica, as well as byproducts such as fly ash, silica fume, slag, rice husk ash and red mud. The choice of source material depends upon the availability, cost and type of application [9, 10 and 11].

Geopolymers offer several advantages over Portland cement. First, it is cost effective to produce because the source material it uses can be any naturally occurring mineral (Kaolinite) or a byproduct of a certain process such as fly ash or rice husk. Second, its production is environmental friendly (i.e., CO_2 released during its production is less significant compared to that of cement production). Finally, geopolymer is better than Portland cement in resisting harsh conditions; this characteristic property is because of its stable microstructure, which is a result of chemical reaction between alkaline liquids and silica and alumina in the source material. Unlike C-S-H gel in cement concrete, geopolymer forms 3-dimensional polymeric chains of Si-O-Al, which are credited with the mechanical strength and other micro-structural properties of geopolymer. In this research, we have investigated the possibilities of using fly ash as a source material for preparing geopolymer.

The civil infrastructure systems are prone to many deterioration mechanisms including fatigue failure (due to repeated live load), environmental degradation (freeze-thaw effect, corrosion), and natural disasters (earth quakes and hurricanes). Coupled with lack of maintenance, these factors lead to deterioration of strength and thereby premature failure of the structure. A study done by Aketan et al. [12] estimates that the lack of performance of infrastructure has an impact up to 1% on nations GDP.

Damage of structural concrete can be major or minor. Major damage includes cracks, spalling, and flaking. These are indications of serious damage and can be detected by visual inspection or by using non-destructive test methods such as ultrasonic and liquid penetration. Minor damages can also pose a severe threat. However, these damages are difficult to detect using commonly employed detection techniques. Electrical measurements of conductive concrete could allow to detect both major and minor damages [13]. To avoid catastrophic failures, structures require routine maintenance, timely rehabilitation and on-going health monitoring. Health monitoring (HM) is a mean of observing the condition of a structure (i.e. to keep track of load acting on it, stresses being developed and performance). Health monitoring mainly involves setting up a baseline data of structural health (levels of stress and strain in different structural members), collection of data (changes in stress and strains), analysis of data (comparison with the baseline data) and structural health assessment (predicting the remaining useful life of a structure).

1.3.2 Objective and Scope

The objectives of this research (Part II) are to develop a conductive geopolymer and a health monitoring technique for structures. Electrical conductivity is induced into

the geopolymer by adding carbon fibers to the fresh cementititous material mixture, and electrical impedance measurements are performed on the hardened concrete matrix. It is hypothesized that the changes in the stress state of conductive concrete lead to changes in its electrical resistance; therefore, by measuring the electrical impedance, the health of a structure can be monitored. AC-impedance spectroscopy was employed for impedance measurements.

1.4 Dissertation Overview

This dissertation is divided into five chapters. Chapter 1 gives the brief introduction to the research topics, including problem statement, objectives and scope of work. Chapter 2 describes the background and earlier work that has been done on these particular topics by others. Chapter 3 describes the experimental design utilized for the electrokinetic coating treatment of concrete pipes. Results from the three Phases of testing and summery of observations are also provided. Chapter 4 describes the experimental design and procedure adopted for developing conductive geopolymer and health monitoring technique; this chapter also contains impedance results from Phases I, II and III as well as the results from a dynamic analysis. Conclusions from the current work and recommendation for the future work are given in Chapter 5.

CHAPTER 2

LITERATURE REVIEW

2.1 Background and Literature Review – Part I

2.1.1 Background on MIC

The first to study micro-bacterial induced corrosion in sewers was Parker [14], whose study isolated the Thiobacillus bacteria from corroded concrete sewers. MIC often involves two types of bacteria common to many sanitary sewer systems, namely sulfate reducing bacteria (SRB) *Desulfovibrio desulfuricans* and sulfide oxidizing bacteria *Thiobacillus thiooxidans* (also known as "concretivorous", or "concrete eater"). Sulfates present in the wastewater are transformed into sulfides by sulfate reducing bacteria which tend to grow on the wet perimeter of the sewer pipe [15]. SRB grows in a slime layer, consisting of bacteria and inert solids held together by a film called Zooglea [16], which forms on the pipe wall below the water level. There are three layers in a typical slime layer, namely inert anaerobic, anaerobic and aerobic zones. The inert anaerobic zone is in contact with the pipe wall while aerobic zone is exposed to the wastewater stream. SRB resides and converts sulfates to sulfides in anaerobic zone residing between these two zones. Due to the aerobic zone being present on top of anaerobic zone, the sulfides produced gets oxidized without getting diffused into the wastewater stream, but when this aerobic zone gets depleted sulfides are released into the wastewater stream [17].

7

The rate at which sulfides are produced in the slime layer depends upon various factors such as BOD (biological oxygen demand) or availability of organic food source, dissolved oxygen concentration, temperature inside the sewer, wastewater stream velocity and area of the pipe wall under the water level [16]. High BOD and high temperatures promotes the growth of bacteria and lowers dissolved oxygen concentration resulting in more sulfides being released into the waste water stream. Waste water stream velocity also plays a key role in the sulfide generation. High stream velocities keep the solids moving with the flow which ensures thin slime layer and more oxygen diffusion into the waste water stream, which in turn, leads to lower production of sulfides. However, if the sulfides are already present in the waste water stream, high velocity leads to rapid release of sulfides into the sewer atmosphere [18]. To avoid build up of solids and to control the release of sulfide, it was proposed that the stream velocity inside a sewer should be maintained at a minimum of 2 to 3.5 ft/s [17].

Once the sulfides are released into the waste water stream, they quickly form a chemical equilibrium among the four forms of sulfide i.e. sulfide ion (S^{-2}), bisulfide or hydrosulfide ion (HS^{-1}), aqueous hydrogen sulfide ($H_2S_{(aq)}$) and gaseous hydrogen sulfide ($H_2S_{(g)}$). Sulfide ions and bisulfide ions do not contribute to the gaseous transformation of hydrogen sulfide, and they remain in the aqueous state. Aqueous hydrogen sulfide leaves the waste water stream to form gaseous hydrogen sulfide. This transformation depends on the rate of change of liquids to gases (Henry's law), as well as the degree of turbulence (i.e. Reynolds number) and pH of the waste water stream. As liquid hydrogen sulfide leaves the stream to form gaseous hydrogen sulfide, bisulfide ion transforms into aqueous hydrogen sulfide and consequently sulfide ion transforms to bisulfide ion to restore the

equilibrium. In this way the generation of hydrogen sulfide is a continuous process as long as there are sulfides in the waste water stream. Thus, the generation of gaseous hydrogen sulfide mainly depends upon the concentration of sulfides produced [19]

$$H_2S_{(g)} \Leftrightarrow H_2S_{(aq)} \Leftrightarrow HS^{-1} \Leftrightarrow S^{-2}. \qquad (2.1)$$
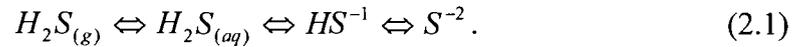
The other factors that can contribute to the increase hydrogen sulfide production are Junctions, force main, high discharge points and siphons in the sewer line creating turbulence. Increased turbulence releases more hydrogen sulfide into the air. Furthermore, inadequate gradient, build up of grit and debris, and poor construction may add up to hydrogen sulfide generation by hindering the waste water flow velocity [18].

2.1.2 Sulfuric Acid Generation and Corrosion Mechanism

In areas of turbulent flow, such as high points in force mains and junctions, the hydrogen sulfide is released into the pipe's head space. The *Thiobacillus* bacteria, which grow on the sewer crown region above the water line, convert the hydrogen sulfide to sulfuric acid in the presence of oxygen [4, 20]. The chemical reaction associated with production of sulfuric acid is [19]

$$H_2S_{(g)} + 2O_2 \longrightarrow H_2SO_4. \qquad (2.2)$$

A freshly placed concrete has a pH of approximately $11 - 13$, depending upon the mix design. This pH is due to the formation of a stable compound, calcium hydroxide $Ca(OH)_2$, a common by-product produced during the hydration of cement. This initial high pH on the surface of the concrete does not allow bacterial growth. However, this high pH state lasts for only a short period, as the pH level slowly declines over time due to interaction with carbon dioxide (CO_2) and hydrogen sulfide (H_2S) gases. These gases form weak acidic solutions when dissolved in water (carbon dioxide forms carbonic acid

and hydrogen sulfide forms thiosulfuric acid and polythionic acid), that lower the pH of the concrete surface to 9 or 8.5 [15]. *Thiobacillus* bacteria that have a unique ability to convert hydrogen sulfide to sulfuric acid in the presence of oxygen start colonizing at a pH of about 9. The first colony of bacteria reduces the surface pH value from 9 to 6.5 by excreting sulfuric acid. These bacteria will not be able to survive at pH values lower than 6.5, and thus, the colony dies, and the residence is then taken over by another species that is capable of surviving below a pH of 6.5. This newly formed species of *Thiobacillus* further reduces the pH value from 6.5 to 4 before dying off. This process of colonizing and dying of bacteria continues, until the pH at the surface of the concrete can be brought to a value as low as 1 or 0.5 [21]. The sulfuric acid produced by the bacteria interacts chemically with the hydration products in the hardened concrete paste. The chemical reactions involved in corrosion of concrete are:

$$H_2SO_4 + CaSi \longleftrightarrow CaSO_4 + 2H^+, \qquad (2.3)$$

$$H_2SO_4 + CaCO_3 \longleftrightarrow CaSO_4 + H_2CO_3, \qquad (2.4)$$

$$H_2SO_4 + Ca(OH)_2 \longleftrightarrow CaSO_4 + 2H_2O. \qquad (2.5)$$
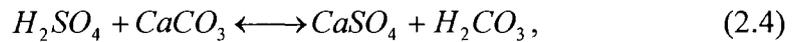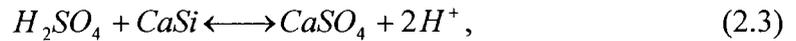
The primary product produced during concrete decomposition by sulfuric acid is calcium sulfate ($CaSO_4$), that when it hydrates becomes "gypsum" [22]. This material has low structural strength, especially when wet. It is usually present in corroded sewers as a pasty white mass at the crown region above the water line. Due to its lower shear strength and poor adhesion, the gypsum is washed off by the wastewater flow, exposing fresh concrete to further acid attack [5]. An example of severe MIC in a 27 year-old concrete sewer pipe is shown in Figure 2.1.
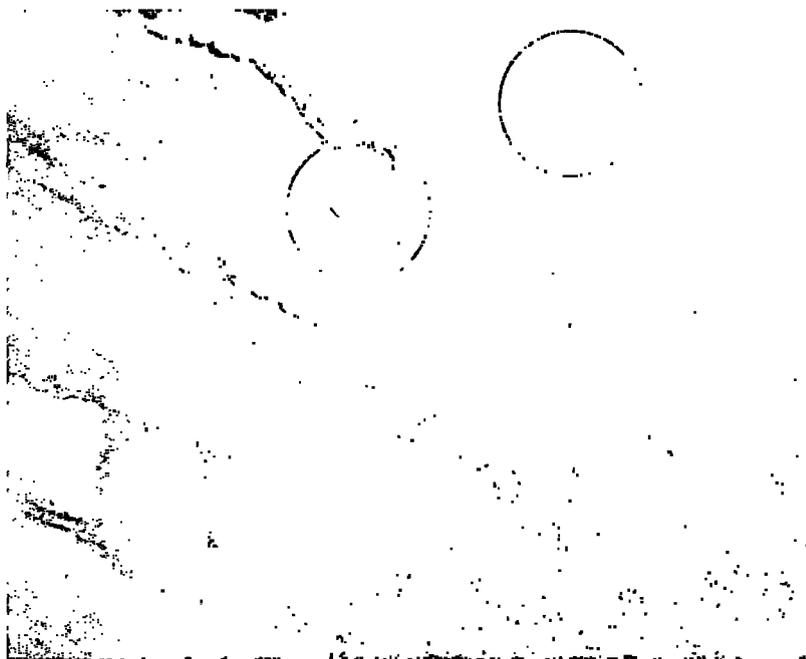
Figure 2.1 Close-up of a 27 year old, 36" diameter concrete sewer pipe that experienced severe MIC.

2.1.3 Available Methods

A large number of methods have been developed to mitigate MIC in wastewater collection systems. To minimize hydrogen sulfide generation in sewage collection systems, the Environmental Protection Agency (USEPA) has recommended the injection of oxygen as well as the addition of various chemicals to wastewater streams [19]. Injection of oxygen increases dissolved oxygen (DO) content in wastewater, which prevents sulfide generation by oxidizing the sulfides entering wastewater streams. The addition of chemicals, such as metallic salts of iron and zinc, results in the formation of precipitates that utilize the sulfides present in the wastewater (e.g., iron sulfide and zinc sulfide) [19]. These methods can considerably minimize the production of hydrogen sulfide in wastewater collection systems, but associated operating and maintenance cost of these processes over the service life of the system could be significant.

Another approach is the utilization of spray-on coating that aims at creating a corrosion resistance barrier (possibly with an embedded biocide agent) between the wastewater stream and the pipe's inner surface. Sample techniques include spraying of the sewer crown region with magnesium hydroxide [22, 24], coating concrete pipe interior surface with 100% solid polyurethane [25], shotcreting with biocrete [26], coating with a sewpercoat [27] as well as mixing antimicrobial chemicals with a cementitious grout or epoxy and spraying them on the sewer wall [28, 29]. However, these methods suffer from several disadvantages. It is often difficult to create proper adhesion between the coating material and the concrete substrate due to the difficulties associated with proper surface preparations, the presence of contaminants (e.g oil and grease) on the surface, entrapment of moisture and the challenges associated in ensuring adequate curing. Further, the "rebound" effect from hurling the coating material at the pipe's wall can result in uneven coating buildup. Combined with a non-uniform rate of application, this uneven layer thickness tends to result in an uneven stress loading and subsequent premature failure of the coating. Since the coating material does not penetrate the pipe surface (i.e., create a mechanical interlock with the concrete substrate), it tends to flake and peel off with time under loading applied by shrinkage, the transported media and/or cracks induced by differential settlement of the pipe [30].

Another common method of protection is lining the pipe's internal surface with a chemically stable material. Over the past 20 years, a large number of lining methods emerged in the market place including cured in place pipe (CIPP), fold and formed (FFP), Deform and reform (DRP), Spiral wounding liners and more [31]. CIPP employs a chemically stable fabric using a thermosetting resin; however, FFP, DRP and spiral

wound lining methods use either PVC or HDPE pipes to form a corrosion resistance barrier at the inner wall of the deteriorated host pipe. Properly applied, these methods will serve their purpose for a long period of time. Shortcomings of lining methods include relatively high costs associated with the required mobilization, preparations and installation activities. In addition, many of these methods require taking the pipe out of service for a significant period of time, which is not feasible for large collectors and interceptors that serve as the backbone of many municipal sewage systems

Almusallam et al. [32] studied the durability of surface coated concrete against sulfuric acid corrosion. Concrete samples were coated with five different types of coating materials (Acrylic coating, Polymer emulsion coating, Epoxy resin coating, Polyurethane coating, and chlorinated rubber coating) and were subjected to degradation by immersing them in a 2.5% sulfuric acid solution. Samples coated with Polymer emulsion and chlorinated rubber did not sustain and deteriorated rapidly; whereas, acrylic coating had edge failures. Only Polyurethane and Epoxy coating were intact after 60 days of immersion. With the better performance of both polyurethane and Epoxy, the author recommends surface coating of concrete with polyurethane and epoxy against chemical attack.

A study of the impact of coating concrete pipe with heavy metal oxides such as Cuprous oxide and Silver oxide was performed by Hewayde et al. [8] and Haile et al. [29]. Cuprous oxide and silver oxide were mixed with epoxy and sprayed on the pipe's internal wall surface. Hewayde et al. [8] demonstrated that the heavy metal oxide coating has a toxic effect on bacteria and significantly reduced its growth. In addition, the slime layer was absent in pipe specimens that were coated. However, leaching of metal oxides

into the simulated sewer solution occurred due to poor bonding of the epoxy to the concrete substrate, leading to flaking and eventually failure of the coating. Leaching of the heavy metals into the effluent stream might also prove detrimental to biological treatment processes at the treatment plant. Cuprous oxide is further used as a conventional biocide against fouling caused by marine bacteria, and it is applied to the surfaces of marine structures and ship hulls by mixing it with marine grade paints [33].

2.1.4 Electrokinetics – An Overview

Electrokinetics is a technique that uses a low DC voltage across the electrodes to move particles or contaminants in a porous medium. Electrokinetics comprises of three major processes--electrophoresis, electro-osmosis and electro-migration. Electrophoresis is the movement of colloids, or charged particles, under the influence of an electrical field; electro-osmosis is the movement of fluid, or in this case, coating solution, through the capillaries and pores from the anode to the cathode. Electro-migration is the movement of ions or ionic complexes. One of the earliest applications of electrokinetics took place during the 1960's, as part of an attempt to extract heavy metals and organic contaminants from soils and ground water [34]. Since then, it has been used as basis for many other applications including:

Steel inside reinforced concrete corrodes when it is exposed to chloride in presence of moisture and oxygen. To ensure the design life of the structure, a constant inspection and repair is necessary. Repair is done by extracting chloride from the concrete and raising the pH of concrete around the reinforcement. By applying an electric field between the reinforcement of the concrete, which acts as cathode and a surface mounted electrode behaving as anode, chloride is drawn out electrokinetically, and

simultaneously, re-alkalization of concrete is achieved by transporting alkaline solution into the concrete through pores. Usually, sodium carbonate is employed as an alkaline solution to increase the pH of concrete [35].

Kim et al. [36] through laboratory experiments on small volumes of contaminated soils, proved that the electrokinetic process can be successfully adopted to remove heavy metals form the soil. By applying an electric field between two electrodes across the soil sample, they were able to move the contaminants through the soil; to increase the mobility of contaminants, distilled water was added to the soil sample. They concluded that the efficiency of electrokinetic heavy metal removal from the contaminated soil depends upon the initial concentration, initial pH value and the way heavy metals exist (i.e., if the metals exist in immobile or bonded form the efficiency of removal will be low). Conversely, if they are loosely bonded, removal efficiency is enhanced greatly.

Bioremediation is a way of restoring contaminated soils which uses naturally occurring bacteria to react with the contaminants and render them less toxic or non-toxic. The method specifically targets organic contaminants such as petroleum products. Using drilling, wells ground water is extracted, essential nutrients are added to it and the water is reinjected back into the ground. Nitrates are added as nutrients to enrich the bacterial life. The water injection process has two important factors that are critical in designing a recovery well for bioremediation, namely soil permeability and flow path. To have a uniform remediation throughout the entire contaminated soil, the process requires relatively large soil permeability, and the flow path should be able to cover the whole treatment area. This permeability and flow path coverage is not possible in all the cases. To overcome this obstacle, Budhu et al. [37] suggested using an electrokinetic

remediation technique. They conducted preliminary tests on small soil samples under laboratory conditions using weak electric field across two electrodes to transport nutrients across the soil sample.

Soil liquefaction is a serious concern in sandy and silty/sandy soils since it may lead to temporary loss of strength and ground settlements. The choices of available methods for improving soil strength are densification, reinforcement and cementation/solidification which depend on soil type, site accessibility and cost. A new technique of injecting grouting material for soil densification deploys electrokinetic permeation. Preliminary experiments conducted on saturated soil samples using dc voltage across the electrodes, grouting material (sodium silicate, colloidal silica and water) was transported through the soil to a particular radial distance away from the electrodes [38].

Cardenas and Strubles [39] work was directed towards reducing the porosity of concrete by electrokinetically transporting colloidal nanoparticles (Silica and Alumina) that formed precipitates in the pore regions. The work done by Cardenas and Goli [40] addressed the effects of electrochemical chloride extraction (ECE) and electrokinetic treatment (EN) on the corrosion potential of steel in concrete. Their studies showed that both ECE and EN will drive the corrosion potential of steel in concrete to a positive shift, but in case of ECE, this effect does not last long. They hypothesized that this result was due to the increase in the permeability caused by ECE; whereas, EN effect on the corrosion potential stayed for a longer period. This effect was attributed to the formation of precipitates in the pores, blocking them. It was also found that EN treatment improves the tensile strength of concrete. Ryu and Ostuki [41] were able to successfully reduce the

crack size in concrete using a electrodeposition technique and suggested that the technique can be adopted to rehabilitate marine concrete structures against chloride corrosion cracking in economic manner.

2.2 Summary of Part I

Biological corrosion of concrete sewer pipes is a common of type of corrosion that takes place mainly due to the presence of two different species of bacteria, sulfate reducing bacteria (SRB) *Desulfovibrio desulfuricans* and sulfide oxidizing bacteria *Thiobacillus thiooxidans.* Sulfate reducing bacteria produces sulfides that combine with the sewage to form hydrogen sulfides. This liquid hydrogen sulfide is slowly released into the sewer atmosphere as hydrogen sulfide gas due to existing ambient conditions inside the sewer. Thiobacillus bacteria consumes hydrogen sulfide for its metabolism in presence of oxygen it producing sulfuric acid though a controlled biological process. This biologically produced sulfuric acid reacts with the hydration products in the hardened concrete matrix leading to deterioration and ultimately premature failure of the sewer system.

Surface treatment is a cost-effective approach for mitigating MIC in concrete sewer pipes. However, current surface treatment has limited useful life (typically months to a couple of years) due to poor adhesion, flaking and shrinkage. The present research aims to overcome these obstacles as well as to break the hydrogen sulfide generation cycle by developing a coating technique that forms a mechanical interlock with the concrete substrate. Using electrokinetics particles of cuprous oxide could be driven into the concrete matrix, forming a biocide layer on and beneath the surface of the pipe

interior. This biocide layer has a toxic effect on the bacteria which prohibits it from colonizing thereby breaking the hydrogen sulfide generation cycle.

2.3 Background and Literature Review – Part II

2.3.1 Background on geopolymer

Geopolymer was first termed by Davidovits in 1978, which also used poly(sialate) as the chemical designation for geopolymers based on silico-aluminates. Sialate is an abbreviation for silicon-oxo-aluminate. Poly(sialates) consists of chain and ring structures of Si^{+4} and Al^{+3} in a four- fold coordination with oxygen (O), and ranges from amorphous to semi-crystalline in nature. SiO_4 and AlO_4 tetrahedral molecules are linked alternately by sharing oxygen. The empirical representation of poly(sialate) is

$$M_n\left[-\left(SiO_2\right)_z - AlO_2\right]_n \bullet wH_2O, \tag{2.6}$$

where 'M' represents a cation such as potassium, sodium and calcium, 'n' is the degree of polymerization or polycondensation, and 'z' is equal to 1, 2, 3 or higher [42]. The hardening mechanism in forming geopolymers involves a chemical reaction between alumino-silicate oxides (Si_2O_5, Al_2O_2) and alkali polysilicates to yield polymeric chains of Si-O-Al. Typically, polysilicates of sodium and/or potassium are used as alkali polysilicates. The polymerization is an exothermic reaction and can schematically be represented as (See Figure 2.2).

$$n(Si_2O_5,Al_2O_2) + 2nSiO_2 + 4nH_2O \xrightarrow{\text{NaOH,KOH}} n(OH)_3\text{-Si-O-}\overset{(-)}{\underset{(OH)_2}{Al}}\text{-O-Si-(OH)}_3$$

$$n(OH)_3\text{-Si-O-}\overset{(-)}{\underset{(OH)_2}{Al}}\text{-O-Si-(OH)}_3 \xrightarrow{\text{NaOH,KOH}} (Na,K)\text{-}(\text{-Si-O-Al-O-Si-O-}) + 4nH_2O$$

Figure 2.2 Schematic representation of polymerization reaction in geopolymer.

The last term in second equation above represents water that is being released during polymerization, which later is expelled during the curing process [43]. Upon

polymerization, geopolymer can take any of the three basic molecular structures, poly(sialate), poly(silate-siloxo) and poly(sialate-disiloxo) (See Figure 2.2).

Poly(sialate)
(-Si-O-Al-O-)

Poly(sialate-siloxo)
(-Si-O-Al-O-Si-O-)

Poly(sialate-disiloxo)
(-Si-O-Al-O-Si-O-Si-O-)
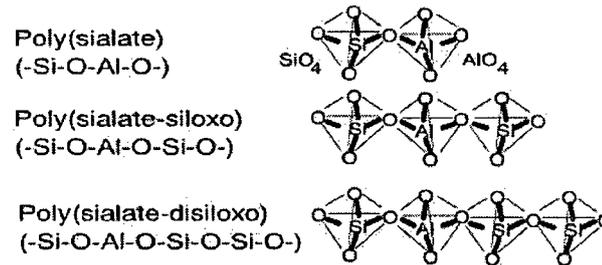
Figure 2.3 Chemical representation of poly(sialate), poly(silate-siloxo) and poly(sialate-disiloxo) [42].

In ordinary Portland cement concrete, hydration of cement leads to the formation of CSH gel, which is responsible for its mechanical strength; whereas, in geopolymers the strength is due the formation of polymeric chains which involves polymerization of silica, alumina with alkaline liquids [10, 44].

2.3.2 Source Materials Required for Making Geopolymer

Similarly to ordinary Portland cement, the making of geopolymer requires a source material and a liquid phase. The source could be any material which is rich in silicon (Si) and aluminum (Al) such as naturally occurring minerals (i.e. kaolinite, mica, garnet, feldspar and clays) [43, 45] or by products of certain industrial processes such as fly ash, blast furnace slag, rice husk ash, and silica fume. Metakaolin (calcined kaolin) can also serve as potential source material in making geopolymer. The choice of source material may depend on local availability, type of application and cost. Metakaolin serves as the perfect source material for making geopolymer because of its rich silicon and aluminum content, high reactivity and ease of control. However, it is not economically

feasible to use Metakaolin for mass production of geopolymer. ASTM class F fly ash could serve as an ideal source material for mass production of geopolymer. Class F fly ash is preferred over class C due to a lower percentage of calcium. Presence of calcium in elevated levels could hinder the polymerization reaction [1] and lead to flash set as well due to formation of calcium hydrate products. Several authors have published a considerable amount of research on utilization of fly ash as a source material for making geopolymer [10, 46, 47, 48, 49 and 50].

Palomo et al. [10] reported that the activation reaction of fly ash with high alkaline solutions involves an exothermic process, and the reaction rate is influenced by temperature, curing time and type of solution used. The study states that the reaction will occur at faster rate if the solution contains soluble silicates (e.g. sodium or potassium silicates) and also with the rise in curing temperature. Mechanical strength of the sample specimens were found to be improved with longer curing times.

Swanepoel and Strydom [49] investigated the potentials of fly ash as a source material for making geopolymer. Their study involved evaluation of the mechanical strength of geopolymer with respect to curing temperatures and time. Geopolymer samples made from fly ash and kaolinite (with NaOH and sodium silicate as activator solution) were subjected to range of temperatures (40° - 70°C) and curing times (6 – 72 hrs) in an oven. The study claims that a curing temperature of 60°C with a curing time of 48 hrs yields the maximum mechanical strength.

Xu and Van Deventer [48] studied three different minerals (fly ash, kaolinite and albite) as the source materials for making geopolymer. X-Ray diffraction, leaching and mechanical strength properties were studied to evaluate the three minerals. Their study

showed that fly ash and albite are reactive compared to kaolinite and suggested that to produce geopolymers with higher compressive strengths, a combination of highly and less reactive materials is required (i.e. fly ash and kaolinite or albite). They also reported that by adding calcined materials (e.g. fly ash) to non-calcined materials (e.g. kaolinite and albite) would significantly reduce the reaction time.

Van Jaarsveld et al. [50] used six different fly ash sources to study the effects that influence the final physical and mechanical properties of fly ash based geopolymers. Their study observed that the source or origin of fly ash plays an important role in dictating the final properties since different fly ash source will contain different percentages of Si, Al and CaO contents. They stated that the presence of calcium content by itself plays a major role in controlling strength and setting time of geopolymers. In addition to calcium content, they found that the zeta potential (surface charge) on fly ash particles, particle size, alkali metal content and water/fly ash ratio also significantly influence the setting time and mechanical strength of fly ash based geopolymers.

Fernandez and Palomo [47] studied various fly ash sources for making geopolymers. They stated features that a fly ash should possess to serve as source material for making geopolymer. Loss of ignition (LOI) or unburnt carbon should be less than 5%, Fe_2O_3 percent should not exceed 10%, CaO content should be low (< 10%) and 80-90% of the particles should be smaller than 45 μm. In another effort, Van Jaarsveld et al. [50] found that the presence of CaO in fly ash results in early development of higher compressive strength geopolymer. They attributed this effect to the formation of calcium-aluminate-hydrate during the early stages of curing.

2.3.3 Liquid Phase Material Required
for Making Geopolymer

Alkaline hydroxides (NaOH, KOH) are the most commonly used liquid phase materials for producing geopolymers. Davidovits was the first to use sodium and potassium hydroxides as the activator solutions for making geopolymer. Many other researchers have also reported using NaOH and/or KOH [10, 45, 51, and 52].

Palomo et al. [10] studied the effects of using alkaline hydroxides with alkaline silicates as activator solutions. They concluded that the use of alkaline silicates (sodium silicate and potassium silicate) in combination with alkaline hydroxides (sodium hydroxide and potassium hydroxide) result in increased reaction rate and better mechanical strengths compared to when only hydroxides are used for producing geopolymers.

Xu and Van Deventer [45] investigated the possibilities of using some 16 naturally occurring Si-Al rich minerals as source materials for making geopolymer. They used concentrated NaOH and KOH as their activator solutions and showed that the dissolution (reaction rate) of minerals increased by adding silicates in addition to the hydroxides.

Kwesi and Trevor [52] used NaOH and sodium silicate for making fly ash based geopolymers. Their work concluded that the strength of geopolymers formed from fly ash depends upon microstructure, mix composition and alkali concentration. High strength geopolymers are characterized by their low porosity and dense microstructure which can be formed by using concentrated alkaline solution. They found that by using approximately equal concentration of sodium to aluminum (Na_2O/Al_2O_3 = 1.0) and high silica to aluminum ratio (SiO_2/Al_2O_3 = 3.5-3.8) can produce dense micro-structured

geopolymers. However, they also observed a decline in the trend after reaching a certain maximum.

Kamhangrittirong et al. [51] studied the effects of sodium hydroxide molarity and fly ash content on setting time and compressive strength of geopolymers. They found that by increasing molarity of NaOH and fly ash content setting time of the geopolymer paste decreased, while there was increase in compressive strength.

2.3.4 Geopolymer Mix Proportions and making

Considering the limited available literature on geopolymer research and with the experimental knowledge gained, Hardjito and Rangan [1] proposed the following mix proportions and quantitative measures of individual materials for making geopolymer.

- ➤ For alkaline liquids the ratio of sodium silicate to sodium hydroxide may be anywhere between 0.4 – 2.5 by mass.

- ➤ Molarity of alkaline solution (NaOH) can range from 8M to 16M depending upon the strength required.

- ➤ Ratio of activator solution to source material (fly ash) can be 0.3 – 0.4.

- ➤ As in Portland cement concrete percentage of coarse and fine aggregate could be 75% to 80%.

- ➤ 0% - 2% super plasticizer by mass of source material (fly ash) could be added to improve workability.

In making geopolymers, researchers have suggested to first dry mix the source materials and aggregates. Next, the alkaline solution ($NaOH/Na_2SiO_3$) is added and further mixing is done for a specific period of time [49, 53]. Teixeira-Pinto et al. [54] suggested the use of shear mixer instead of gravity since mixing increased the viscosity

and also found that increase in mixing time increases the temperature of the fresh geopolymer, thus affecting workability. For curing geopolymers, a wide range of temperatures and curing times have been suggested, curing can be done anywhere between room temperature to 90°C, and the period of curing can be from 1 hour to more than 24 hrs [1, 10, 49, and 54].

2.3.5 Applications of Geopolymers

Geopolymer has interesting properties such as high early strength gain, fast setting, low permeability, resistance to chemical attack and cost efficiency in production [1, 10, 46, 47, and 48].

In a review while explaining the theory behind geopolymer, the reactions involved, formation of the structure and its properties, van Jarsveld et al. [11] quoted the following potential applications of geopolymer

- Surface capping and low permeability base liners for waste dumps and landfills where high strength barrier is needed to avoid leakage and infiltration.

- Construction of dams and stabilization of tailings dams.

- Can serve as cheap, non porous, non permeable and non reactive pads in case of leaching and collection of leachate.

- Intermediate horizontal barriers to separate waste masses from contact between layers.

- Structural floors, storage areas, runways and in pre-cast industry to make simple structures such as fences, pavements, and pipes.

- Immobilization of heavy metals such as arsenic, mercury and lead, and also to encapsulate hazardous materials such as asbestos and radioactive wastes.

➤ A replacement for Portland cement in building components to make bricks and ceramic tiles.

– The utilization of geopolymer composites as a protective coating for transportation structures was investigated by Defazio et al. [55]. They have successfully applied and improved the strength of concrete beams by applying geopolymer composite coating and reported that the performance was better than organic coating in terms of fire resistance. The application is further said to serve as a graffiti-resistant coating since it provides a hard and smooth surface with low porosity, which prevents the graffiti paint from adhering to the surface and making it easy to be removed by abrasion wheels.

Palomo et al. [56] investigated the potential of using fly ash based geopolymer concrete for making railway sleepers. They reported that geopolymer concrete could be easily be produced and used for making structural member with the existing concrete technology. The performance of these produced members was considered to be satisfactory and little drying shrinkage was noted.

In building civil infrastructure, there could be several uses of geopolymer. A study conducted by Hardijito and Rangan [1] showed that fly ash based geopolymer can serve as potential source for replacing Portland cement concrete in construction due to properties such as lower shrinkage, elevated resistance to sulfate and acid attack and high strength gain rate. In another study, Rangan et al. [57] concluded that the elastic properties of reinforced structural members of geopolymer were similar to that of OPC, and so design codes and standards currently employed for OPC based structures could be potentially used for designing geopolymer concrete structure.

Zhao et al. [58] studied a geopolymer composite for applications for which there is a need to resist fire and high temperature exposures. The composite combines the high strength and stiffness of metal wires with high temperature resistance and chemical stability of geopolymers. In their experimental work, they showed that the composite retained almost 50% of its original ductility even after exposing it to high temperatures such as 800°C to 1050°C.

2.3.6 Reinforcing Effects of Fibers in Cementitious Matrices

Reinforcing concrete using fibers is a not a new concept when it comes to improving the strength and ductility of structures. There are several ways fibers could be used in construction to meet the day-to-day demand for sustainable and better performing structures. Fiber usage can be classified into three main categories, namely: a) providing internal reinforcement; b) increasing the performance of existing structure by external wrapping and plating; and c) adding short random fibers to increase tensile strength, resistance cracking and ductility.

2.3.7 FRP (Fiber Reinforced Polymer)

Glass fiber was first used to reinforce polymers during late 1940's by the petrochemical industry which required light, high strength and high performing materials. During 1960's and 70's, usage of FRP was limited to high-end technologies such as space explorations and defense, due to high cost. In the 80's and 90's, the demand for FRP increased around the world paving a way to increase in FRP production and lower prices. Today, FRP has applications in a multitude of fields. FRP usage in construction consists mainly of pultruded structural products for load bearing and general construction applications, fiber reinforced polymer bridge decks, internal reinforcement with FRP

grids and bars and external reinforcing with bonded FRP grids, wrapping and plating, mechanical fastening and spraying [59, 60, 61 and 62].

2.3.8 Short Fiber Reinforced Cementitious Matrices

The present work concerns short fibers reinforced cementitious materials, specifically, exploiting the conductivity property induced by the addition of short fibers (carbon fibers) to the cementitious matrices. A significant amount of research has been done on this particular topic by Chung and her associates, who suggested that by adding short carbon fibers to the cementitious matrix, its conductivity can be significantly improved [63, 64, and 65].

Chen and Chung [63] were the first to study the electrical properties of carbon fiber reinforced mortar for electrical probing of existing concrete structures. They studied the contact electrical properties between metal and the carbon fiber entrained mortar, and stated that for achieving good electrical contact, the metal does not need to be embedded in the curing concrete. This property means that the metal probe or electrical lead can be placed on the surface of the conductive concrete after curing for electrical probing. Their study also concluded that bulk electrical resistivity value of conductive mortar will be lower if methylcellulose in combination with silica fume were used as dispersing agents in place of latex.

Xuli Fu and Chung [64] studied the self monitoring properties of short fiber reinforced cement mortar. They used short carbon fibers (5mm in length), 0.5% by weight of cement, with methylcellulose and silica fume as dispersing agents for making specimen samples. They studied the self monitoring effects of conductive mortar by performing cyclic loading on the specimen samples and simultaneously measuring the

electrical resistivity of the samples. They observed decrease in fractional electrical resistance with increase in loading cycles and attributed this changes to the damage in cement matrix separating the fibers. This phenomenon enables the cement mortar to detect fatigue damages, by observing changes in volume resistivity of the conductive mortar.

In another study, Zeng and Chung [65] investigated the possibilities of using conductive concrete for traffic monitoring and weighing in motion applications. Laboratory experiments were performed to record the speed and weight of a moving car wheel. The car wheel was allowed to rotate against a conductive concrete cylinder that had electrical contacts which provided the information regarding the resistivity changes in the cylinder. Using this resistivity data, the authors were able to calculate the speed and weight of the moving car wheel. They were successful in recording the speeds up to 55 mph. The authors say that this property could be effectively used in monitoring traffic speed and weighing in motion.

Chung [66] explained that the conductive concrete could be used for both strain sensing and damage detection applications. In case of strain sensing that electrical resistance varies with changes in strain, (i.e. increases reversibly upon tension and decreases reversibly upon compression due to fiber pull out and pull in), Chung suggests that a gage factor could be assigned for fractional change in resistance per unit strain, using this fractional change, strain could be monitored in a particular conductive structural member. Chung also writes that addition of large aggregate to the cement matrix will decrease this gage factor but will not hinder strain sensing ability. In case of damage detection, Chung says that electrical resistance increases permanently, (i.e.

during the loading when damage occurs, resistance cannot be brought back to the original baseline resistance upon unloading). This permanent shift in resistance could be used to detect damages in the structures.

2.3.9 Importance of Electrical Interrogation

Following the work done by Chung, other researchers have published their work on carbon fiber reinforced conductive cement (CFRCC). The significant difference between Chung's work and the latest published research is the use of alternating current (AC) for electrical interrogation rather than direct current (DC) [67, 68, & 69]. Chung used DC electrical resistance measurements for the characterization of CFRCC. It is known that DC measurements will produce false polarization potentials that arise from chemical reactions at the electrodes. This false potential is also known as back emf, since it opposes the flow of current. To avoid the problems of false potential, AC is often preferred over DC for electrical resistivity measurements. Using AC the polarization potential is not completely eliminated, but rather transformed into a capacitive resistance in series or in parallel with the true resistance of the material, and can be subtracted in the resistance calculations. When AC is used, electrical resistance measurements are termed as impedance (Z), which is a combination of real impedance (true resistance) and imaginary impedance (capacitance or inductance). Imaginary impedance (in this case capacitance) is frequency dependent, (i.e. as the frequency of the applied alternating current increases, the capacitance decreases, and the total impedance approaches real impedance). In this way, capacitance or polarization potential can be eliminated from total impedance measurements (See Eq. 2.8, Eq. 2.9 and Eq. 2.10) [70].

$$Z = \sqrt{\left(R^2 + X_C^2\right)}$$

(2.8)

$$Z = \cfrac{1}{\sqrt{\left(\cfrac{1}{R^2} + \cfrac{1}{X_C^2}\right)}} \qquad (2.9)$$

$$X_C = \cfrac{1}{2\pi * f * C}, \qquad (2.10)$$

where Z = total impedance,

R = real part of the impedance,

X_c = imaginary part of the impedance due to capacitance,

f = frequency of current applied,

C = capacitance.

Another reason to adopt AC over DC is to make use of frequency dependent behavior exhibited by carbon fibers in the cementitious matrices. When carbon fibers are added to the cementitious matrix, a potential barrier (charge transfer resistance) is formed around the fibers which will not allow them to conduct electricity at very low AC frequencies or DC measurements. Using high frequency AC causes displacement currents to short circuit the barrier, and the fibers start conducting through the matrix [71, 72]. Torrents et al. [71] and Mason et al. [72] employed AC impedance spectroscopy technique to characterize CFRCC. A frequency response impedance analyzer was used to collect the impedance data while the frequency was swept from 10 MHz to 0.1 MHz with an excitation amplitude of 1 V. Nyquist 3D plots were obtained from the analyzer with real impedance values plotted on X axis, imaginary impedance values on the Y axis and frequency on the Z axis. The value of frequency reduces from left to right on a Nyquist plot. The authors observed two bulk arcs on Nyquist plot for cement with short fibers in contrast to a single bulk arc for cement alone. They claim that this dual arc behavior is exhibited due to the frequency dependent behavior of CFRCC (See Figure 2.3). The

single bulk arc in case of cement alone splits into two smaller arcs for CFRCC; the arc on the left is formed when fibers are contributing towards conductivity (i.e. at high frequency), and the arc on the right is due to matrix conductivity alone. The point of intersection of two arcs represents the composite resistance (Rcusp) while the point on the extreme right represents the value of resistance with or without the contribution of the fibers (Rdc). That is when DC or low frequency AC is employed for resistance measurements on CFRCC, we measure Rdc (which does not include the contribution of the carbon fibers to the composite's conductivity). But when appropriate high frequency AC is used, we measure Rcusp, which is a combination of both matrix and fiber conductivity.
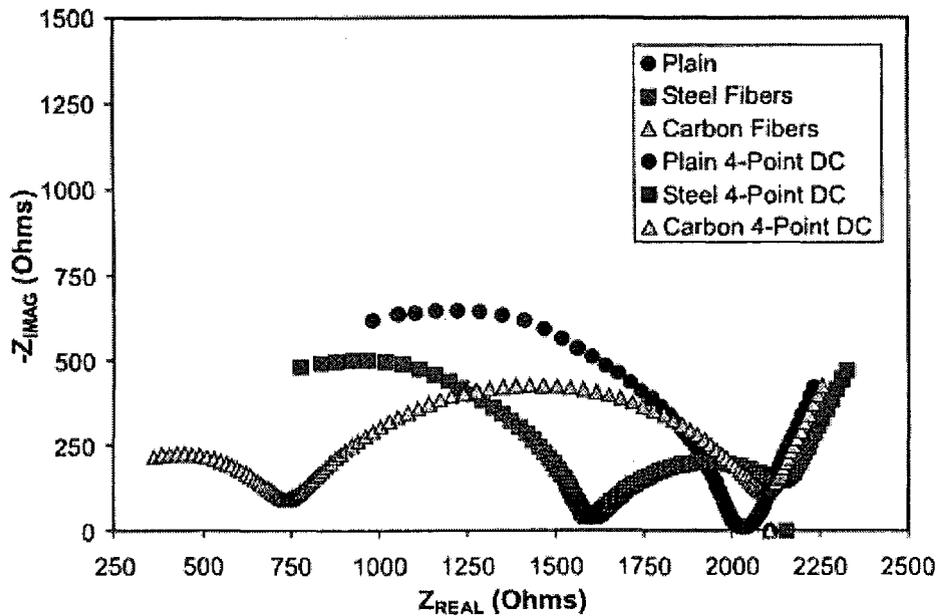
Figure 2.4 Nyquist plot for carbon fiber reinforced cement [71].

Considering the importance of using high frequency AC on conductivity of fiber reinforced cementitious composites, researchers have opted use AC over DC for the characterization of CFRCC [67, 68, and 69].

Farhad et al. [68] studied changes in electrical resistance of carbon fiber reinforced cement composite under dynamic compressive loading. An LCR (inductance, capacitance and resistance) meter was used to record the resistance data at a frequency of 100 Hz. During their experimental study, they observed that with the increase in load electrical resistance decreased. They attribute this change to reduction in conduction length and fiber contact in the matrix. During the cyclic loading, they further found reversible change in resistance when there is no significant cracking, (i.e. resistance could gain its original value upon unloading with the exception of no cracking). They claim that the technique could be used as a nondestructive testing method for monitoring structural integrity.

Bing Chen et al. [67] and Manuela et al. [69] studied the effects of fiber volume, size, relative humidity and curing age of cement on electrical conductivity of carbon fiber reinforced cementitous composite (CFRCC). AC voltage amplitude of 10 mV with a frequency of 100 KHz was used in their parametric study. They stated that the composite conductivity and fiber volume fraction could be analyzed using classic percolation theory. From the experimental data obtained, they were able to state that by increasing fiber volume fraction and length of fibers electrical conductivity increases up to a point (threshold fraction) after which there will be little or no effect of fiber volume increments on conductivity. They also observed that the resistivity of material decreased with the increase in hydration (i.e. curing time in water) and relative humidity in case of

composites with lower fiber volume fraction, but this phenomenon becomes less significant once the percolation threshold was reached. That is, once a continuous conductive path develops in the composite, the effect of fiber volume fraction, humidity and curing age become less significant.

Xiufeng Wang et al. [73] also investigated the influence of fiber volume fraction and length on electrical conductivity of CFRCC and stated that fiber volume fraction and length had an inverse relation with electrical resistivity. They observed that increasing fiber fraction and fiber length leads to decrease in resistivity of the composite. In addition, they performed flexure tests on the CFRCC and stated that the composite can behave as a stress sensor. They claim that once the percolation threshold is reached, then with the increase in flexure load, the composite resistivity decreases. In other words, upon attaining the percolation network, the CFRCC behaved as smart material.

Mingqing et al. [74] studied the piezoelectric behavior of CFRCC. Short carbon fibers were added to cement to form CFRCC. Based on experimental observations, it was stated that CFRCC can act as smart sensor on its own (i.e. the CFRCC was able to produce minute amounts of electrical current under compressive load). They attributed the source of current to the flow of ions in the double layer under shear stress from the loading.

2.4 Summary of Part II

Geopolymers, introduced by Davidovits in 1978, has captured the imagination of many researchers working in multitude fields. In the construction industry, it is believed to have the potential to serve as a substitute for Portland cement due to properties such as high early strength and resistance to elevated temperatures, corrosion and freeze thaw

effect, while maintaining low shrinkage. Just as in Portland cement concrete, geopolymers also require a pozzolanic source and a liquid phase for making a cementitious material. Source material could be any material which is rich in silicon (Si) and aluminum (Al), such as naturally occurring minerals (e.g. kaolinite, mica, garnet, feldspar and clays) or byproducts of industrial processes such as fly ash, blast furnace slag, rice husk ash, and silica fume. For the liquid phase alkaline hydroxides, such as NaOH or KOH, in combination with sodium silicate or potassium silicate are commonly be used.

Traditionally, fibers are used in concrete to improve tensile strength, ductility and resistance to crack propogation. Chen and Chung in 1993 [63] were the first to exploit the electrical conduction behavior of concrete rendered by the addition of carbon fibers to the cementitious matrix. Follow up work resulted in different concepts and methods as to how to maximize the output conductivity of conductive concrete. One such technique is ACIS (alternating current impedance spectroscopy) interrogation, in which a low amplitude AC current is swept from high frequency to low frequency (10 MHz to 1Hz) through the conductive concrete and simultaneously impedance measurements are recorded.

This research is aimed at making conductive geopolymer and using it as a smart material for sensing stress related changes in conductivity. In the first Phase of the research, sample specimens were subjected to ACIS interrogation, while in the 2nd Phase a particular maximum frequency was selected from the obtained impedance charts for dynamic testing, in which conductive geopolymer samples were mechanically loaded and simultaneous resistivity changes were recorded. Specimens made from OPC were used as

comparison. To the best knowledge of the author, this is the first attempt to develop conductive geopolymer (CFRGC).

.

CHAPTER 3

EXPERIMENTAL EVALUATION OF ELECTROKINETIC COATING TREATMENT FOR CONCRETE PIPES

3.1 Introduction

This chapter contains the details of experimental design and procedure that was adopted for all the three Phases of electrokinetic coating treatment process. Mock concrete pipe specimens were used in Phases I and II, while for Phase III a 15" diameter commercial concrete pipe was used. Atomic Absorption Spectroscopy (AAS) analysis was performed on the samples to find the percentage of copper that penetrated into the concrete matrix.

3.2 Experimental Design and Procedure

The experimental work was conducted in three Phases. In Phases I and II, mock concrete pipe cylinder specimens were used to evaluate the coating effectiveness while in the Phase III, a 15" diameter commercially produced, steel reinforced pre-cast concrete pipe was electrokinetically coated. The mock cylindrical specimens were 12" in height and 6" in diameter, with a central void of 1.5" in diameter and 10" in depth. The concrete mix design for all the specimens consisted of Type II Portland cement with a water-cement ratio of 0.45, and 3/8" diameter coarse aggregate (Coarse to fine

aggregate ratio 1:1.08). A super plasticizer was added to mix at a ratio of 8 fl oz per 100 lbs of cement, to reduce the vibration force required to properly consolidate the specimens.

Commercially available plastic cylindrical molds (12" X 6") were used to prepare the specimens. The central void was formed by inserting a 1.5" diameter PVC tube into the center of the mold. The lower end of the insert was sealed using expandable foam to prevent fresh concrete from entering the cavity and was secured to the mold to prevent it from 'floating' during the casting of the concrete. The steel reinforcement consisted of fine gauge welded wire reinforcement fabric that served as both, transverse and longitudinal reinforcement. The mesh was cut into rectangular shapes of 11.5" X 12.56". The reinforcement fabric was then wrapped around four ¼" diameter threaded rods to form a cylinder 4" in diameter. Steel ties were used to secure the reinforcement fabric to the threaded rods. The threaded rods were 14" in length and served as a longitudinal reinforcement as well as the terminals for the power supply. Figure 3.1 shows a schematic diagram of a mock pipe specimen.
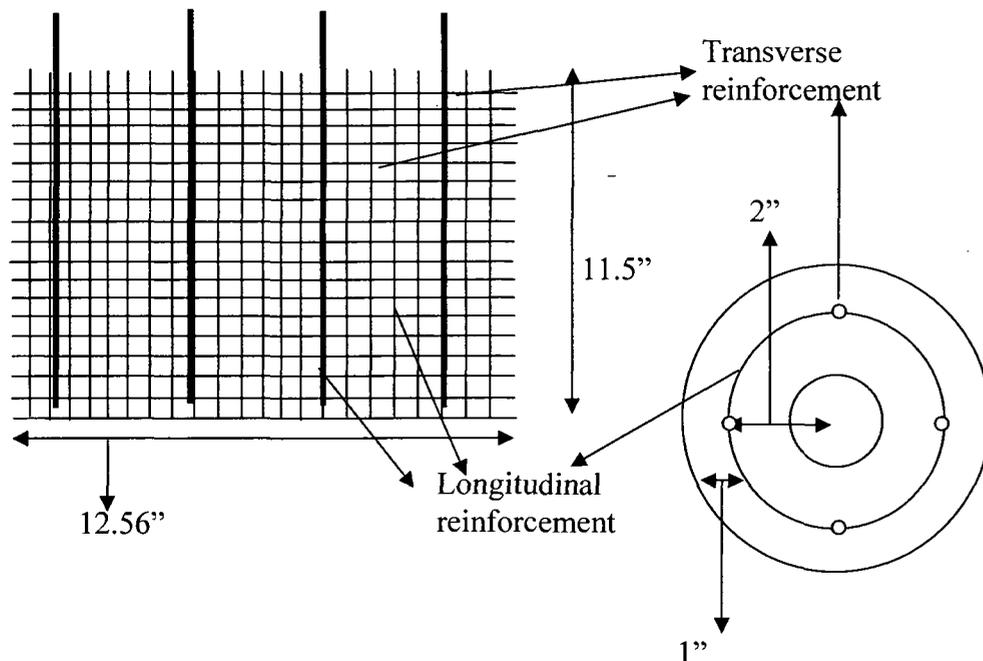
Figure 3.1 Schematic diagram of a mock pipe specimen.

The reinforcement cage was placed inside the cylindrical mold and fresh concrete was poured while the PVC insert was maintained at the center of the mold. The PVC insert was removed with care three hours following placement of the concrete. No breaking agents were applied to the PVC pipe inserts to avoid altering the surface characteristic of the specimens' inner wall. The specimens were allowed to cure in a water holding tank for a period of 28 days as per ASTM C 31. Following the curing period, the specimens were removed from the tank and air dried. The 28 days compressive strength of the batch was obtained by conducting a standard compression test on 3 solid cylinder specimens, resulting in an average compressive strength of 5456 psi (37.6 MPa).

3.2.1 Solution Preparation

The chemical solution used for cuprous oxide deposition was prepared partially based on work reported by Jongh et al. [75], which successfully electrodeposited Cu_2O - (cuprous oxide) on a transparent conducting substrate using an alkaline Cu (II) lactate solution. The pH of the solution was maintained between 8 and 9 so as to optimize the amount of cuprous oxide that can be electrodeposited. Forty five gm of Cu_2SO_4 (copper sulfate) were dissolved in 75 mL of lactic acid to obtain the copper lactate solution. Next, 225 mL of 5 M NaOH (sodium hydroxide) were added in a titration-like fashion to maintain the pH of the solution. The solution was stirred for 12 hrs prior to being poured into the void in the concrete specimens (See Figure 3.2).
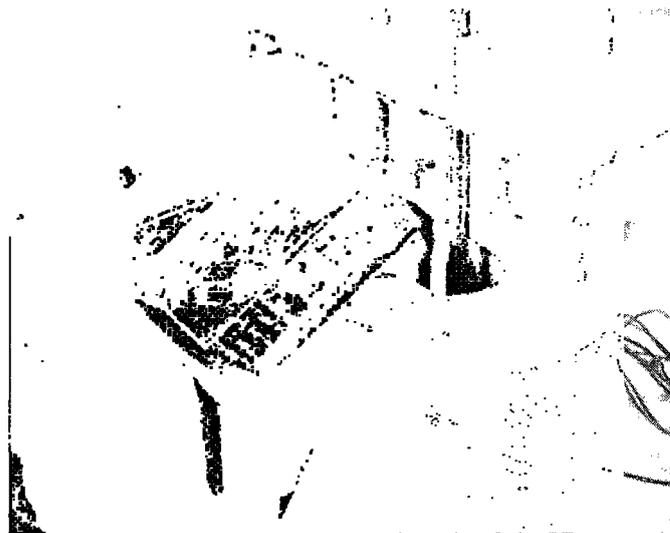
Figure 3.2 Copper lactate solution being poured into the specimen.

3.3 Phase I

In Phase I of the experimental work, a pilot study was performed to evaluate the effectiveness of the proposed coating procedure for the cases of undamaged, moderately deteriorated and severely deteriorated concrete pipes. Of the three specimens tested, one serves as a control (simulating a newly installed pipe); the second specimen was degraded to represent a partly corroded pipe (i.e., exposure of the coarse aggregates), while the third specimen was degraded to represent a moderate-to-severely corroded pipe (i.e., loss of coarse aggregates; random exposure of steel reinforcement). Degradation of the specimens was accomplished by filling the cavity in their centers with sulfuric acid solution (pH = 0.7), which was refreshed regularly until the desired effect was achieved. Following the degradation process, the specimens were rinsed with distilled water and drained several times repeatedly.

The electrokinetic process took place by applying 0.3 Amp (i.e., current density of $0.5mA/cm^2$) of current continuously over a period of 5 hrs. A copper rod was placed in the solution to serve as the anode, while the steel reinforcement served as the cathode (See Figure 3.3 for electrokinetic coating process for mock pipes). The time of application of the electrical current was selected as an initial estimate of the minimum needed application period for the electrokinetic process. Following the surface preparation treatment, the three specimens were electrokinetically coated using a cuprous oxide solution. Next, the solution remaining in each of the specimen was removed and the inner wall of the "pipe" exposed. Optical and chemical tests were undertaken to evaluate the effectiveness of the coating process in terms of the extent of penetration of the copper oxide particles into the hardened cement matrix and the concentration of the

heavy metal as a function of depth. Slices from the wall of each specimen were cut using a masonry diamond saw. The slices were inspected using an optical microscope (X 25) for the evidence of copper particles deposited in the binder matrix. Figure 3.4 presents selected snap shots from the microscopy examination. Copper depositions can be identified as green colored stains on the gray-white background of the hardened cement matrix. Figures 3.4 a and b display distinct green areas within the gray-white background typical for hardened Portland cement paste. These areas are suspected to be traces of copper oxide driven into the concrete matrix via the electrokinetics process. Figures 3.4 a & b were taken from the non-corroded and partially corroded specimens, respectively. In contrast, Figure 3.4 c displays a uniform gray color, with no traces of green stains. This result suggests that the copper oxide did not penetrate the severely corroded specimen during the electrokinetics process. A possible explanation is that exposing the reinforcement resulted in a "short-circuit" with the electrical current gradient flowing primarily to the partially exposed reinforcement rather than moving through the less conductive cementitious material.
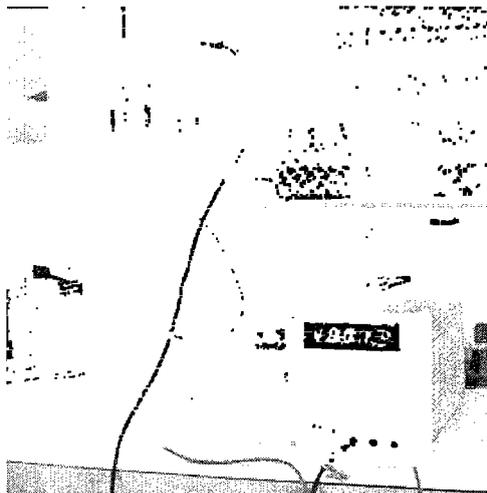
Figure 3.3 Electrokinetic coating process for mock concrete pipes.

25X   25X

(a)   **(b)**

(c)
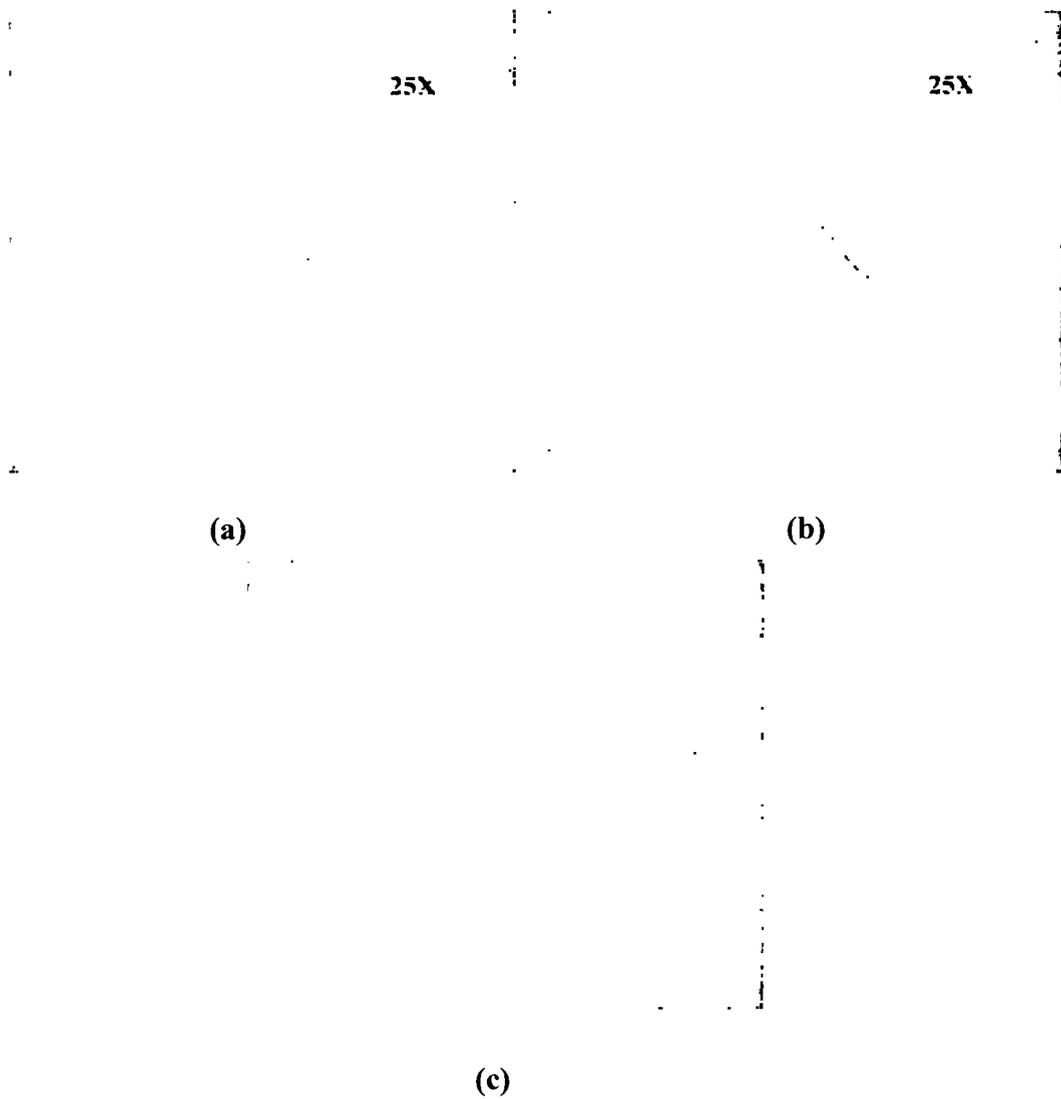
Figure 3.4 Optical microscopy images.

To confirm the hypothesis that copper oxide particles migrated into the concrete matrix, Atomic Absorption Spectroscopy (AAS) analysis was performed on the three specimens and on an untreated concrete specimen. Sample preparation and testing procedure for the AAS analysis are described in the next section, while the results of the AAS analysis are summarized in Table 3.1.

Table 3.1 Atomic absorption spectroscopy results from Phase I

Quantity Measured	Non-Corroded (Inner surface intact)	Partially Corroded (Coarse aggregate exposed)	Fully Corroded (Reinforcement exposed)	Untreated concrete sample ('black')
Absorbance	0.012	0.013	0.003	FAIL
Concentration of copper (ppm)	1.232	1.355	0.308	--
Amount of copper (μg)	308.008	338.809	77.002	--
Weight of cement dissolved (g)	1.398	0.528	0.867	0.912
Percentage of copper (by wt)	0.022	0.064	0.009	--

3.3.1 Sample Preparation and AAS Testing

Following the electrokinetic coating process, samples were taken from the inner wall of the mock concrete pipe for AAS Testing. Using a diamond saw, cubes approximately 0.08 in^3 each, were removed from the inner surface of the sliced concrete. Each sample was dried and weighed before it was placed in 100 ml of 98% concentrated Nitric acid. The solution was filtered through a 2.7 micron filter paper. The filtered solids (coarse and fine aggregate) were then dried and weighed (i.e. only the hardened cement binder was dissolved in the acid). By subtracting the weight of filtered solids from the original weight of the dissolved binder material, the weight of the dissolved cement matrix was obtained. The dissolved matrix material also contained the copper that penetrated into the concrete by the electrokinetic process. Distilled water was added to the filtrate to make it up to 250 ml standard solution for AAS Testing. GBC Avanta Atomic Absorption Spectrometer was used to measure the copper concentrations in the sample solutions. A calibration curve for known values of copper concentrations verses

the corresponding values of absorption was developed using the AAS unit. A slope intercept equation with intercept at the origin was fitted to this curve (See Figure 3.5). The concentration of copper in each of the test samples was calculated using this regression curve. Great care was taken in obtaining the weights of the samples and during solution preparations. A digital balance accurate to 0.001 g was used for weighing samples and pipettes with a precision of 0.001 ml were used for preparing the solutions.
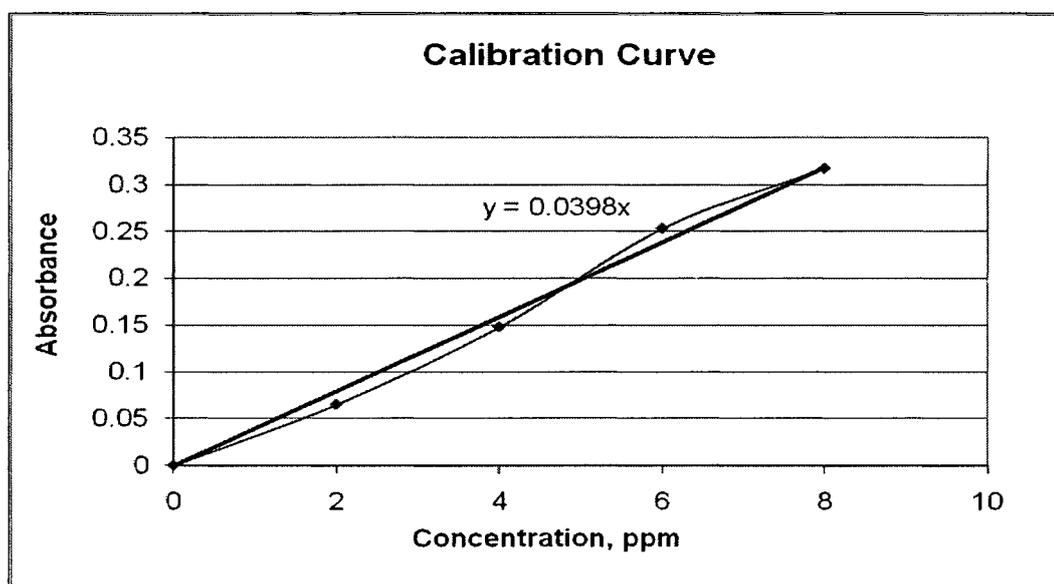
Figure 3.5 Calibration curve plotted using known concentrations of copper vs absorbance obtained from AAS.

3.4 Phase II

Results from Phase I suggest that the coating procedure is most effective on partially corroded concrete pipes. The authors attribute this effect to the larger surface area and reduced wall thickness from the degradation process that resulted in a lower resistance to the flow of electric current. The process was found to be not effective for fully corroded concrete pipes due to the exposed steel reinforcement "short-circuiting" the electric current. Background measurements conducted on untreated ('blank') concrete

samples revealed no traces of copper. Phase II of the study was aimed at optimizing the coating process for partially corroded and non-corroded concrete pipes. Six mock pipe specimens were electrokinetically coated, with three representing undamaged (i.e., non-corroded) pipes and three partially corroded concrete pipes (i.e. chemically degraded to expose the coarse aggregates). Degradation was achieved using 0.7 pH sulfuric acid. All six specimens were electrokinetically coated applying 0.3 Amp of current over a period of 8 hrs. Atomic Absorption Spectroscopy results from Phase II are summarized in Table 3.2. Each data point represents the average of three readings. It can be seen that by increasing the treatment time from 5 to 8 hours (60% increase), the amount of copper increased from 0.024% and 0.064% to 0.053% and 0.11% by weight of matrix digested for non-corroded and partially corroded specimens, respectively. Thus, a 60% increase in treatment time resulted in more than 100% increase in the amount of copper that was deposited in the concrete matrix. It could also be seen that the process is most effective in the case of partially corroded concrete, which presents the main application of the proposed technology.

Table 3.2 Atomic absorption spectroscopy results from Phase II

Quantity Measured	Non-Corroded (Inner surface intact)	Partially Corroded (Coarse aggregate exposed)
Absorbance	0.072	0.151
Concentration of copper (ppm)	2.654	5.580
Amount of copper (μg)	663.580	1,395.062
Weight of cement dissolved (g)	1.219	1.446
Percentage of copper (by wt)	0.053	0.111

3.5 Phase III

Results from Phase II confirmed that the process is most effective for partially corroded concrete pipes and time dependent as well, since the amounts of copper deposited within the hardened cement matrix were found to more than double when treatment time was extended from 5 to 8 hrs. In Phase III, the specimen used was a commercially manufactured, steel reinforced, pre-cast concrete pipe with an internal diameter of 15", an external diameter of 18", and a length of 36". The concrete cover over the reinforcement (measured from the inner wall of the pipe) was 38 mm thick. The pipe was made to stand upright on a wooden base frame for ease of access. To minimize the amount of chemical solution used in the coating process, an annulus space was created by placing a tin metal sheet inside the concrete pipe. A tin metal sheet was folded to form a 13" diameter inner tube, which was coated with fiber glass on its outside surface to enhance its resistance to buckling as well as to improve its chemical resistance (See Figure 3.6 a). The bottom of the experimental setup was also coated with epoxy to prevent leakage of the chemical solution (See Figure 3.6 b). Following the fiber glass coating, the tin tube was placed and fixed inside the concrete pipe. A drain was installed at the bottom of the experimental setup to drain the chemicals at the end of the test (See figure 3.6 for electrokinetic coating procedure employed for commercial concrete pipe).

(a)

(b)

(c)
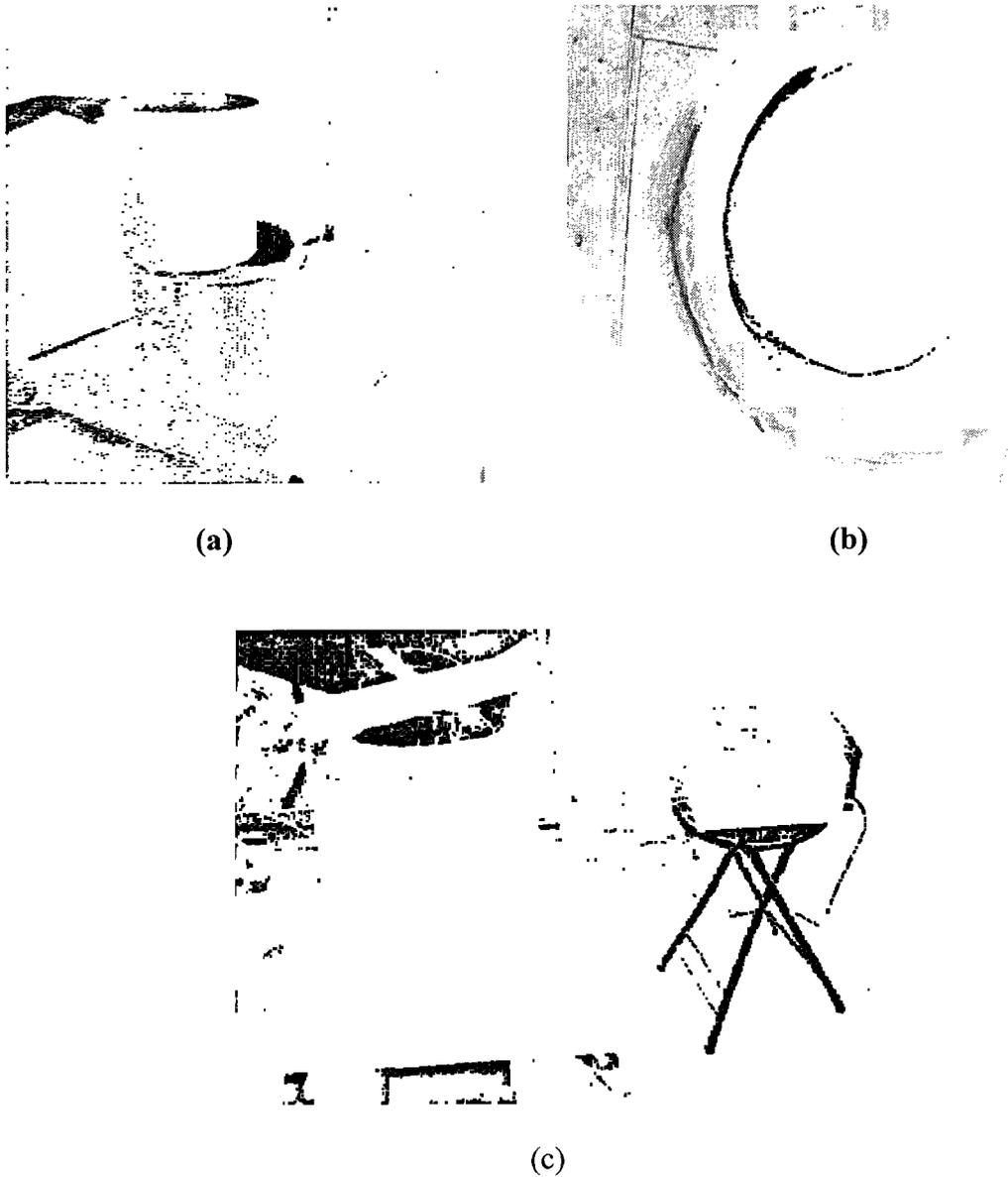
Figure 3.6 Experimental setup for electrokinetic coating on commercial concrete pipe.

Partial degradation of the inner surface of the concrete pipe was achieved using 0.5 pH sulfuric acid. Following the degradation process, the annulus space was rinsed with distilled water and drained several times, repeatedly. The space was then filled with copper lactate solution to a depth of 15", and two copper rods were placed opposite to each other to serve as anodes, while the steel reinforcement in the concrete pipe acted as

cathode. The electrokinetic coating process took place by applying a current of 6.5 Amp (i.e., current density of $0.5mA/cm^2$) for a period of 8 hrs. Following the coating process, samples were obtained by core drilling the pipe in three locations (top, middle and bottom). The samples were then prepared for AAS analysis following the procedure described earlier in the chapter. The results obtained from the AAS test on the commercial concrete pipe are summarized in Table 3.3. Each data point in the table represents the average of three independent measurements.

Table 3.3 AAS results of partially degraded pre-cast concrete pipe

Quantity Measured	Partially Corroded Concrete Pipe (Coarse aggregate exposed)
Absorbance	0.202
Concentration of copper (ppm)	5.084
Amount of copper (μg)	1,270.938
Weight of cement dissolved (g)	1.379
Percentage of copper (by wt)	0.111

3.6 Summary

Results from Phase I confirmed the feasibility of depositing copper ions inside hardened concrete paste using electrokinetics. Images from optical microscopy revealed what appeared to be copper oxide inside the hardened cement matrix that can be seen as green stains on a graish-white background in the case of new and partially deteriorated mock pipe specimens. No color traces of copper were observed for the fully deteriorated specimen, leading to the conclusion that little, if any, copper had penetrated the concrete. A possible explanation is the development of a "short-circuit" via the exposed reinforcement mesh that came into contact with the copper lactate solution. An atomic absorption spectroscopy analysis suggested that copper was deposited in the concrete

matrix of all three specimens. However, in the case of the undamaged and partially deteriorated specimens, the percentage of copper was considerably higher than for the fully-deteriorate specimen. Phase II results revealed that the coating procedure is most effective for partially deteriorated concrete pipes. Possible explanations are the larger surface area due to the degradation process and reduced wall thickness resulting in a higher concentration per unit volume between the pipe surface and the reinforcement cage. The effectiveness of the process was also found to be time dependent (i.e., the percentage of copper being deposited is a function of time of application of the coating procedure). Reviewing the AAS test results for all the partially corroded specimens (See Table 3.4), it could be seen that the average concentration of copper measured for the case of a full scale commercial pipe treated for 8 hrs was very similar to that measured for the partially degraded mock specimens treated for the same duration, thus providing a level of confidence in the validity of the results obtained from the bench-scale tests in Phase I and II.

Table 3.4 Comparison of results obtained from 5 hr and 8 hrs Electrokinetic coating on corroded specimens

Quantity Measured	5 hour Test on Mock Pipe	8 hour Test on Mock Pipe	8 hour Test on Commercial Pipe
Absorbance	0.013	0.151	0.202
Concentration of copper (ppm)	1.355	5.580	5.084
Amount of copper (μg)	338.809	1,395.062	1,270.938
Weight of cement dissolved (g)	0.528	1.446	1.379
Percentage of copper (by wt)	0.064	0.111	0.111

CHAPTER 4

EXPERIMENTAL EVALUATION OF
CONDUCTIVE GEOPOLYMER
FOR HEALTH MONITORING
APPLICATIONS

4.1 Introduction

Chapter 4 describes the experimental design and procedure used to evaluate the electrical conduction properties of both Portland cement and Geopolymer mortar and concrete with and without fibers. The experimental procedure is divided into three Phases. In Phase I, mortar specimens were used to evaluate the percentage effect of fiber present in the cementitious material on the electrical conduction of the matrix. Phase II and III utilized concrete specimens using the maximum beneficial fiber percentage determined from the results of Phase I. In Phase II, effect of curing time on electrical conduction of cementitious material was evaluated, and in Phase III, dynamic testing was performed on the concrete specimens and stress related conductivity measurements were recorded. The chapter concludes with a summary of the results and observations from the three Phases.

4.2 Experimental Design for Phase I

In Phase I of the experimental procedure, rectangular bar specimens 1" x 1" x 11" of both Portland cement and geopolymer mortar were prepared (See Figure 4.1). Portland

cement of Type II was used in making cement mortar specimens with a water cement ratio of 0.4 and sand to cement ratio of 1.0. Whereas, in geopolymer specimens a commercial fly ash (FA) from Ohio was used. The particle size distribution and chemical analysis of FA used are listed in Tables 4.1 & 4.2 (more than 80% of the particles were smaller than 45 μm).
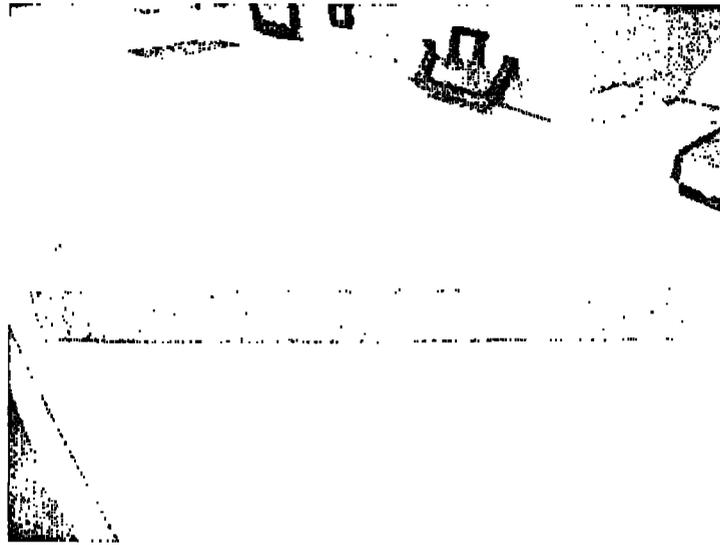
Figure 4.1 A rectangular bar specimen with embedded steel electrodes.

Table 4.1 Particle size distribution of fly ash stockpile

Size(um)	Percent Passing
10.00	43.41
20.00	64.27
30.00	76.49
40.00	82.99
45.00	85.71
50.00	88.54
60.00	93.74
70.00	97.40
80.00	99.24
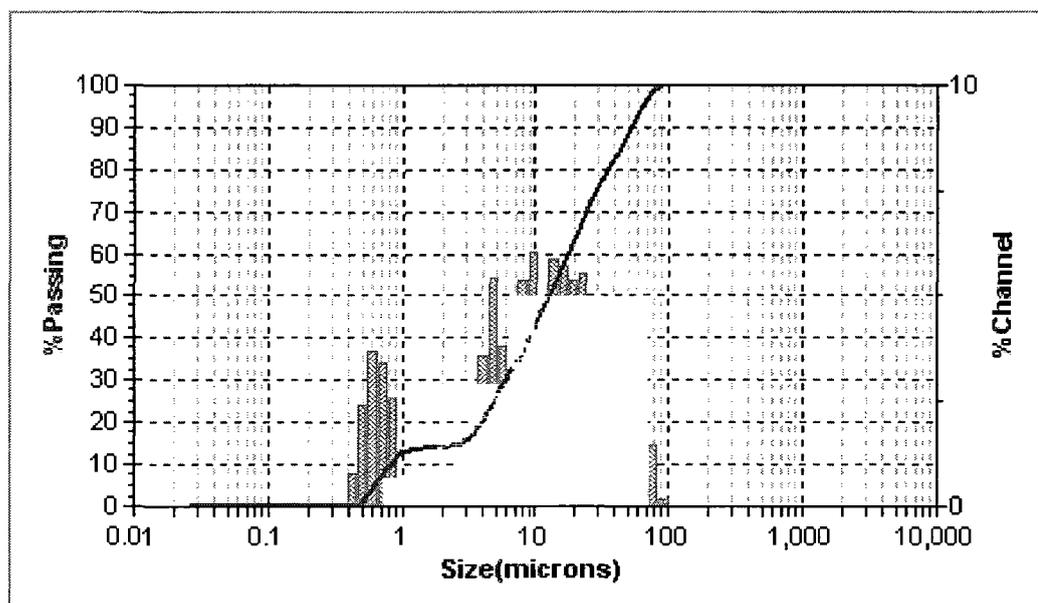
Figure 4.2 Particle size distribution for fly ash stockpile.

Table 4.2 Chemical composition of fly ash stockpile

Chemical analysis of FA, wt %	
Silicon Dioxide, SiO$_2$	55.07
Aluminum Oxide, AL$_2$O$_3$	28.61
Iron Oxide, Fe$_2$O$_3$	6.22
Calcium Oxide, CaO	1.97
Magnesium Oxide, MgO	1.08
Sodium Oxide, Na$_2$O	0.38
Potassium Oxide, K$_2$O	2.63
Titanium Oxide, TiO$_2$	1.56
Manganese Dioxide, MnO$_2$	0.02
Phosphorus Pentoxide, P$_2$O$_5$	0.16
Strontium Oxide, SrO	0.08
Barium Oxide, BaO	0.21
Sulfur Trioxide, SO$_3$	0.19
Total	98.18
Loss on Ignition	1.82

For making geopolymer specimens, a 2:1 combination of sodium silicate to sodium hydroxide were used as the liquid phase materials, with an activator to source

material (FA) ratio of 0.5 and sand to cementitious material (FA) ratio of 1.0. The sodium

hydroxide used was 10 M (400 gm of sodium hydroxide mixed in 1 L of water), prepared

in the laboratory by dissolving sodium hydroxide pellets in distilled water. The sodium

silicate used was a Type N commercial grade product obtained from PQ_{INC}. To induce

conductivity through the cementitious matrix, carbon fibers were added while mixing.

Fibers were provided by TAHO TANEX and their properties are shown in Table 4.3.

Stainless steel plates 0.4" x 1.38" x 0.015" served as electrical contacts in the specimens.

The two steel electrodes were embedded in the bar specimens while placing the fresh

cementitious material in the molds. Rheobuild super plasticizer 2% by weight of

cementitious material was added while mixing to increase the workability, and methyl

cellulose of 0.4% by weight of cementitious was added to increase the fiber dispersion

throughout the cementitious material. Following specimen preparation and an adequate

curing period, impedance measurements were conducted to evaluate the effect fiber

percentage or the bulk resistivity of the cementitious matrix.

Table 4.3 Properties and dimensions of carbon fiber used

Length, mm	Diameter, μm	Tensile Strength, Ksi	Tensile Modulus, Msi	Resistivity, $\mu\Omega$-cm	Density, lb/in^3
6	7	500	30	1,670	0.065

4.2.1 Preparation of the Specimens

To evaluate the effect of the fiber addition on the electrical conductivity of the

cementitious composite, fiber percentage was varied from 0 to 0.8% by weight of

cementitous material in both cases (OPC and geopolymer). A set of three specimens were

prepared for each fiber percentage fraction (See Table 4.4 for number of specimens

prepared). During mixing, the cementitious material and sand were mixed first for a minute, and then fibers and methylcellulose were added and mixed for two additional minutes. The liquid phase material and super plasticizer were added slowly while mixing immediately following the addition of the fibers. Upon mixing, the mortar was then taken out of the mixer and placed in bar molds in layers. Each layer was tamped and steel electrodes were embedded in the specimens. Specimens were left in the molds to set for one day, before they were taken out of the molds for curing. Portland cement specimens were cured in lime water for 3 days while geopolymer specimens were placed in an oven at 60°C for 24 hours to achieve complete curing.

Table 4.4 No. of specimens prepared for Phase I experiments

Fiber percentage WRT cementitious material	No. of cement specimens (W/C = 0.4, S/C = 1)	No. of geopolymer specimens (A/S = 0.5, S/C = 1)
0	3	3
0.008	3	3
0.02	3	3
0.04	3	3
0.06	3	3
0.08	3	3
0.2	3	3
0.4	3	3
0.6	3	3
0.8	3	3
Total	30	30

4.2.2 Experimental Procedure

Following the curing process, cement specimens were taken out of the water and surface dried while the geopolymer specimens were left outside the oven for at least 2 hrs to attain room temperature before performing conductivity measurements. High

frequency alternating current (AC) was used to perform electrical measurements on fiber reinforced cementitious materials, even though AC measuring equipment is more costly compared with direct current (DC) measuring devices. The reasons for choosing high frequency AC over DC was to avoid problems of false potential (or polarization potential) and to exploit the frequency dependent behavior exhibited by carbon fibers in the cementitious matrices (See Section 2.3.9). At high frequency AC carbon fibers start conducting (they lay inert when low frequency AC or DC currents are applied) and the value of the imaginary impedance (X_c), due to capacitance, approaches zero with increased frequency, so the impedance measured using high frequency AC is the true impedance of the conducting material without deleterious effects due to polarization potential. However, using very high frequency AC causes the current to flow through the outer surface of the material instead of flowing through its cross section (also known as "skin effect"). In order to find appropriate maximum frequency at which fibers in the matrix are fully conductive while keeping the skin effect and imaginary impedance minimum, AC impedance spectroscopy is employed. AC-IS contained a potentiostat in conjunction with an impedance analyzer, potentiostat provided the necessary voltage while impedance measurements are recorded by the impedance analyzer. Bode plots (magnitude of impedance Vs frequency and phase Vs frequency) generated by AC-IS were used to analyze the results. Impedance measurements on all the specimens were conducted using 1V voltage amplitude while the frequency was swept from 10 MHz to 1 Hz. Two measurements were recorded for each specimen i.e. a total of six readings for each fiber fraction.

4.2.3 <u>Analysis of AC-IS Results</u>

Bode plots consists of two different plots, one magnitude of impedance Vs frequency and the other phase Vs frequency. In magnitude of impedance and frequency plot, the X axis is representing the frequency (logarithmic scale) while the Y axis representing the magnitude of impedance. In data sets, as frequency of the current increases from left to right, the value of impedance decreased. However, above certain frequency (Ft), the value of impedance drops rapidly, likely due to the skin effect (See Figure 4.3). That is, above the threshold frequency (Ft), the current instead of flowing through the cross sectional area of the specimen chooses to flow only through a zone around the perimeter of the sample, and with the increasing frequency, this zone decreases and reaches a minimum at very high frequency (i.e. skin effect See Figure 4.4). Skin effect causes the magnitude of impedance to drop fast, making the specimen appear to be a superconductor at very high frequency. This appearance is, of course, not true since the current is flowing only through the skin of the specimen not through its entire cross sectional area. Therefore, in all the cases, Ft was chosen as the maximum allowable frequency for the impedance measurements, while impedance readings above Ft were discarded. In each measurement, the value of impedance at frequency Ft is considered as the total impedance of the composite (i.e. including fiber contribution).
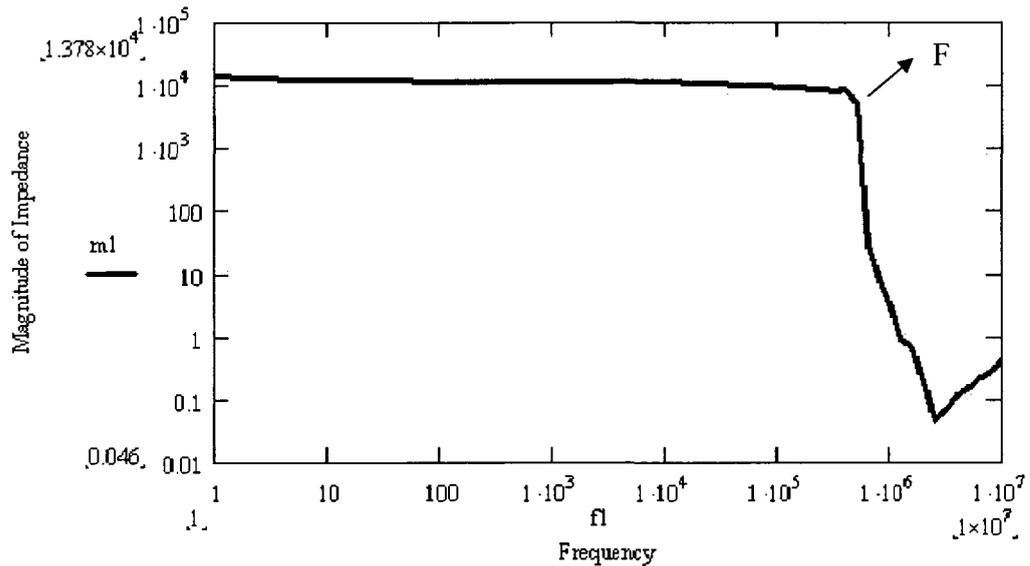
Figure 4.3 Magnitude of impedance Vs frequency plot.

Ft

Increasing frequency
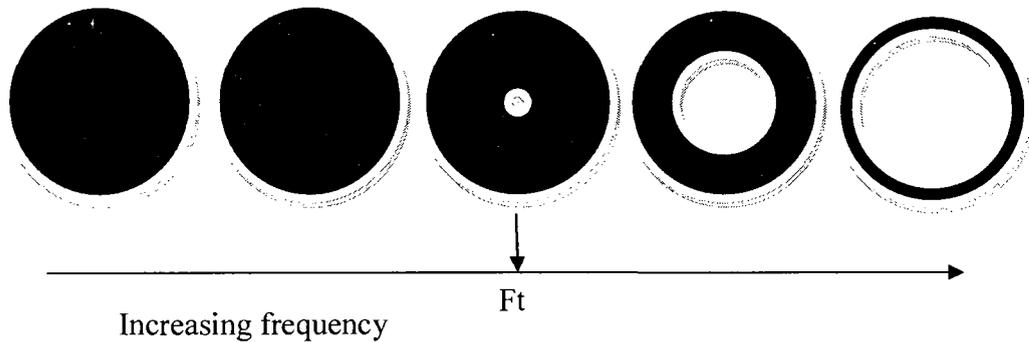
Figure 4.4 Illustration of skin effect.

4.2.4 Sample of Data Interpretation

Section 4.2.4 presents a comparison of Bode plots for Portland cement with and without fibers. Figure 4.5 represents magnitude and phase plots versus frequency of Portland cement specimens without fiber; whereas, Figure 4.6 represents the same information for Portland cement grout with 0.8% fibers by weight of cement. In both cases, the impedance dropped rapidly after Ft. However, the value of impedance remains almost unchanged prior to reaching Ft in case of cement without any fibers (See Figure

4.5 a); whereas, in case of cement with fibers, the impedance value drops slowly and reaches a minimum at Ft. This intermediate drop of impedance in case of Portland cement with fibers is due to the contribution of the fibers to the electrical conduction of the material. At low frequencies, fibers in the matrix would not contribute towards electrical conduction due to polarization of the double layer around them until certain frequency is reached above which the double layer breaks down and the fibers start conducting (See Figure 4.6a). Therefore, the value of impedance at Ft is considered the true impedance of the composite material.

Frequency dependent behavior of the imaginary impedance could be observed in the phase plots where X axis represents the frequency (logarithmic scale), and the Y axis represents phase between voltage and current. At low frequencies, the voltage and current are in the same phase, but as the frequency increases above Ft, there is a shift in the phase. A change in phase between voltage and current indicates capacitance or inductance in the circuit. A positive shift in the phase indicates inductance and a negative shift is due to capacitance. The shift in phase is observed only above the frequency Ft, implying that impedance measurements conducted at frequency Ft are pure impedances of the material, free of imaginary impedance (capacitance and inductance).

1.378×10^4

$1 \cdot 10^5$

$1 \cdot 10^4$

$1 \cdot 10^3$

100

10

1

0.1

0.046 0.01

Magnitude of Impedance

m1

Ft

1 10 100 $1 \cdot 10^3$ $1 \cdot 10^4$ $1 \cdot 10^5$ $1 \cdot 10^6$ $1 \cdot 10^7$

$.1$ fl 1×10^7

Frequency

(a)

$.172$ 200

100

0

-100

$- 131.56$ -200

Phase

p1 − 1

Ft

1 10 100 $1 \cdot 10^3$ $1 \cdot 10^4$ $1 \cdot 10^5$ $1 \cdot 10^6$ $1 \cdot 10^7$

$.1$ fl 1×10^7

Frequency
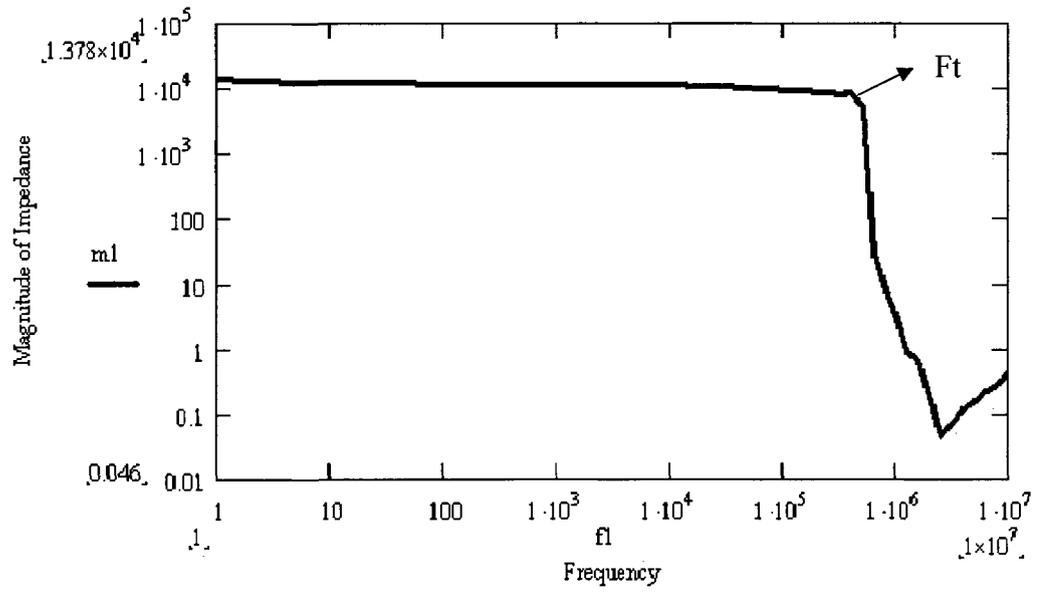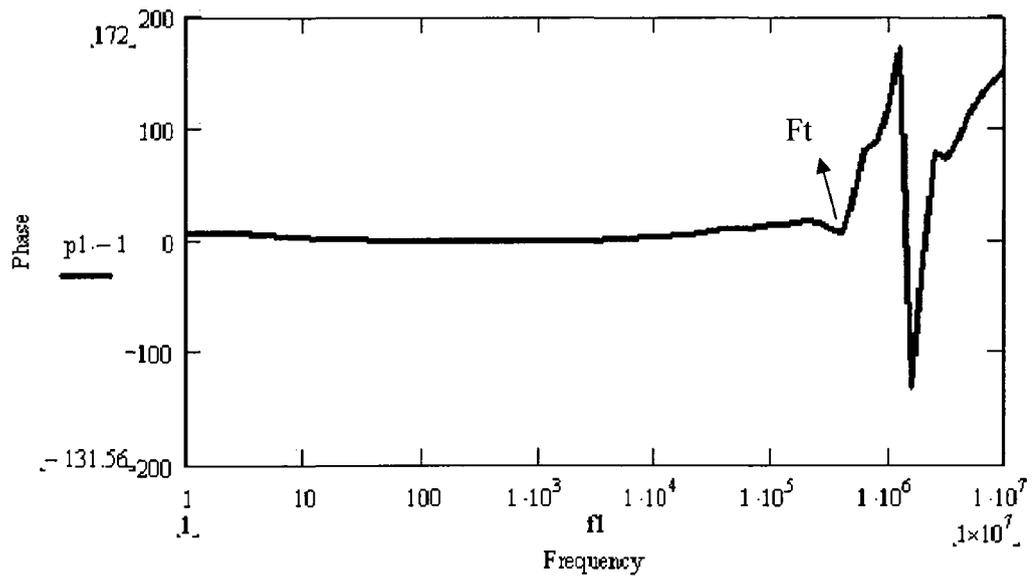
(b)

Figure 4.5 Bode plots for Portland cement mortar without fibers.
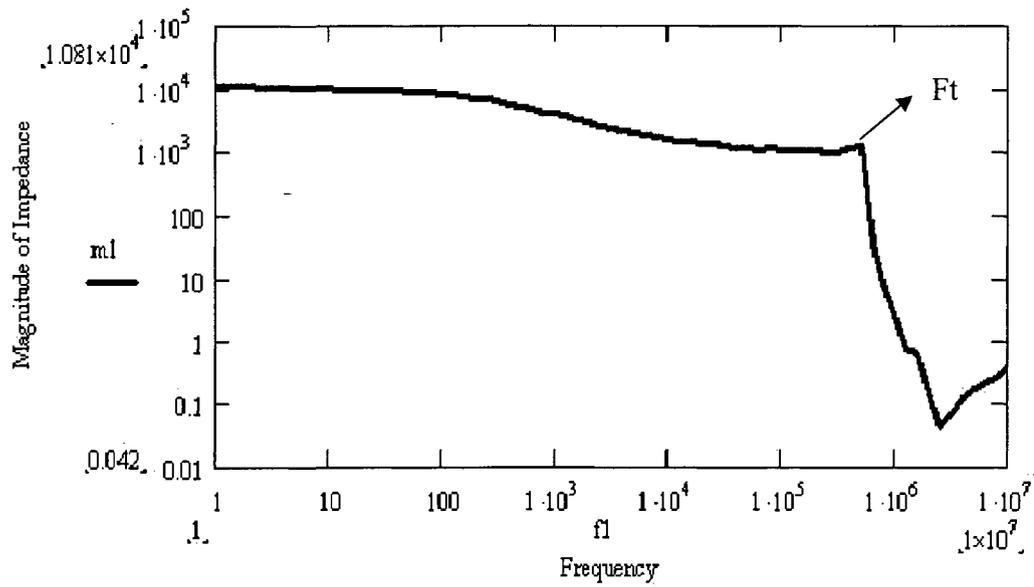
(a)
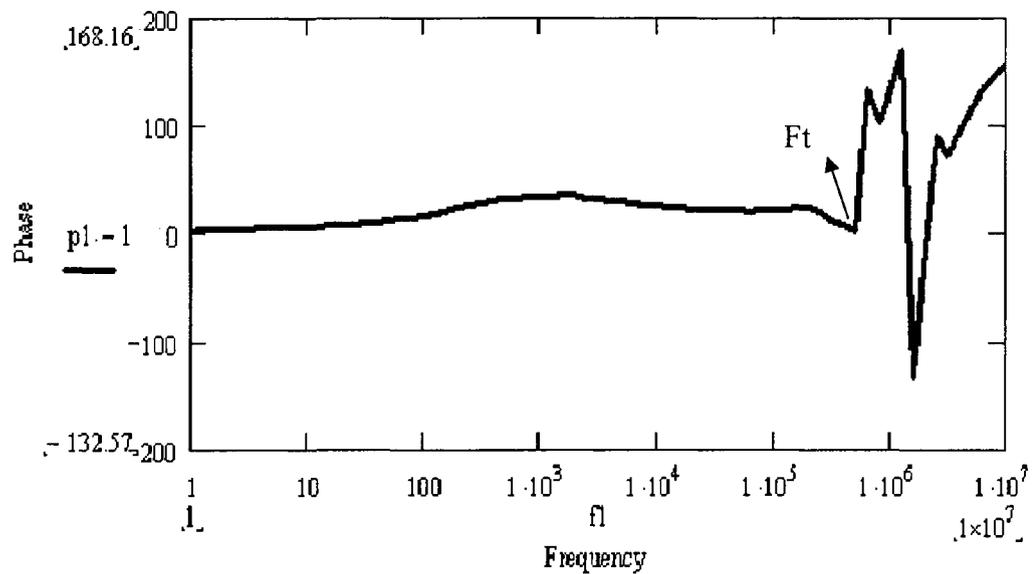
(b)

Figure 4.6 Bode plots for Portland cement mortar with 0.8% fibers WRT cement

4.2.5 Results from Phase I

AC-IS was performed on all Portland cement and geopolymer mortar specimens, and the value of impedance was calculated at frequencies Ft in each case as explained in

Section 4.2.4. The results obtained from Phase I are summarized in Tables 4.5 and 4.6 while Figures 4.7 a and b represent the resistivity of Portland cement and geopolymer mortar with respect to changes in fiber fraction. In both the plots, X axis represents fiber percentage and Y axis the resistivity of the samples (Ohms-in). Electrical resistivity of the sample is calculated by using the following equation (See Eq. 4.1)

$$\rho = \frac{(R * A)}{L},$$

(4.1)

where, ρ = Resistivity (Ohm – in),

R = real impedance obtained from bode plots (Ohms),

A = Embedded cross sectional area of electrode (Sq. in),

L = Length between the electrodes (in).

The separation length between the electrodes and the cross sectional areas of the embedded electrodes for all specimens were 10 in and 0.4 in^2, respectively. The value of real impedance (R) for each point on the plot is an average of six readings per fiber percentage (a set of two readings per specimen and three specimens per fiber percentage) obtained at threshold frequency Ft.

(a)

(b)
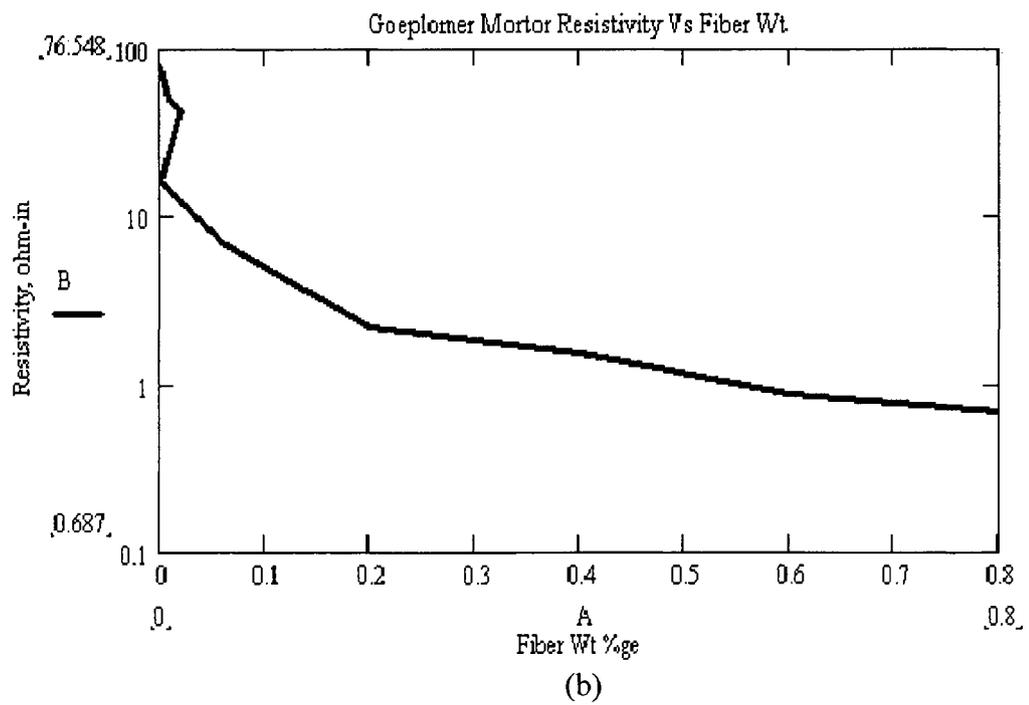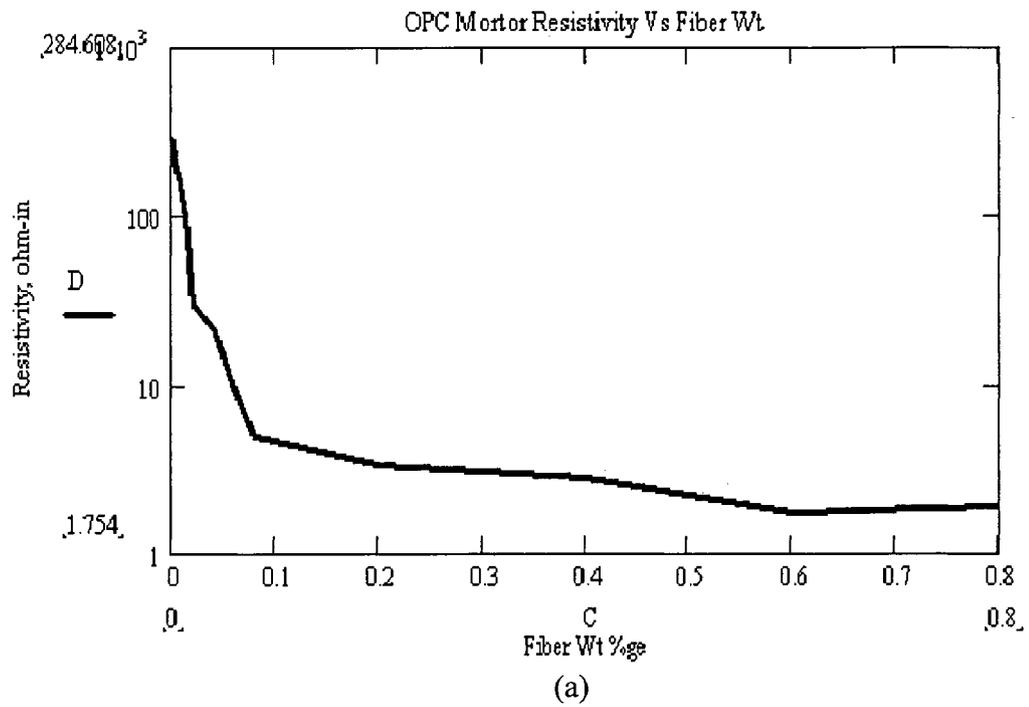
Figure 4.7 Resistivity of mortar specimens WRT fiber percentage

Table 4.5 Summary of results obtained for Portland cement specimens

Percentage of fiber WRT Portland cement	Electrical resistance, ohms	Electrical resistivity, ohms-in
0.000	7115.20	284.61
0.008	3912.63	156.51
0.02	741.40	29.66
0.04	545.38	21.82
0.06	237.73	9.51
0.08	123.28	4.93
0.20	84.49	3.38
0.40	70.36	2.81
0.60	43.85	1.75
0.80	47.93	1.92

Table 4.6 Summary of results obtained for geopolymer specimens

Percentage of fiber WRT Fly ash	Electrical resistance, ohms	Electrical resistivity, ohms-in
0	1913.70	76.55
0.008	1249.30	49.97
0.02	1083.70	43.35
0.04	400.63	16.03
0.06	176.03	7.04
0.08	143.53	5.74
0.20	54.90	2.20
0.40	38.57	1.54
0.60	21.81	0.87
0.80	17.18	0.69

4.2.6 <u>Analysis of Results from Phase I</u>

A review of the results obtained from Phase I reveals that in both cases (OPC and Geopolymer), resistivity decreased with increase in fiber percentage (as expected). In case of Geopolymer specimens without any fibers, resistivity measured was 77 ohm-in after one day of curing at 60 °C, and for Portland cement specimens it was 285 ohm-in after curing them in lime water for 3 days. Portland cement after 3 days is not fully cured; there is still water present inside the cementitious gel that contributes towards electrical conductivity (specimens were only surface dry). Whereas, geopolymer specimens are fully cured after one day at 60 °C. With full curing and little to no free water presence geopolymer specimens exhibited less resistivity compared with their Portland cement counter parts. This effect suggests that geopolymer could serve as a better candidate when used as a conductive material.

4.3 <u>Phase II</u>

In Phase II, to test the hypothesis that conductivity could also be induced into concrete, concrete cylinders were casted from both Portland cement (OPC) and geopolymer (GPC), with and without carbon fibers. AC-IS analysis was performed on all the specimens to obtain the electrical impedance. Testing was performed after one day of curing at 60°C for geopolymer specimens; whereas, concrete specimen were tested after 7, 14 and 21 days to see the effect of the curing period on electrical conduction. The pilot study conducted on mortar specimens provided a basis for selecting the proper combination of fiber percentage ratio and liquid to source material ratio, in order to achieve the needed workability for making the specimens.

4.3.1 <u>Experimental Design</u>

For making concrete samples, 4" x 8" plastic cylinder molds were used. Portland cement of Type II with water cement ratio of 0.4 and 1:2:2 ratio of cement to sand to aggregate was used in making the OPC concrete specimens. As for geopolymer specimens, the Ohio fly ash whose properties are listed in Table 4.2 was used with an activator to source material ratio of 0.5 and fly ash to sand to aggregate ratio of 1:2:2 ratio. Pea gravel (3/8") was used as coarse aggregate in making concrete samples from both Portland cement and geopolymer. The activator solution for making geopolymer consisted of 2:1 ratio of sodium silicate to sodium hydroxide. A set of six concrete cylinders were poured for Portland cement and geopolymer, three with embedded carbon fibers (See Table 4.3 for properties) and three plain (control) specimens. Two stainless steel electrodes 0.4" x 4" x 0.015" served as the electrical contacts inside the specimens. Prior to pouring, the concrete the steel electrodes were inserted into the plastic cylinder mold by making inserts at its top & bottom. The separation distance between the two electrodes was 7". Rheobuild super plasticizer 2% by weight of cementitious material was added while mixing to increase workability and methyl cellulose of 0.4% by weight of cementitious was added to increase the fiber dispersion (See Figure 4.8 for specimen).
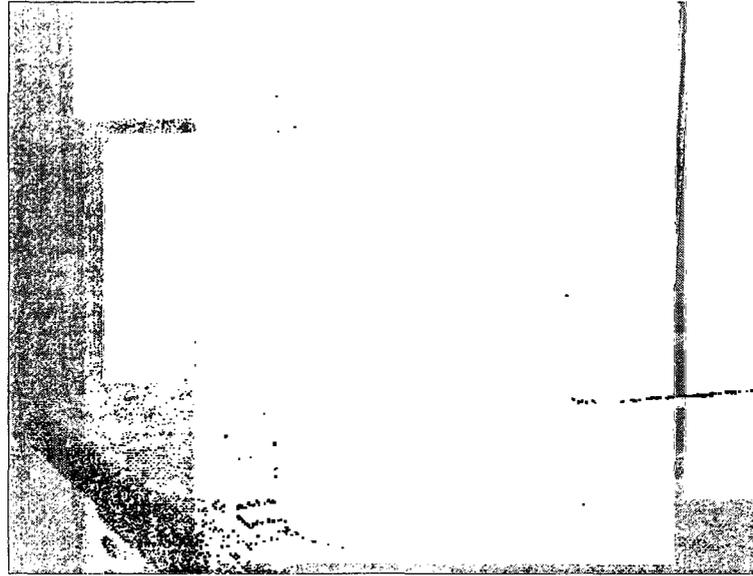
Figure 4.8 A concrete cylinder specimen with embedded steel electrodes.

4.3.2 Preparation of Concrete Specimens

From the study conducted in Phase I, it was decided that fiber content of 0.4% by weight of cementitious material would be appropriate for making concrete samples. During mixing, the coarse aggregate and sand were mixed for a minute and then cementitious material was added and mixed for another minute. Next, the fibers and methylcellulose were added and mixed for 2 minutes, followed by the liquid phase material and super plasticizer that were added while the mixing continued for the final two minutes. The fresh concrete was then taken out of the mixer and placed in plastic cylinder molds in three layers, tamping each layer. Care was taken not disturb steel electrodes in the molds. Specimens were left in the molds to set for one day before de-molding. OPC specimens were placed in lime water bath for curing while the geopolymer specimens were cured at 60°C for 24 hours in an oven.

4.3.3 Experimental procedure

Following the curing process, cement specimens were taken out of the water and surface dried while geopolymer specimen were left outside the oven for at least 2 hrs to attain room temperature before performing conductivity measurements. AC-IS analysis was performed on all geopolymer specimens after one day of curing, while in case of OPC concrete, testing was performed on specimens after 7, 14 and 21 days of curing. Bode plots (magnitude of impedance Vs frequency and phase Vs frequency) generated by AC-IS were used to analyze the results. The impedance measurements on all the specimens were conducted using 1 volt voltage amplitude while the frequency was swept from 10 MHz to 1 Hz.

4.4.4 Analysis of Results

Below are the results obtained from AC-IS analysis for all the specimens, Table 4.7 summarizes the resistivity values for Portland cement concrete, while Table 4.8 summarizes the test data collected for geopolymer concrete. Each resistivity value in the tables is an average of six readings. Resistivity was calculated using Eq. 4.1, where R is the real impedance obtained from AC-IS at frequency Ft for each sample, and, A is the embedded cross sectional area (1.2 in^2) and L is the separation length between the electrodes (7").

Table 4.7 Summary of results obtained from Phase II testing on OPC

Curing period	Electrical Resistance of OPC (Ohms)		Electrical Resistivity of OPC (Ohm-in)	
	0% by wt fibers	0.4 % by wt fibers	0% by wt fibers	0.4 % by wt fibers
7 days	1259.37	533.15	216.61	91.70
14 days	1450.84	631.58	249.54	108.63
21 days	1404.82	657.75	250.23	110.55

Table 4.8 Summary of results obtained from Phase II testing on GPC

Curing period	Electrical Resistance of GPC (Ohms)		Electrical Resistivity of GPC(Ohm-in)	
	0% by wt fibers	0.4 % by wt fibers	0% by wt fibers	0.4 % by wt fibers
24 hrs @ 60°C	486.98	157.91	83.76	27.16

The data reveal that the conductivity of both OPC and GPC has improved by the addition of carbon fibers. This change in conductivity proves the hypothesis that conductivity can also be induced into the concrete and presence of aggregate would not affect it. From the OPC results, it could be inferred that curing of cement does have a detrimental effect on electrical conductivity during early stages, but this effect will slowly wear off as the curing continues. It is expected that as curing becomes substantially complete, the electrical conductivity of the specimen stabilizes.

AC-IS testing on all the OPC samples were performed shortly after taking them out of the lime water and surface drying them. To isolate the effect of water content on the electrical conductivity, three OPC samples with 0.4% fibers were tested after 28 in lime water and 7 days of open air drying. The average electrical resistivity obtained on these samples was 411.5 Ohm-in (Table 4.9).

Table 4.9 Results obtained for OPC after 28 days of curing

Curing period	Electrical Resistance of OPC with 0.4% fibers (Ohm-in)	Electrical Resistivity of OPC with 0.4% fibers (Ohm-in)
28 days in water & 1 week open air	2392.53	411.51

By comparing the results in Tables 4.7 and 4.9, it can be observed that the resistivity measured for air dry OPC samples with 0.4% fibers is significantly higher than that measured for surface dry OPC without any fibers. This increase in resistance shows that the electrical resistivity in OPC is highly dependent on the water content of the matrix. On the other hand, GPC samples containing no free water exhibit significantly lower electrical resistivity compared with OPC specimens, for the case of no-fibers presence and entrained fibers. Keeping this in mind, only GPC samples were chosen for Phase III (dynamic testing), as the practicality of using OPC for health monitoring was put to question by the high variability with moisture content.

4.5 Phase III

A set of three geopolymer concrete cylinders and two beams with carbon fiber ratio of 0.4% by wt of fly ash were prepared. Compressive load was applied onto the cylinders while the beams were centrally loaded to observe the changes in stress related electrical resistivity in the GPC specimens. Electrical resistance strain gages were bonded onto the surface of GPC specimens to keep track of changes in stress related strain.

4.5.1 Experimental Design

For making GPC beam specimens, 4" x 4" x 16" steel molds were used and for cylinder specimens 4" X 8" plastic cylinder molds were used. The same mix design and

preparation techniques that were used for making samples in Phase II were employed to prepare geopolymer concrete specimens (See Section 4.3 for mix design). A 24 gage thin copper wire was used the electrical contact. The wire was tightly wound around the specimens in two separate locations. On the beam, the separation distance between the two electrodes (copper wire wounds) was 8" and on the cylinder it was 6". Conductive silver paste was applied on to the copper wire wounding to improve the contact between the concrete surface and copper wire electrode. Electrical resistance strain gages were used to measure the changes in strain under the applied load. The gages were applied in the direction of load for cylinders and in the tensile region for the beams. The length of the strain gages used was 2" for beams and 1" for the cylinders. The strain gages were connected to a DAQ HP 3479A data acquisition unit to collect the strain data. A servo-controlled MTS machine (load and displacement control) was used to apply the flexure load on the beams and axial compressive load on the cylinders. Frequency/arbitrary wave form generator (HP33120A) was used as the power source with Tektronix 2430A digital oscilloscope to collect voltage and current data. The digital oscilloscope utilized a generic voltage probe to measure the voltage data while a Tektronix A6303 current probe was used to measure variations in current. The current probe was used in conjunction with a Tektronix TM502A current amplifier.

4.5.2 Experimental Procedure

After the preparation and curing of the specimens, AC-IS analysis was performed to determine the appropriate frequency (Ft) for dynamic testing. Based on the AC-IS results, it was inferred that a frequency of 795 KHz would be appropriate for the dynamic

testing (See Figure 4.9). Figure 4.9 represents the magnitude of impedance versus

frequency plot for the conductive geopolymer concrete beam.
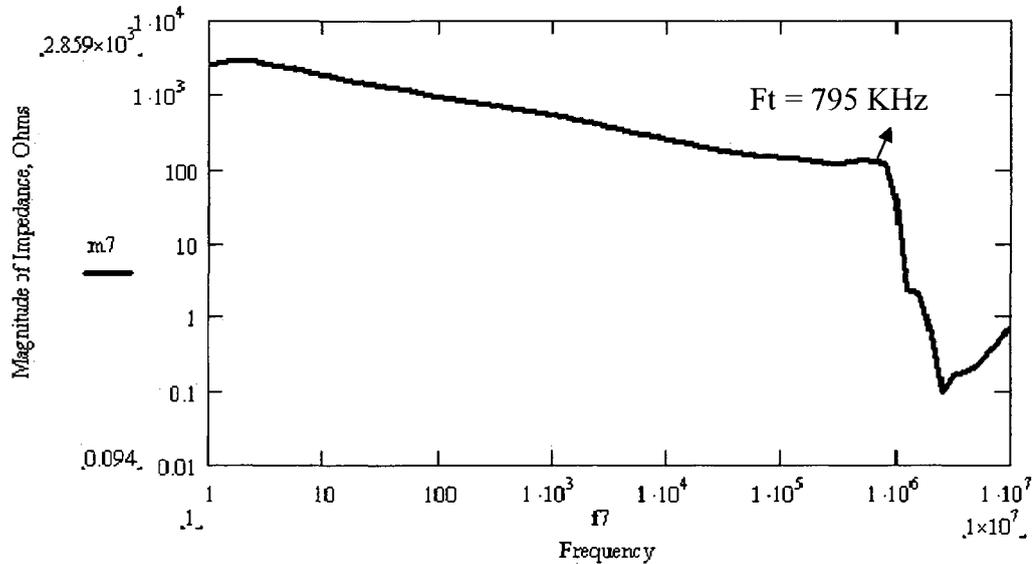
Figure 4.9 Magnitude of impedance Vs Frequency for GPC beam

The beams were subjected to a three point bending while the cylinders were

subjected to a standard compressive test; all the specimens were electrically isolated.

Voltage, current and strain data were acquired during all the tests. The beams were placed

on a bending setup with a separation distance between the two supports of 12". The point

load on the beams was applied by the MTS hydraulic actuator at a load rate of 100 lbs per

minute. Care was taken to not to disturb the strain gage located on the bottom face of the

beam.

Current leads from the wave form generator (HP33120A) were connected to the

specimen electrodes (copper wire electrode) on each side of the beam. One of the current

leads was looped through the current probe to be able to read the current being applied.

The current probe (Tektronix A6303) was connected to the current amplifier (Tektronix

TM502A) which, in turn, was connected to the oscilloscope where the current was measured. The voltage probe from the oscilloscope was also connected to the two electrodes on the specimen to read the voltage (See Figures 4.10 & 4.11 for instrument and equipment setup).
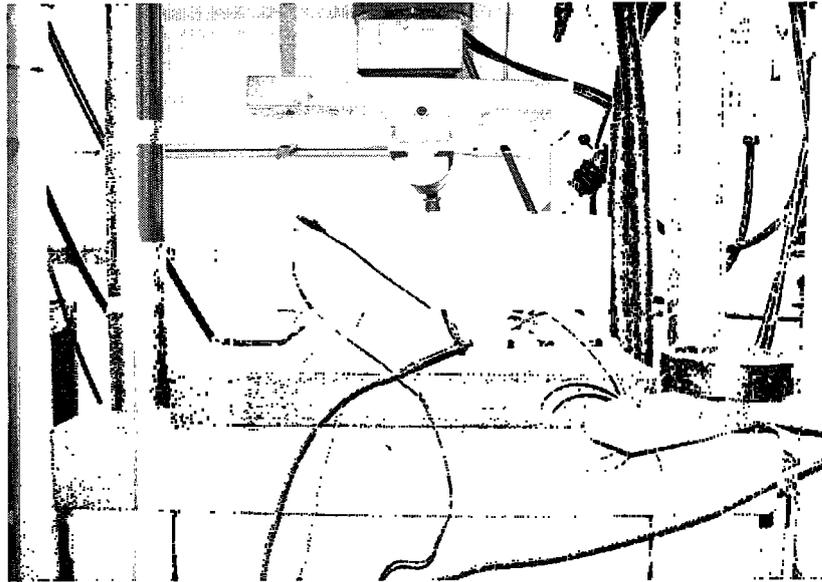
Figure 4.10 GPC beam mounted on the three point bending set up, with current leads, voltage probe and current probe.

Figure 4.11 Data acquisition units' digital oscilloscope, current amplifier and strain gage data acquisition system.

During the test, the input voltage amplitude from the wave form generator was set to 4 V with a frequency of 795 KHz. Leads from the strain gage were hooked to the data acquisition unit (DAQ HP 3479A) to record changes in strain. For every 100 lbs applied, the MTS machine was paused to maintain the load while the voltage, current and strain gage data were recorded for that particular load step. In this way, a maximum of 2100 lbs load was applied on to each beam. Results from the dynamic testing on the beams are given in section 4.6. Similarly, in case of the carbon fiber entrained geopolymer cylinders compressive load was applied on each cylinder using a servo-controlled MTS hydraulic actuator (See Figure 4.12) while voltage, current and strain gage data were recorded at

particular load intervals using the same equipment and setup used for the beams (See

Figure 4.13 for experimental setup). The results from the compressive loading are given

below (See Section 4.6).
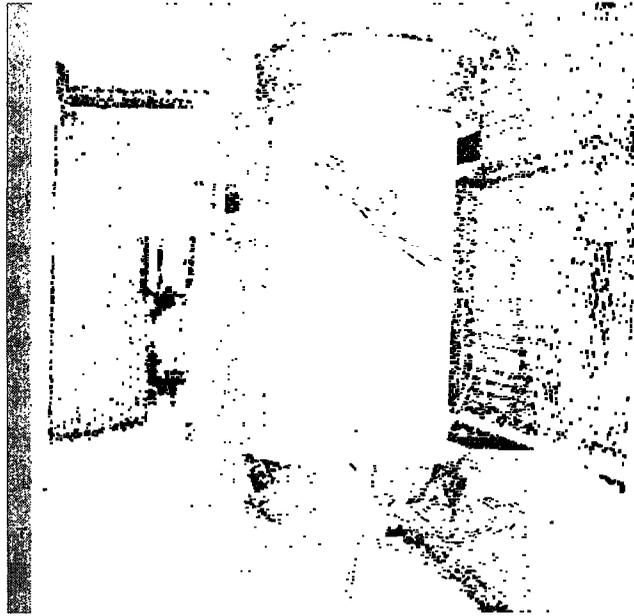
Figure 4.12 GPC cylinder under compressive test setup with voltage probe and current
            leads.
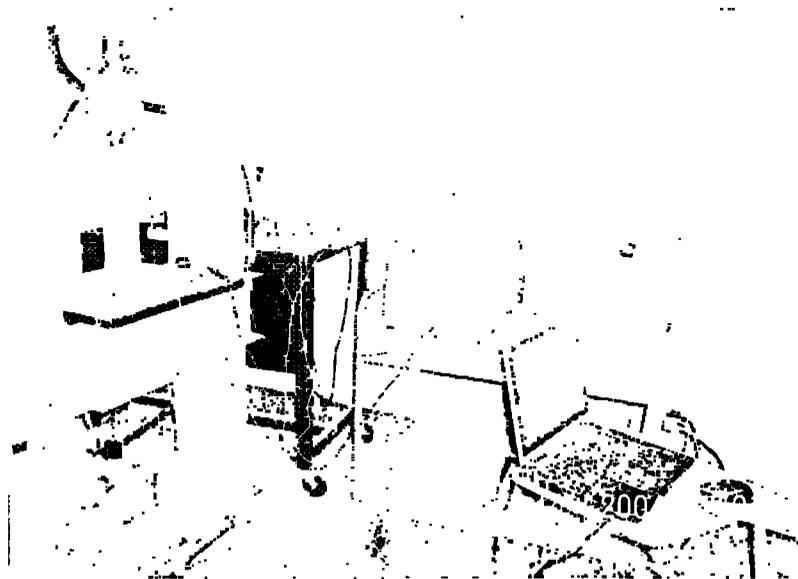
Figure 4.13 Experimental setup for compressive load testing.

4.6 <u>Analysis of Results</u>

4.6.1 <u>GPC Beams Under Flexure Load</u>

Results from dynamic testing on the beam specimens are summarized in Tables A1 through A4 in Appendix 'A'. A discussion of the results is provided below.

Figure 4.14 shows the loading condition, shear force and bending moment diagrams for the beams. Figure illustrates the deformed geometry of the beam under load, (vertical displacement at the center of the beam is equal to the distance moved by the edge of the beam). Figures 4.16 & 4.17 display the electrical resistance (ohms) versus the flexural stress (psi) of the GPC beam specimens (Beam1 and Beam2). The electrical resistance was measured directly between two electrodes placed on the beam specimens, and the flexure stress was calculated using the Eq. A4 ($S_f = 3PL/2bd^2$). Figures 4.18 & 4.19 depict the stress versus strain and electrical resistance for both beams as recorded by the data acquisition system. The flexure stresses are derived from the applied load and the geometry of the specimens, while the strain readings are calculated from the strain gage data placed at the point of loading on tensile face. Details of the calculations can be found in Appendix A. Figure 4.20 shows the electrical resistivity versus the vertical displacement of the beam specimens recorded by the MTS hydraulic ram unit.

From the Figures 4.14 through 4.20, it can be observed that with increase in flexure stress and curvature, the electrical resistance decreases for the two GPC beams in a linear fashion at a rate of approximately 3.3 Ohms-in per 1000 psi of flexure stress for Beam 1 and 4.1 Ohms-in per 1000 psi of flexure stress for Beam 2. Thus, there is an inverse relationship between the tensile strain at the outer most surface at the bottom of the beam and the beam's electrical resistance. Similarly, an inverse relationship appears

to exist between the vertical displacement of the beam and its resistivity. Thus, monitoring the electrical resistance of geopolymer members could potentially provide information regarding their serviceability criteria (i.e., vertical deflection of beams and other flexure members) as well as permanent damage (strain). The decrease in electrical resistance may be due to increase in flexure stress that tends to curve the beams, leading to a reduction in the separation distance between the electrodes (i.e. shortening the conduction path) and subsequently causing the electrical resistance to decrease (See Figure 4.15). This decrease in resistance could potentially be reported using the concept of apparent conductive length. The electrical resistance is calculated using the expression $R = (\rho {*}L)/A$, where R is the resistance, ρ is the bulk resistivity of the material, L is the physical length between the electrodes and A is the cross sectional area of the specimen. The apparent change in conductive length can be calculated using the expression below (Eq. 4.2). Conductive path through a structural cementitious element under load is a complex and dynamic function which depends on the factors such as void ratio, the presence and degree of micro-cracks and the interface between the cementitious grout and the aggregate (both fine and coarse, the gravel and sand are rendered non-conductive)

$$\Delta L_c = \frac{\dfrac{\rho \cdot L_i}{R_i \cdot A}}{\dfrac{\rho \cdot L_f}{R_f \cdot A}} = \frac{L_i \cdot R_f}{L_f \cdot R_i}, \tag{4.2}$$

where ΔL_c = Apparent change in conduction length,

A = Cross sectional area (A = 16 in^2 for Beam specimens),

ρ = Bulk resistivity of the material,

L_i = Initial separation distance between the electrodes,

L_f = Final separation distance between the electrodes (L_f = 7.912 for Beam 1 and 7.9052 for Beam 2),

R_i = Initial electrical resistance measured without any load,

R_f = Final electrical resistance measured before failure.

For both the beams, the change in conductive length was found to decrease as the flexural load increased. The electrical resistance also decreased with increasing flexural stress. Thus, the change in the conductive length is directly proportional to the resistivity of the specimen. The conductivity of a geopolymer concrete matrix is affected by several micro structural changes such as collapse of pores that changes the void ratio and could lead to increase in fiber-fiber interaction, development of micro-cracks at the interface of the matrix-aggregate and at the interface of coarse and fine aggregate. Whatever may be the reason, all the factors come under changes in apparent conductive length, and when apparent conductive length is less than 1 (ΔL_c = 0.928 for Beam 1 and 0.891 for Beam 2, in both the cases it is less than 1), electrical resistance decreases.
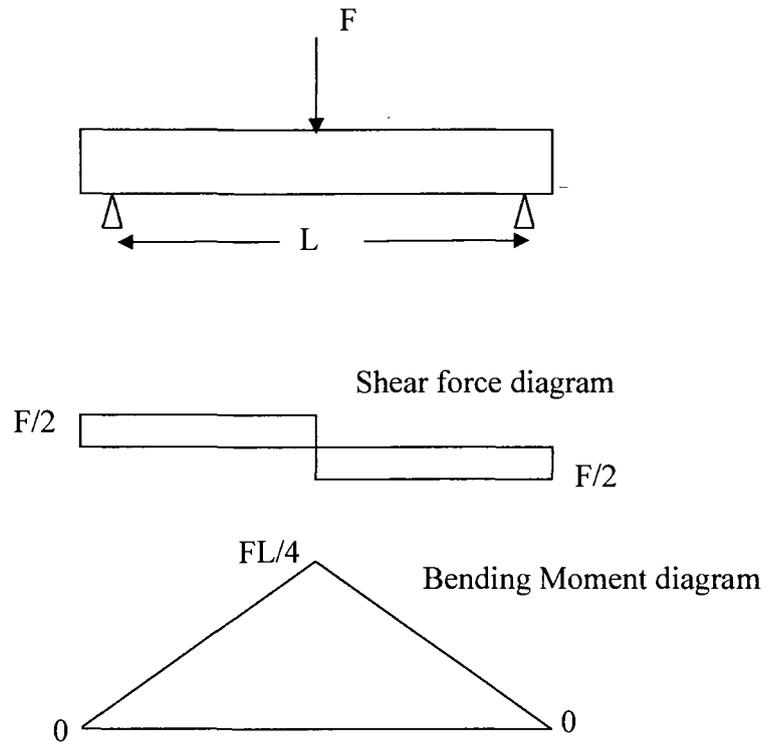
Figure 4.14 Loading of beams, shear force and bending moment.
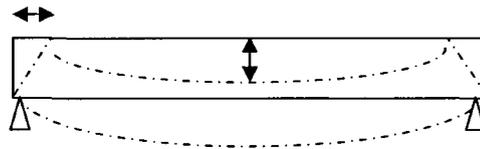
Figure 4.15 Deformed shape of beam under 3 point loading.
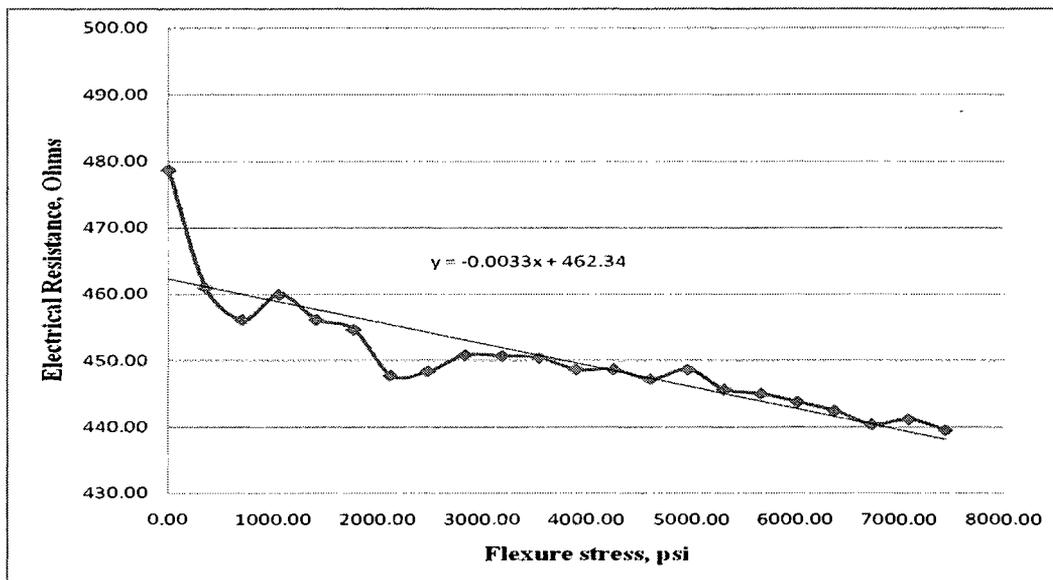
Figure 4.16 Electrical resistance Vs flexure stress for Beam 1.
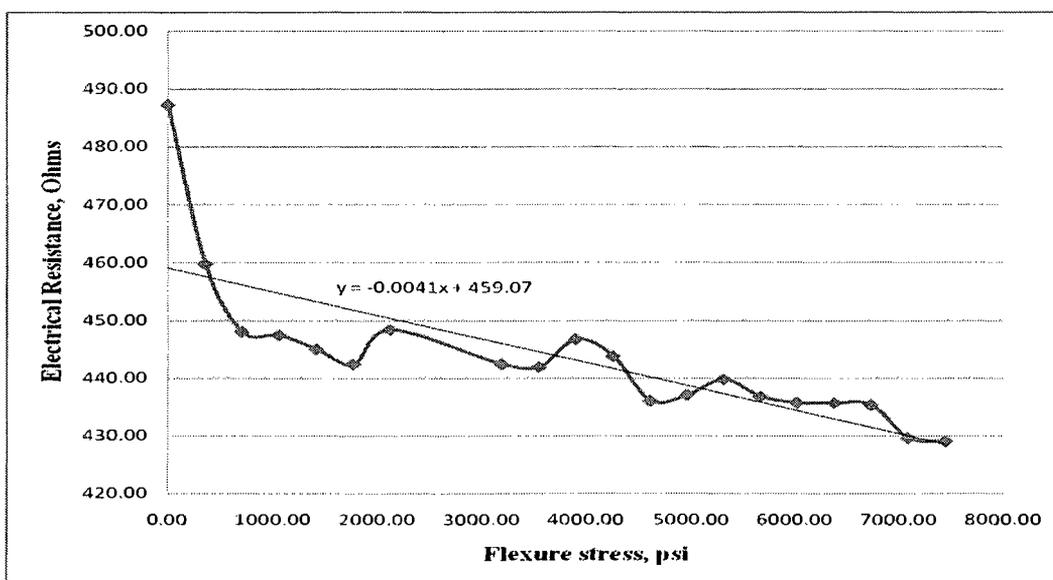
Figure 4.17 Electrical resistance Vs flexure stress for Beam 2.
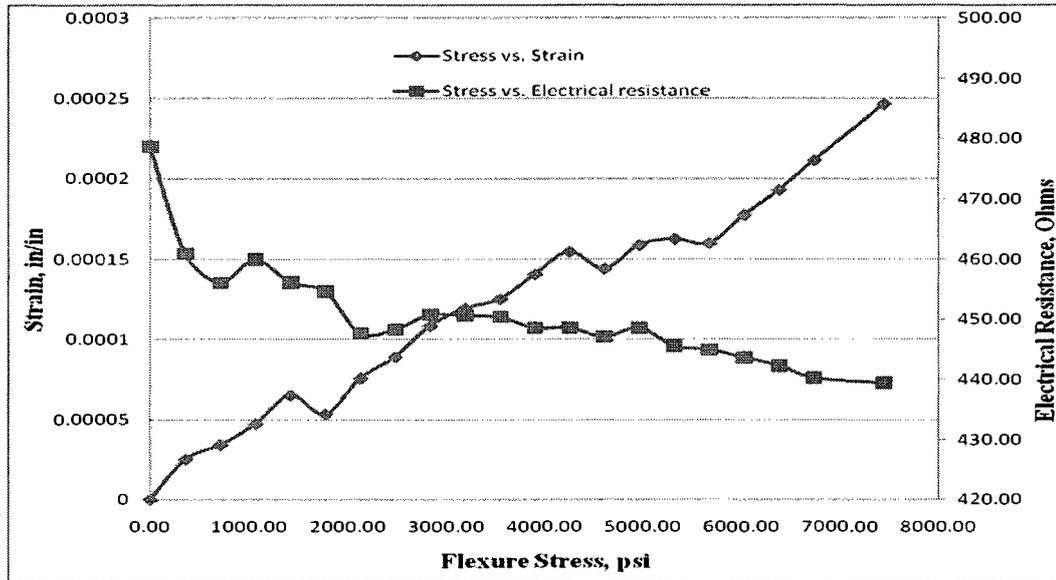
Figure 4.18 Flexure stress vs. strain and electrical resistance for Beam 1.
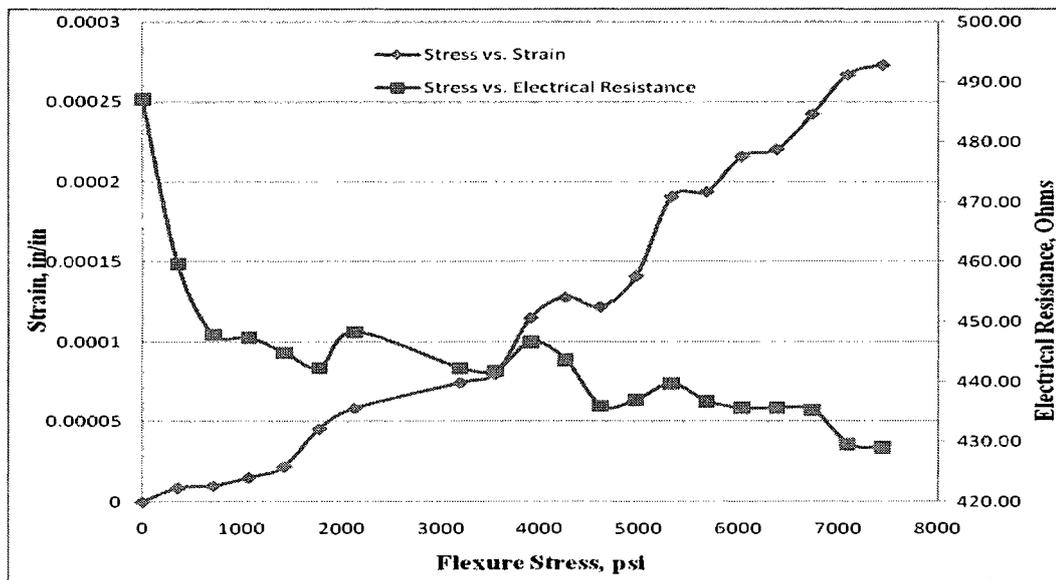
Figure 4.19 Flexure stress vs. strain and electrical resistance for Beam 2.
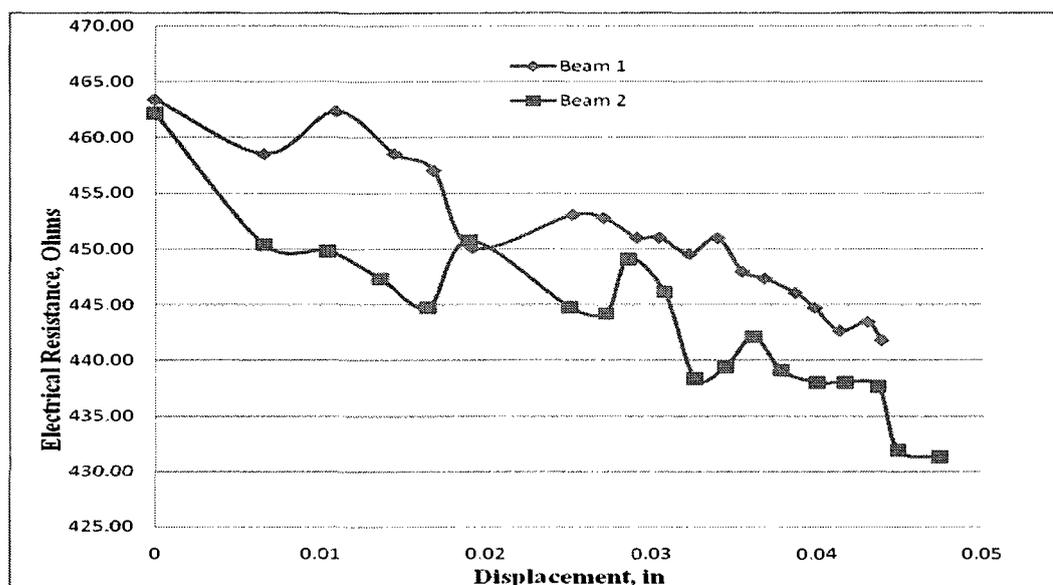
Figure 4.20 Electrical resistance vs. vertical displacement for Beam 1.

4.6.2 GPC Cylinders Under
Compressive Load

Results from the compressive testing of three GPC cylinders are summarized in Tables B1 through B6 in Appendix B. A analysis of the results is provided below.

Figures 4.21, 4.22, and 4.23 display the in change electrical resistivity of the GPC cylinders verses the uni-axial compressive stress in the specimens. The electrical resistance was measured using surface mounted electrodes attached to each of the cylinders. Figure 4.24 displays plots of stress versus strain for the three cylindrical specimens obtained from strain gauge data.

From the Figures 4.21 through 4.25, it can be observed that electrical resistance generally increases with the increase in compressive stresses. This increase could be explained by the changes in apparent conductive length, with the increase in compressive stresses electrical resistance increased. The changes in apparent conductive length are calculated using the Eq. 4.3.

$$\Delta L_C = \frac{L_i \cdot R_2}{L_2 \cdot R_i},$$ (4.3)

where L_i = Initial separation distance between the electrodes,

L_2 = reduced separation distance with the increase in load, obtained from strain gage readings,

R_i = Initial resistance without any load,

R_2 = Electrical resistance measured under each load.

Changes in apparent conductive length could be potentially due to several reasons including increase in the density of the concrete mass under the externally applied load and the development of micro-cracks which conversely effect electrical resistance. With the increase in compressive stress, micro voids in the concrete collapse, leading to reduction in conductive path and subsequently reduction in resistance. Further, with the increase in axial load, concrete mass develops internal cracks leading to increase in the conductive path which, in turn, leads to increase in electrical resistance. A third potential contributor are changes in the interface between the aggregates and the cementations matrix (the sand and gravel aggregates are non-conductive, thus the electrical current must travel around these obstacles). These processes result in opposite effects on the electrical resistance of the specimens with increase in compressive load. The result is that the instantaneous resistivity readings change in a dynamic fashion as the externally applied load (and degradation of the concrete paste) increases.

Figure 4.25 displays the changes in change in apparent conductive length versus compressive stress for the three specimens. It can be seen that the behavior of the three specimens follows a similar pattern, as peaks and valleys occurs within the similar ranges of applied axial stress. The valleys represent a decrease in resistivity (lower apparent

conductive length), while the peaks represent a increase in resistivity. Upon the loading on the specimens, there is a general decrease in resistivity due to the shortening of the conductive length, up to about a stress level of 1000 psi, where a sudden increase in resistivity is noted for all three specimens, indicating the onset of micro-cracks in the geopolymer paste matrix. The process of densification and micro-crack propagation continues until the specimen fail.
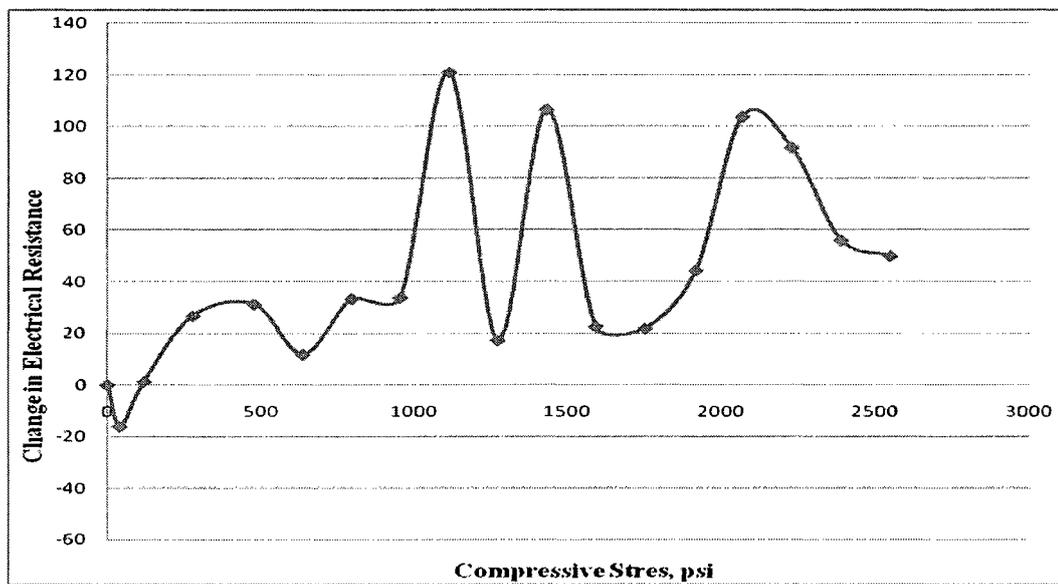
Figure 4.21 Change in electrical resistance vs compressive stress for Cylinder 1.
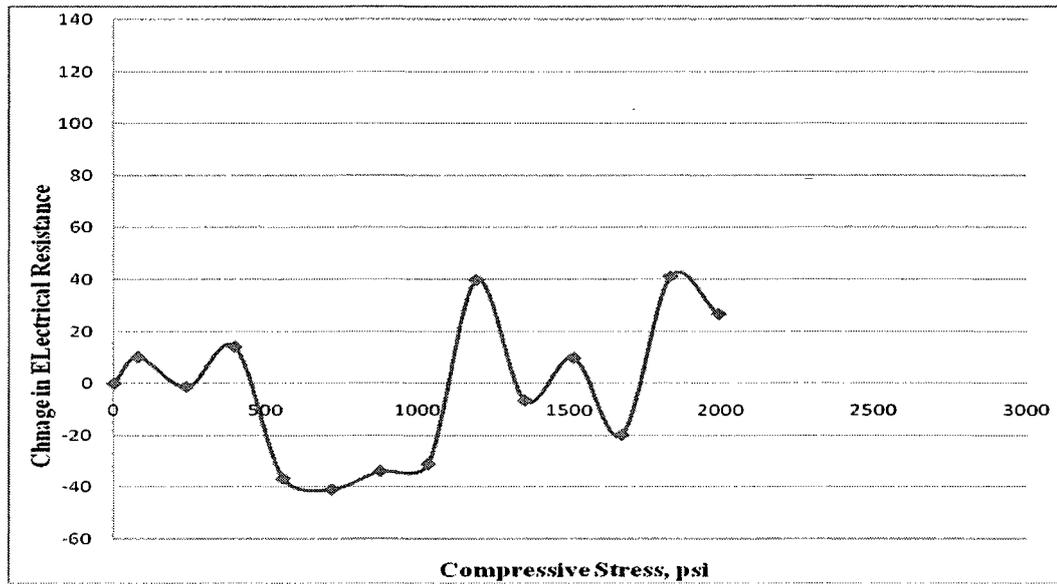
Figure 4.22 Change in electrical resistance vs. compressive stress for Cylinder 2.
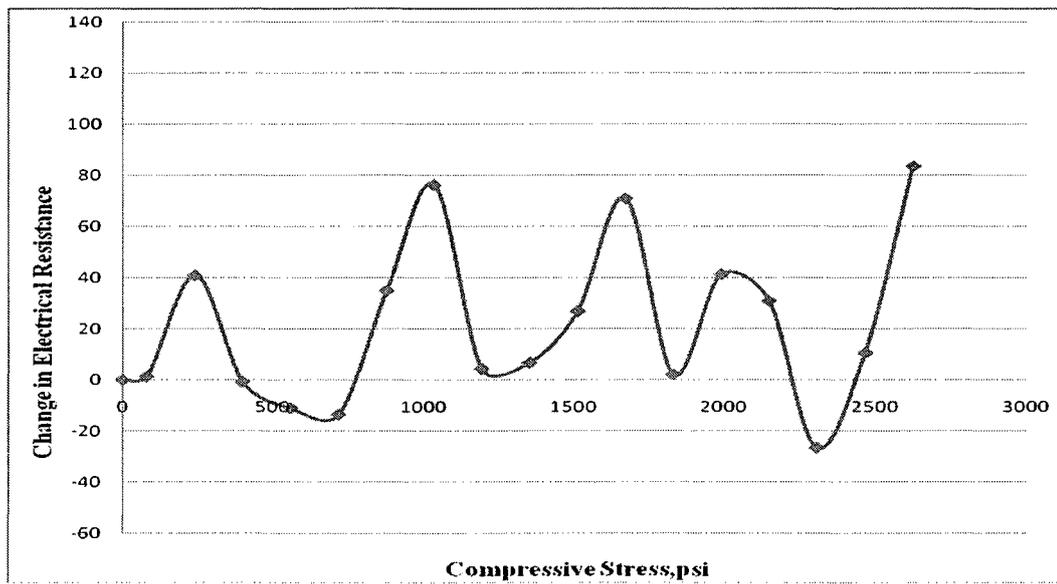
Figure 4.23 Change in electrical resistance vs. compressive stress for Cylinder 3.
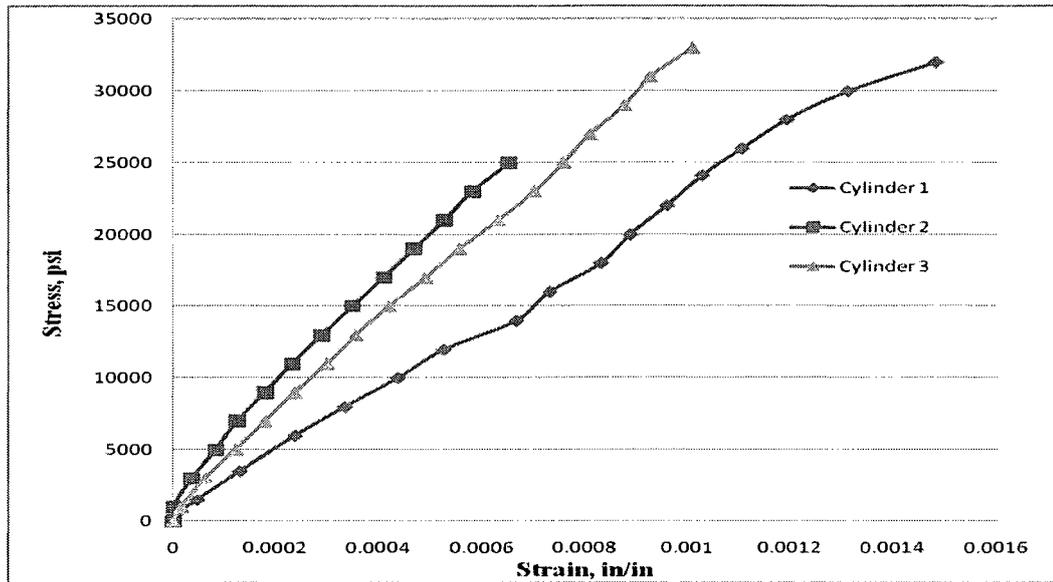
Figure 4.24 Compressive stress vs. strain for Cylinders 1, 2 and 3.
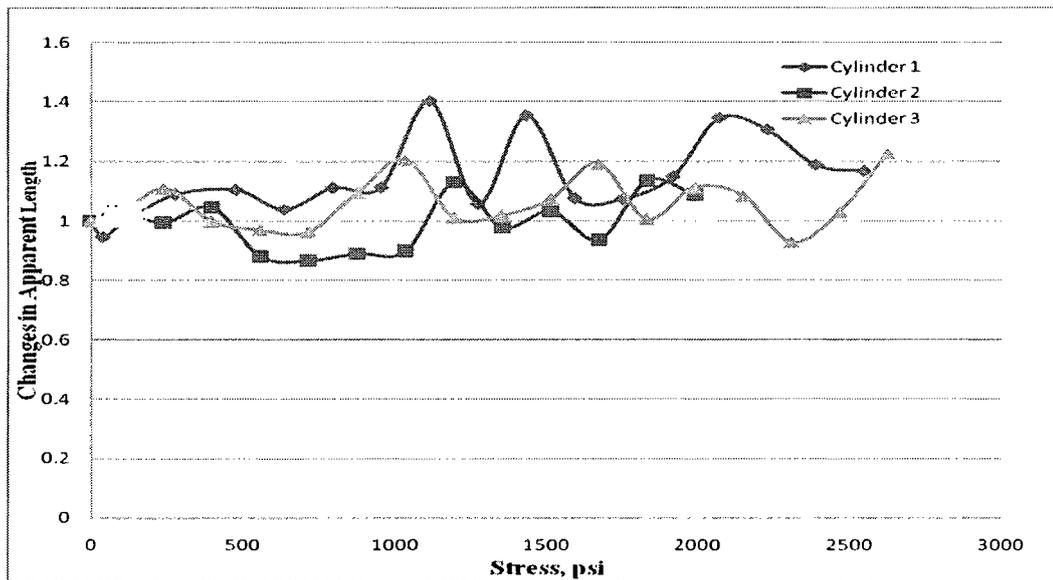
Figure 4.25 Changes in apparent length vs. stress.

4.6 Summary

Reviewing the results from Phase I of the experimental study, it can be observed that with increased fiber percentile fraction, the resistivity of the cementitious matrix decreased in both Portland cement and geopolymer mortar specimens. Geopolymer mortar specimens exhibited lower resistivity to the passage of electrical current compared with Portland cement mortar specimens regardless of the fact that there is little or no free water in geopolymer specimens after curing at 60 °C in an oven for 24 hours. This observation suggests that geopolymer could serve as a better choice of cementitious material for electrical conduction applications.

Results from Phase II suggest that electrical conductivity could also be induced in concrete specimens (using Portland cement or geopolymer as binder) by the addition of carbon fibers. In the case of OPC, it was observed that the electrical conductivity decreased with age of concrete (degree of hydration) before approaching a steady value. This decrease was attributed to the reduced amount of free water within the cemntitious matrix as the hydration process progress. Results from impedance tests on air dry OPC samples (28 day curing and 7 day air dry) revealed that the moisture content in OPC plays a key role on its ability to conduct electric current. The dependency of OPC on free water within the pores for electrical conduction leads to the conclusion that applications of conductive OPC concrete in the real-world could be limited because variations in electrical conduction with moisture content of the OPC might over shadow the changes relating to the change in the stress state of the member.

In Phase III of the experimental study, GPC concrete specimens were subjected to three-point bending and axial compressive load to examine the relationships between changes in the specimens' stress state and electrical resistance. Stress calculations were backed by

strain gauge data. Results from three-point bending tests demonstrated that resistance followed a descending trend with increase in bending stresses which could be attributed to reduction in the conduction length due to the physical shortening of the compression surface of the beam and/or micro-structural changes within the geopolymer matrix, which were lumped under the term "changes in the conductive path", acknowledging that the path of least resistance between the two electrodes is a complex one as the gravel and sand particles, that represents 75% of the volume of the geopolymer concrete, are esesentialy non-conductive. In the case of axial compressive stresses electrical resistance was observed to be fluctuating. This behavior might be attributed to the densification of the geopolymer paste on one hand, and the development of micro-cracks on the other. These two processes occur simultaneously with increase in compressive load, but have the opposite effect on the electrical resistance of the specimen.

CHAPTER 5

CONCLUSIONS AND RECOMMENDATIONS

5.1 Conclusions and Recommendations from Part I

The first part of this dissertation describes a new approach for the rehabilitation of deteriorated concrete sewer pipes. The objective of the study was to investigate the technical feasibility of an innovative coating procedure that could be used for inoculating pre-cast concrete pipes against microbial induced corrosion using eletrokinetics. Results from the preliminary Phases of the study (Phases I and II) suggested that the electrokinetic coating procedure could be used to transport corrosion inhibiting coating material (copper oxide) into the hardened concrete matrix, and that the procedure is most effective in the case of partially deteriorated concrete pipes. For testing the field applicability of the electrokinetic coating technique, a 15" diameter commercial pre-cast concrete pipe was electrokinetically coated using copper oxide in Phase III. Quantitative measures of elemental copper concentration within the concrete matrix obtained using AAS on the specimens treated during the three phases of the study suggest the effectiveness of the coating procedure is time dependent, and provided an indication that the results from the mock specimens can be scaled up (i.e. the concentration of copper measured for the mock specimens was the same measured for the full-scale test using the same duration of treatment).

The proposed electrokinetic coating process could be considered viable as far as laboratory tests are concerned. Implementing this technology in the field requires additional consideration of the application mechanism (e.g. utilization of fabric material impregnated with the chemical solution placed on a bladder system). While the study was conducted with pre-cast concrete pipes in mind, alternative applications include manholes, storage facilities and drop structures where access to the steel reinforcement could be secured with greater ease. Other applications outside of the rim of municipal engineering include the protection of structures that house livestock (swine farms). Further studies should include evaluating the durability of the coating under physical, thermal and chemical loadings, as well as exposing the treated specimens to simulated wastewater colonized with bacteria cultures. Furthermore, a long term leach test should be performed on the coating to evaluate the amount of copper leaching out.

5.2 Conclusions and Recommendations from Part II

The second part of this dissertation is aimed at developing a conductive geopolymer concrete to be used in health monitoring applications for civil infrastructure. Carbon fibers were mixed with fresh cementitious materials to enhance the electrical conductivity of the resulting matrix. AC-IS analysis was performed on the specimens and their electrical resistivity was recorded for a wide range of current frequencies. The experimental study was divided into three Phases. Mortar specimens (Portland cement and geopolymer) with varying fiber percentages were tested in Phase I. In Phase II, concrete specimens (Portland cement and geopolymer) with selected optimum fiber percentage were tested to evaluate the effect of curing time/degree of hydration and moisture content on the specimens electrical conductivity. In Phase III, dynamic load

tests were performed on prism and cylindrical geopolymer concrete specimens to establish the relationships between the electrical resistance and the stress state of the specimen (under flexure and compression).

Results obtained from Phase I of the study suggest that by increasing fiber percentage, resistivity of the material decreases. It was also found that geopolymer specimens exhibit a significantly lower resistivity compared with the Portland cement specimens. Phase I provided the basis for selecting the optimum fiber percentage values based upon electrical conductivity and workability of the cementitious materials. Based on the results, a fiber content equal to 0.4% by weight of the cementitious material was selected as an optimum value from the conductivity and workability prospective. The results from Phase II suggested that electrical conductivity could be induced into concrete matrices (both Portland cement and geopolymer). In case of OPC water content was found to play a key role in determining the electrical conductivity of the hardened paste. In fact, the "noise" associated with the changes in electrical conductivity as a function of the OPC paste moisture content appears to be significantly greater than the changes attributed to the member's stress state. Observations from Phase II resulted in only GPC samples used in the dynamic load testing. Two beams and three cylinders of GPC with optimum fiber percentage (0.4% by wt of cementitious binder) were casted. Results from dynamic load testing suggest that as flexure stresses in the beams increase, their electrical resistance decreases. This decrease could be attributed to the shortening of the outer most chord at the compression face of the beam which resulted in a shorter conduction path. Another possible explanation is reduction in the apparent conduction length, a term used to lump micro-structure processes within the cementitious matrix that impact the

electrical resistance of the specimens (i.e., densification, micro-cracking). In the case of cylindrical specimens, the electrical resistance fluctuated with increase compressive stress. It is hypothesized that contributing factors to this behavior are process of densification of the concrete paste under the externally applied load, the development of micro-cracking and changes at the interface between the paste and the aggregates (both fine and coarse), that make 75% of the volume of the geopolymer concrete specimens. Each of these processes has an impact on the length of the path electrical current needs to traverse between the two electrodes and thus on the bulk resistivity of the specimen. As some of the processes will result in reducing the bulk electrical resistivity of the specimen others tend to increase it, the total sum of changes in electrical resistivity is a dynamic function which changes with increase in applied load, up to the failure of the member.

Geopolymer concrete is potentially suitable for many applications because of its mechanical, chemical and electrical properties, providing a "green" alternative to OPC as a construction material. The research conducted here lays the foundation for a new and improved cementitious material (carbon fiber reinforced geopolymer concrete-CFRGC) that could be used in building of smart and sustainable infrastructure. This study provides a characterization of basic electrical properties of CFRGC and demonstrates that CFRGC offers superior performance compared to carbon fiber entrained OPC. Further studies on CFRGC should include examination of the effect of moisture content in GPC and carbon content in the fly (LOI) ash on its electrical properties. It is also beneficial to study means to improve the conductivity of GPC such as ion substitutions as well as evaluation of other fiber types such as stainless steel. A study correlating the densification of CFRGC and micro-cracking development with electrical resistance should be performed with the

aid of acoustic emission detectors (elastic energy stored in the concrete will be released as sound wave under loading which can be detected). Such a study will confirm or discard the hypothesis made in chapter 4 that electrical resistance changes closely follow micro-structural changes within the geopolymer mass.

APPENDIX A

RESULTS FROM DYNAMIC TESTS
ON GPC BEAM SPECIMENS

Tables A.1 through A.4 represents the results obtained on Beams 1 and Beam 2. The electrical resistance was calculated from voltage and current readings obtained from the digital oscilloscope. During the test, channel 1 on digital oscilloscope represented voltage readings while channel 2 the current reading. The magnification for channel 1 was set to 2 V per division while for channel 2 was set to 10 mV. The current amplifier through which a current probe was connected to the oscilloscope was set to 20 mA per division. Each division on the digital oscilloscope represented 25 units. During the data acquisition, for each particular load point, the oscilloscope gives 463 readings of voltage and current in units, which when plotted individually, resemble a sinusoidal wave form. Electrical resistance was obtained by calculating the RMS (root mean square) values of both the voltage and current units. Before substituting the values into Ohm's law for calculating the electrical resistance, the RMS values of voltage and current units were converted into volts and amperes which was done using the following equations:

$$\text{Voltage in Volts, } V = \left(\frac{2V}{division}\right) * \left(\frac{1.division}{25.units}\right) * (V.RMS) \tag{A.1}$$

$$\text{Current in Amperes, } I = \left(\frac{20mA}{division}\right) * \left(\frac{1.division}{25.units}\right) * (I.RMS). \tag{A.2}$$

Electrical resistance in Ohms:

$$R = \frac{(V).Volts}{(I).Amperes}.$$ (A.3)

The voltage, current, resistance and resistivity values in the tables A.1 & A.3 were calculated using Eq. A.1, A.2 & A.3 (where A/L for the beams is 1.0054" and for the cylinders it is 0.9027"). The flexure stress values in Tables A.1 and A.3 were calculated using Eq. A.4. Tables A.2 & A.4represents the stress Vs strain data obtained from strain gage data acquisition unit.

Flexure Stress:

$$S_F = \frac{3*P*L}{2*b*d^2},$$ (A.4)

where, P = Load, lbs

L = Separation distance between the supports (12")

b = Breadth of the beam (4")

d = Depth of the beam (4").

Table A. 1 Summary of dynamic test results on Beam 1

Load, lbs	Flexure Stress, psi	Voltage, units	Current, units	Voltage, volts	Current, mA	Resistance, ohms
0	0.00	31.05	6.49	2.48	5.19	478.69
100	354.61	30.68	6.66	2.45	5.32	460.95
200	709.22	30.98	6.79	2.48	5.43	456.11
300	1063.83	30.91	6.72	2.47	5.38	459.92
400	1418.44	30.90	6.77	2.47	5.42	456.13
500	1773.05	30.88	6.79	2.47	5.43	454.63
600	2127.66	30.82	6.88	2.47	5.51	447.69
700	2482.27	30.82	6.87	2.47	5.50	448.34
800	2836.88	30.78	6.83	2.46	5.46	450.78
900	3191.49	30.69	6.81	2.46	5.45	450.64
1000	3546.10	30.71	6.82	2.46	5.46	450.36
1100	3900.71	30.77	6.86	2.46	5.49	448.59
1200	4255.32	30.77	6.86	2.46	5.49	448.61
1300	4609.93	30.71	6.87	2.46	5.50	447.14
1400	4964.54	30.64	6.83	2.45	5.46	448.58
1500	5319.15	30.65	6.88	2.45	5.50	445.58
1600	5673.76	30.70	6.90	2.46	5.52	444.95
1700	6028.37	30.64	6.91	2.45	5.52	443.68
1800	6382.98	30.67	6.93	2.45	5.55	442.35
1900	6737.59	30.77	6.99	2.46	5.59	440.28
2000	7092.20	30.68	6.96	2.45	5.56	441.07
2100	7446.81	30.60	6.96	2.45	5.57	439.44

Table A. 2 Summary of strain gage data for Beam 1

Load, lbs	Stress, psi	Resistance, R	Initial resistance, Ro	Change in resistance over Initial resistance (R-Ro)/Ro	Strain
0	0	120.38632	120.386	0	0
100	354.61	120.39269	120.386	5.29395E-05	2.5E-05
200	709.22	120.39496	120.386	7.1782E-05	3.4E-05
300	1063.83	120.39825	120.386	9.90899E-05	4.7E-05
400	1418.44	120.40279	120.386	0.000136821	6.5E-05
500	1773.05	120.3998	120.386	0.000111927	5.3E-05
600	2127.66	120.40544	120.386	0.000158824	7.6E-05
700	2482.27	120.40887	120.386	0.000187278	8.9E-05
800	2836.88	120.41372	120.386	0.000227593	0.00011
900	3191.49	120.41649	120.386	0.000250598	0.00012
1000	3546.1	120.41795	120.386	0.000262702	0.00013
1100	3900.71	120.42187	120.386	0.000295264	0.00014
1200	4255.32	120.42539	120.386	0.000324535	0.00015
1300	4609.93	120.42272	120.386	0.000302344	0.00014
1400	4964.54	120.42647	120.386	0.00033346	0.00016
1500	5319.15	120.4274	120.386	0.000341189	0.00016
1600	5673.76	120.42673	120.386	0.000335689	0.00016
1700	6028.37	120.43118	120.386	0.000372584	0.00018
1800	6382.98	120.43513	120.386	0.000405446	0.00019
1900	6737.59	120.43978	120.386	0.00044404	0.00021
2100	7446.81	120.44871	120.386	0.000518201	0.00025

Table A. 3 Summary of dynamic test results for Beam 2

Load, lbs	Flexure Stress, psi	Voltage, volt	Current, units	Voltage, volts	Current, mA	Resistance, ohms
0	0.00	31.49	6.46	2.52	5.17	487.20
100	354.61	31.09	6.76	2.49	5.41	459.72
200	709.22	31.01	6.92	2.48	5.54	447.96
300	1063.83	30.97	6.92	2.48	5.54	447.40
400	1418.44	30.96	6.96	2.48	5.57	444.96
500	1773.05	30.98	7.00	2.48	5.60	442.38
600	2127.66	30.91	6.89	2.47	5.51	448.33
900	3191.49	30.97	7.00	2.48	5.60	442.35
1000	3546.10	30.93	7.00	2.47	5.60	441.83
1100	3900.71	30.91	6.92	2.47	5.54	446.66
1200	4255.32	30.86	6.95	2.47	5.56	443.71
1300	4609.93	30.82	7.07	2.47	5.65	436.04
1400	4964.54	30.75	7.04	2.46	5.63	437.04
1500	5319.15	30.81	7.01	2.46	5.61	439.73
1600	5673.76	30.79	7.05	2.46	5.64	436.76
1700	6028.37	30.77	7.06	2.46	5.65	435.67
1800	6382.98	30.82	7.07	2.47	5.66	435.67
1900	6737.59	30.83	7.08	2.47	5.67	435.29
2000	7092.20	30.74	7.15	2.46	5.72	429.62
2100	7446.81	30.75	7.17	2.46	5.73	429.03

Table A. 4 Summary of strain gage data for Beam 2

Load, lbs	Stress, psi	Resistance, R	Initial resistance, Ro	Change in resistance over Initial resistance (R-Ro)/Ro	Strain
0	0	120.509445	120.5094452	0	0
100	354.61	120.507192	120.5094452	1.86997E-05	8.9E-06
200	709.22	120.512038	120.5094452	2.15195E-05	1E-05
300	1063.83	120.513293	120.5094452	3.19325E-05	1.5E-05
400	1418.44	120.515063	120.5094452	4.66133E-05	2.2E-05
500	1773.05	120.521012	120.5094452	9.59809E-05	4.6E-05
600	2127.66	120.524282	120.5094452	0.000123119	5.9E-05
700	2482.27	120.525272	120.5094452	0.000131331	6.3E-05
800	2836.88	120.527792	120.5094452	0.000152247	7.2E-05
900	3191.49	120.528374	120.5094452	0.000157074	7.5E-05
1000	3546.1	120.529735	120.5094452	0.000168366	8E-05
1100	3900.71	120.538633	120.5094452	0.000242207	0.00012
1200	4255.32	120.541871	120.5094452	0.000269077	0.00013
1300	4609.93	120.540358	120.5094452	0.000256519	0.00012
1400	4964.54	120.545224	120.5094452	0.000296893	0.00014
1500	5319.15	120.557786	120.5094452	0.000401135	0.00019
1600	5673.76	120.558509	120.5094452	0.000407138	0.00019
1700	6028.37	120.564133	120.5094452	0.000453808	0.00022
1800	6382.98	120.565229	120.5094452	0.000462904	0.00022
1900	6737.59	120.570838	120.5094452	0.00050944	0.00024
2000	7092.2	120.5771	120.5094452	0.000561407	0.00027
2100	7446.81	120.578608	120.5094452	0.000573916	0.00027

APPENDIX B

RESULTS FROM DYNAMIC TESTS
ON GPC CYLINDER SPECIMENS

Tables B1 through B6 represents results obtained on cylinder 1, cylinder 2 and cylinder 3. The voltage, current and electrical resistance values in the Tables B1, B.3 and B.5 were calculated using Eq. A.1, A.2 & A.3. The compressive stress values in Tables B.1, B.3 and B.5 were calculated using Eq. B.1. Tables B.2, B.4 & B.6 represents the stress versus strain data obtained from strain gaga data acquisition unit.

Compressive Stress:

$$S_C = \frac{P}{A_c},$$ (B.1)

where, P = Load, lbs

A_c = Surface area of the cylinder (12.57 in^2).

Table B. 1 Summary of dynamic test results for Cylinder1

Load	Compressive Stress, psi	Voltage, units	Current, units	Voltage, Volts	Current, mA	Resistance, Ohms
0	0	9.54768	7.9324	1.90954	6.34592	300.908
500	39.7867	9.43233	8.28057	1.88647	6.62446	284.773
1500	119.36	9.20223	7.61397	1.84045	6.09118	302.149
3500	278.507	9.39054	7.16451	1.87811	5.73161	327.676
6000	477.441	9.30086	7.00118	1.86017	5.60094	332.118
8000	636.588	9.361	7.48775	1.8722	5.9902	312.544
10000	795.735	9.31876	6.96969	1.86375	5.57575	334.26
12000	954.882	9.32494	6.96459	1.86499	5.57167	334.727
14000	1114.03	9.07536	5.3781	1.81507	4.30248	421.866
16000	1273.18	9.09634	7.15178	1.81927	5.72142	317.975
18000	1432.32	9.03152	5.54255	1.8063	4.43404	407.372
20000	1591.47	9.12923	7.05379	1.82585	5.64303	323.558
22000	1750.62	8.9864	6.96157	1.79728	5.56925	322.715
24100	1917.72	8.88725	6.43455	1.77745	5.14764	345.294
26000	2068.91	9.00027	5.55982	1.80005	4.44785	404.702
28000	2228.06	8.87456	5.64874	1.77491	4.51899	392.767
30000	2387.2	8.80674	6.16813	1.76135	4.93451	356.945
32000	2546.35	8.98653	6.40494	1.79731	5.12395	350.766

Table B. 2 Summary of strain gage data for Cylinder 1

Load, lbs	Compressive stress, psi	Resistance, R	Initial resistance, Ro	Change in resistance over initial resistance, (R-Ro)/Ro	Strain
0	0	121.196	121.196	0	0
500	39.7867	121.196	121.196	3.57827E-06	3.6E-06
1500	119.36	121.19	121.196	-4.6757E-05	4.7E-05
3500	278.507	121.18	121.196	-0.00012927	0.00013
6000	477.441	121.167	121.196	-0.00023672	0.00024
8000	636.588	121.155	121.196	-0.00033356	0.00033
10000	795.735	121.143	121.196	-0.00043501	0.00044
12000	954.882	121.132	121.196	-0.00052491	0.00052
14000	1114.03	121.115	121.196	-0.00066578	0.00067
16000	1273.18	121.107	121.196	-0.00073074	0.00073
18000	1432.32	121.095	121.196	-0.00083095	0.00083
20000	1591.47	121.088	121.196	-0.00088734	0.00089
22000	1750.62	121.08	121.196	-0.00095904	0.00096
24100	1917.72	121.071	121.196	-0.00102757	0.00103
26000	2068.91	121.062	121.196	-0.00110481	0.0011
28000	2228.06	121.051	121.196	-0.00119179	0.00119
30000	2387.2	121.037	121.196	-0.0013112	0.00131
32000	2546.35	121.016	121.196	-0.0014817	0.00148

Table B. 3 Summary of dynamic test results for Cylinder 2

Load, lbs	Compressive stress, psi	Voltage, units	Current, Units	Voltage, Volts	Current, mA	Resistance, Ohms
0	0	24.0617	7.87111	1.92493	6.29689	305.696
1000	79.5735	22.2687	7.04826	1.7815	5.6386	315.946
3000	238.72	22.3203	7.33106	1.78563	5.86485	304.462
5000	397.867	21.5755	6.74645	1.72604	5.39716	319.806
7000	557.014	21.2174	7.88266	1.69739	6.30613	269.165
9000	716.161	20.7391	7.8315	1.65913	6.2652	264.816
11000	875.308	20.2861	7.45777	1.62289	5.96622	272.013
13000	1034.46	20.6642	7.52129	1.65314	6.01703	274.743
15000	1193.6	20.6672	5.98166	1.65337	4.78533	345.509
17000	1352.75	20.2367	6.76351	1.61894	5.41081	299.205
19000	1511.9	20.3738	6.45497	1.6299	5.16398	315.629
21000	1671.04	20.3256	7.10965	1.62605	5.68772	285.888
23000	1830.19	20.4778	5.90433	1.63822	4.72346	346.827
25000	1989.34	20.0343	6.02865	1.60274	4.82292	332.318

Table B. 4 Summary of strain gage data for Cylinder 2

Load, lbs	Compressive stress, psi	Resistance, R	Initial Resistance, Ro	Change in Resistance over initial resistance, (R-Ro)/R	Strain
0	0	121.146	121.146	0	0
1000	79.5735	121.146	121.146	-3E-06	1.6E-06
3000	238.72	121.137	121.146	-8E-05	3.6E-05
5000	397.867	121.125	121.146	-0.0002	8.3E-05
7000	557.014	121.114	121.146	-0.0003	0.00012
9000	716.161	121.1	121.146	-0.0004	0.00018
11000	875.308	121.087	121.146	-0.0005	0.00023
13000	1034.46	121.073	121.146	-0.0006	0.00029
15000	1193.6	121.057	121.146	-0.0007	0.00035
17000	1352.75	121.042	121.146	-0.0009	0.00041
19000	1511.9	121.027	121.146	-0.001	0.00047
21000	1671.04	121.012	121.146	-0.0011	0.00053
23000	1830.19	120.998	121.146	-0.0012	0.00058
25000	1989.34	120.98	121.146	-0.0014	0.00065

Table B. 5 Summary of dynamic test results for Cylinder 3

Load, lbs	Compressive stress, psi	Voltage, Units	Current, Units	Voltage, Volts	Current, mA	Resistance, Ohms
0	0	26.0187	7.02576	2.08149	5.62061	370.332
1000	79.5735	25.5008	6.85954	2.04007	5.48764	371.757
3000	238.72	25.1692	6.1202	2.01353	4.89616	411.247
5000	397.867	25.1284	6.79961	2.01027	5.43969	369.556
7000	557.014	25.042	6.96866	2.00336	5.57493	359.352
9000	716.161	25.2206	7.07025	2.01765	5.6562	356.714
11000	875.308	25.6008	6.31717	2.04807	5.05374	405.258
13000	1034.46	25.1003	5.61937	2.00803	4.4955	446.675
15000	1193.6	25.1426	6.71086	2.01141	5.36869	374.656
17000	1352.75	25.4604	6.75235	2.03683	5.40188	377.059
19000	1511.9	25.2608	6.35947	2.02087	5.08758	397.216
21000	1671.04	25.4787	5.77224	2.03829	4.61779	441.4
23000	1830.19	25.0086	6.7149	2.00069	5.37192	372.435
25000	1989.34	24.7928	6.02238	1.98342	4.8179	411.678
27000	2148.48	24.9046	6.20549	1.99237	4.96439	401.332
29000	2307.63	24.892	7.24295	1.99136	5.79436	343.672
31000	2466.78	24.9021	6.53802	1.99216	5.23041	380.881
33000	2625.93	24.8257	5.46868	1.98606	4.37495	453.962

Table B. 6 Summary of strain gage data for Cylinder 3

Load, lbs	Compressive stress, psi	Resistance, R	Initial Resistance, Ro	Change in resistance over initial resistance, (R-Ro)/Ro	Strain
0	0	121.089	121.089	0	0
1000	79.5735	121.085	121.089	-3E-05	1.6E-05
3000	238.72	121.073	121.089	-0.0001	6.3E-05
5000	397.867	121.058	121.089	-0.0003	0.00012
7000	557.014	121.044	121.089	-0.0004	0.00018
9000	716.161	121.029	121.089	-0.0005	0.00024
11000	875.308	121.013	121.089	-0.0006	0.0003
13000	1034.46	120.999	121.089	-0.0007	0.00035
15000	1193.6	120.983	121.089	-0.0009	0.00042
17000	1352.75	120.965	121.089	-0.001	0.00049
19000	1511.9	120.948	121.089	-0.0012	0.00056
21000	1671.04	120.929	121.089	-0.0013	0.00063
23000	1830.19	120.911	121.089	-0.0015	0.0007
25000	1989.34	120.897	121.089	-0.0016	0.00076
27000	2148.48	120.883	121.089	-0.0017	0.00081
29000	2307.63	120.866	121.089	-0.0018	0.00088
31000	2466.78	120.853	121.089	-0.0019	0.00093
33000	2625.93	120.832	121.089	-0.0021	0.00101

APPENDIX C

POISSON RATIO OF GEOPOLYMER
CONCRETE

To find the Poisson ratio of geopolymer concrete, a standard ASTM test (ASTM c

469) was conducted on a 6" X 12" geopolymer concrete specimen (see figure below for

Poisson ratio test). The same mix design and preparation techniques that were used in

making the samples for Phase II and Phase III were adopted to make the specimen for

Poisson ratio test. Results from the test are summarized in Table C-1.
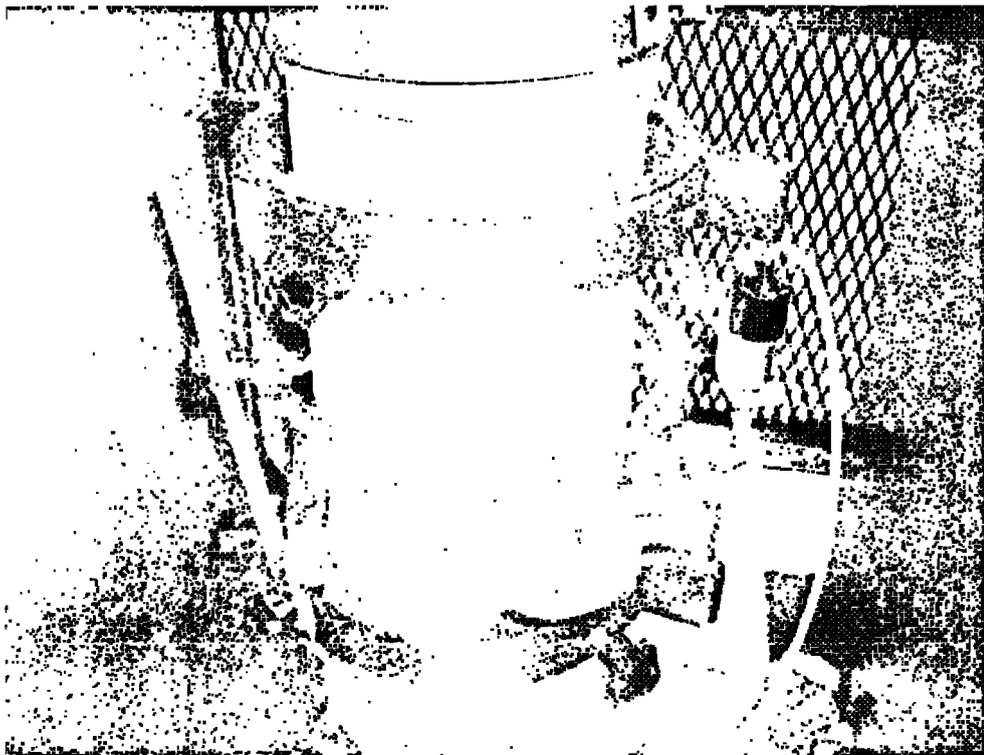
Figure C.1 Experimental setup for Poisson ratio test.

The longitudinal and transversal strains in the table below are calculated using the Eq. 4.7 & 4.8 and Poisson ratio is obtained using the Eq. 4.9

Longitudinal strain:

$$\varepsilon_l = \frac{d_l}{L} = \frac{(g_l.e_h)/(e_h + e_g)}{8}.$$

(4.7)

Transverse strain:

$$\varepsilon_t = \frac{d_r}{r} = \frac{(g_r.e_r)/(e_r + e_g)}{7.5},$$

(4.8)

where, d_l & d_r = deformation in longitudinal and transverse directions

L & r = actual separation distances between the pivots (8" & 7.5")

g_l & g_r = gage readings in longitudinal and transverse directions

e_h & e_r = distance measured between the center pivot and extreme end

e_g = distance measured between the center pivot and the gage location.

Poisson ratio:

$$\mu = (\varepsilon_{t2} - \varepsilon_{t1})/(\varepsilon_2 - 0.00005),$$

(4.9)

where, ε_{t2} = transverse strain at mid-height of the specimen produced by 40% of the ultimate load ($9.42E^{-05}$)

ε_{t1} = transverse strain at mid-height of the specimen produced by initial load ($8.31E^{-06}$)

ε_2 = longitudinal strain produced by 40% of the ultimate load (0.000674).

Therefore:

$$\mu = (9.42E^{-05} - 8.31E^{-06})/ (0.000674 - 0.00005)$$

$$\mu = 0.14 \text{ (approximately)}.$$

Table C. 1 Summary of results obtained from Poisson ratio for GPC

Load, lbs	Stress, psi	Measured Longitudinal deformation, x 10^{-5}	Longitudinal Strain	Measure Radial deformation, x 10^{-5}	Transversal Strain
0	0	0	0	-5	0
5000	176.928521	85	5.28E-05	-20	8.31E-06
10000	353.857042	160	9.94E-05	-30	1.38E-05
15000	530.785563	240	0.000149	-45	2.22E-05
20000	707.714084	320	0.000199	-55	2.77E-05
25000	884.642604	405	0.000252	-65	3.32E-05
30000	1061.57113	480	0.000298	-80	4.15E-05
35000	1238.49965	555	0.000345	-90	4.71E-05
40000	1415.42817	645	0.000401	-105	5.54E-05
45000	1592.35669	730	0.000453	-120	6.37E-05
50000	1769.28521	815	0.000506	-130	6.92E-05
55000	1946.21373	910	0.000565	-150	8.03E-05
60000	2123.14225	1000	0.000621	-160	8.59E-05
65000	2300.07077	1085	0.000674	-175	9.42E-05
70000	2476.99929	1165	0.000724	-190	0.000102
75000	2653.92781	1260	0.000783	-205	0.000111
80000	2830.85633	1350	0.000839	-220	0.000119
85000	3007.78485	1455	0.000904	-240	0.00013
90000	3184.71338	1550	0.000963	-260	0.000141
95000	3361.6419	1690	0.00105	-295	0.000161
110000	3892.42746	1915	0.00119	-340	0.000186
120000	4246.2845	2120	0.001317	-390	0.000213
130000	4600.14154	failure	failure	failure	failure

REFERENCES

[1]   D, Hardjito and B. V. Rangan, "Development and properties of low calcium fly ash based geopolymer concrete," Curtin University of Technology, Perth, Australia, Research Report GC 1, 2005.

[2]   EPA, "Hydrogen sulfide corrosion in wastewater collection and treatment system," U. S. Environmental Protection Agency, Tech. Rep. EPA/430/09-91-010, 1991.

[3]   L. Zhang, P. De Schryver, B. De Gusseme, W. De Muynck, N. Boon, and W. Verstraete, "Chemical and biological technologies for hydrogen sulfide emission control in sewer systems: A review," *Water Research*, vol. 42, pp. 1 – 12, 2008.

[4]   J, Monteny, E. Vincke, A. Beeldens, N. De Belie, L. Taerwe, D. Van Gemert, W. Verstraete, "Chemical, microbiological and in situ test methods for biogenic sulfuric acid corrosion of concrete," *Cement and Concrete Research*, vol. 30, pp. 623-634, 2000.

[5]   T. Mori, T. Nonaka, K. Tazaki, M. Koga, Y. Hikosaka, and S. Noda, "Interaction of nutrients, moisture and pH on microbial corrosion of concrete sewer pipes," *Water Research*, vol. 26, no. 1, pp. 29-37, 1992.

[6]   R. Pomeroy, and J. Parkhurst, "The forecasting of sulfide build-up rates in sewers," *Water Technology*, vol. 9, pp. 621-628, 1997.

[7]   W. Sand, and E. Bock, "Concrete corrosion in Hamburg sewer system" *Environmental Technology Letters*, vol. 5, pp. 517-528, 1984.

[8]   E. Hewayde, G. F. Nakhla, and E. N. Allouche, and P. Mohan, " Beneficial Impact of Coatings on Biological Generation of Sulfides in Concrete Sewer Pipes," *Journal of Structures and Infrastructure Engineering, Maintenance, Management, Life-cycle, Design & Performance*, vol. 3, no. 3, pp. 267-277, 2007.

[9]   T. W. Cheng, and J. P. Chiu, "Fire-resistant geopolymer produced by granulated blast furnace slag," *Minerals Engineering*, vol. 16, no. 3, pp. 205-210, 2003.

[10]   A. Palomo, M. W. Grutzeckb and M. T. Blancoa, "Alkali-activated fly ashes a cement for the future," *Cement and Concrete Research*, vol. 29, pp. 1323–1329, 1999.

[11]   J. G. S. Van Jaarsveld, J. S. J. Van Deventer, and L. Lorenzen, "The potential use of geopolymeric materials to immobilize toxic metals: Part I. Theory and Applications," *Minerals Engineering*, vol. 10, no. 7, pp. 659-669, 1997.

[12]   A. E. Aktan, A. J. Helmicki, and V. J. Hunt, "Issues in health monitoring for intelligent infrastructure," *Smart Materials and Structures*, vol. 7, pp. 674–692, 1998.

[13]   B. Dragos-Marian, D. D. L. Chung, G. C. Lee, "Damage in carbon fiber-reinforced concrete, monitored by electrical resistance measurement," *Cement and Concrete Research*, vol. 30, pp. 651-659, 2000.

[14]   C. D. Parker, "The isolation of species of bacterium associated with the corrosion of concrete exposed to atmospheres containing hydrogen sulfide," *Australian Journal of Experimental Biology and Medical Science*, vol. 23, pp. 81-90, 1945.

[15]   W. Sand, "Microbial mechanisms of deterioration of inorgainc substrates-A general mechanistic overview," *International Biodeterioration & Biodegradation*, vol. 40, no. 2-4, pp. 183-190, 1997.

[16]   EPA, "Sewer sediment and control-A management practice reference guide," U. S. Environmental Protection Agency, Tech. Rep. EPA/600/R-04/059, 2004.

[17]   D. K. Thistlethwayte, *The control of sulfides in sewage system*, Ann Arbor, MI: Ann Arbor Science, 1972.

[18]   E. Hawayde, "Investigation on degradation of concrete sewer pipes by sulfuric acid attack," PhD dissertation, The University of Western Ontario, London, Ontario, Canada, 2005.

[19]   EPA, "Odor and corrosion control in sanitary sewage systems and treatment plants," U. S. Environmental Protection Agency, Tech. Rep. EPA/625/1-825/018, 1985.

[20]   R. D. Pomeroy, "Control of hydrogen sulfide generation in sewer," *Water and Sewage Work*, pp. 133-137, 1956.

[21]   R. L. Islander, J. S. Devinny, F. Mansfeld, A. Postyn, and H. Shih, "Microbial Ecology of Crown Corrosion in Sewers", *Journal of Environmental Engineering*, vol. 117, no. 6, pp 751-770, 1991.

[22]   E. Bock and W. Sand, "Applied electron microscopy on the biogenic destruction of concrete and blocks-use of transmission electron microscope for identification of mineral acid producing bacteria," in *Proc. eighth Int. Conf. on Cement Microscopy*, 1986, International Cement Microscopy Association, Duncanville, Texas.

[23]   E. Esfandi, "Proposal to conduct research for control of sewer corrosion," Districts of Los Angles County, County Sanitaion Internal Rep. 1986.

[24]   J. James, "Controlling sewer crown corrosion using the crown spray process with magnesium hydroxide," in *Underground Construction Technology Conference*, 2003, Houston, TX.

[25]   G. Shiwei, "Synergistic protection against microbiologically induced corrosion using a 100% solid polyurethane incorporated with antimicrobial agent," 2006. [Online]. Available: http://www.madisonchemical.com/pdf_tech_papers/Synergistic_Protection_Again st_MIC.pdf [Accessed: July 10, 2009]

[26]   G. Nelson, "In-sewer trail of biocrete sewer lining," Sydney Water Corporation, Investigation Report, May 2004. [Online]. Available: http://www.cticonsultants.com.au.

[27]   T. Graham, "Corrosion and rehabilitation of concrete access chambers," in *Sixty third Annual Water Industry Engineers and Operators Conference*, Sept. 2000, Warrnambool, Australia.

[28]   W. E. Shook, and W. Bell, "Corrosion control in concrete pipe and manholes," in *Water Environmental Federation Conference*, 1998, Orlando, Florida.

[29]   T. Haile, G. F. Nakhla, and E. N. Allouche, "Evaluation of the resistance of mortars coated with silver bearing zeolites to bacterial – induced corrosion," *Corrosion Science*, vol. 50, no. 3, pp. 713-720, 2008.

[30]   D. Stein, *Rehabilitation and maintenance of drains and sewers*, Germany: Vch Verlagsgesellschaft Mbh, 2001.

[31]   R. Sterling, E. N. Allouche, M. Bob, W. Lili, S. Jadranka, W. E. Condit, S. Sunil, Ed. Kampbell, C. Abraham, "White paper on rehabilitation of wastewater collection and water distribution systems," USEPA Forum, Edison, N.J, Tech. Rep. Sept 9-10, 2008.

[32]   A. Almusallam, F. M. Khan, S. U. Dulaijan, O. S. B. Al-Amoudi, "Effectiveness of surface coatings in improving concrete durability," *Cement & Concrete Composites*, vol. 25, pp. 473–481, 2003.

[33]   L. V. Evans and N. Clarkson, "Antifouling Strategies in the Marine Environment," *Journal of Applied Bacteriology-Symposium Supplement*, vol. 74, pp. 119S-124S, 1993.

[34]   Y. B. Acar. and A. N. Alshawabkeh, "Principles of electrokinetic remediation," *Environmental Science and Technology*, vol. 27, no 13, pp. 2638-2647, 1993.

[35]   E. Velivasakis, S. K. Henriksen, and D. Whitmore, "Chloride extraction and re-alkalization of reinforced concrete to stop corrosion," *Journal of Performance of Constructed Facilities*, vol. 12, no. 2, pp.77-84, 1998.

[36]   S. Kim, W. Kyoung, and D. Stuben, "Evaluation of electrokinetic removal of heavy metals from tailing soils," *Journal of Environmental Engineering*, vol. 128, no. 8, pp. 705-715, 2002.

[37]   M. Budhu, M. Rutherford, G. Sills, and W. Rasmussen, "Transport of nitrates through clay using electrokinetics," *Journal of Environmental Engineering*, vol. 123, no. 12, pp. 1251-1253, 1997.

[38]   S. Thevanayagam, and W. Jia, "Electro-osmotic grouting for liquefaction mitigation in silty soils," in *Third International Specialty Conference on Grouting and Ground Treatment*, 2003, pp. 1507-1517, New Orleans, Louisiana, USA.

[39]   E. H. Cardenas, J. S. Leslie, "Electrokinetic nanoparticle treatment of hardened cement paste for reduction of permeability," *Journal of Materials in Civil Engineering*, vol. 18, no. 4, pp. 554-560, 2006.

[40]   E. H. Cardenas, G. Nagaraju, "Investigation of electrokinetic nanoparticle technology for corrosion mitigation in reinforced concrete," in *Concrete Solutions: Proceedings of Second International Conference*, June. 2006, St Malo, France.

[41]   R. Jae-Suk, and N. Otsuki, "Crack closure of reinforced concrete by electrodeposition technique," *Cement and Concrete Research*, vol. 32, no. 1, pp. 159-164, 2002.

[42]   J. Davidovits, "Properties of geopolymer cements", in *proceedings first international conference on alkaline cements and concretes*, 1994, pp. 131-149.

[43]   S. E. Wallah, and B. V. Rangan, "Low-calcium fly ash based geopolymer concrete : Long term properties," Curtin University of Technology, Perth, Australia, Research Report GC 2, 2006.

[44]   J. Davidovits, "High alkali cements for 21st century concretes," Presented at Symposium on Concrete Technology: Past, Present and Future, University of California, Berkeley, 1994a.

[45]   H. Xu, J. S. J. Van Deventer, "The geopolymerisation of alumino-silicate minerals," *International Journal of Mineral Processing*, vol. 59, no. 3, pp. 247-266, 2000.

[46]   T. Bakharev, "Resistance of geopolymer materials to acid attack", *Cement and Concrete Research*, vol. 35, pp. 658–670, 2005.

[47]   A. Fernandez-Jimenez, & A. Palomo, "Characterisation of fly ashes. Potential reactivity as alkaline cements," *Fuel*, vol. 82, no. 18, pp. 2259-2265, 2003.

[48]   H. Xu, J. S. J. Van Deventer, "Geopolymerisation of multiple minerals," *Minerals Engineering*, vol. 15, pp. 1131–1139, 2002.

[49]   J. C. Swanepoel, C. A. Strydom, "Utilisation of fly ash in a geopolymeric material," *Applied Geochemistry*, vol. 17, pp. 1143–1148, 2002.

[50]   J. G. S. Van Jaarsveld, J. S. J. Van Deventer, and G. C. Lukey, "The characterisation of source materials in fly ash-based geopolymers," *Materials Letters*, vol. 57, pp. 1272–1280, 2003.

[51]   P. Kamhangrittirong, P. Suwanvitaya, P. Suwanvitaya, "The effect of fly ash content and sodium hydroxide molarity on geopolymer," in *International Conference on Pozzolan, Concrete and Geopolymer*, 2006, Khon Kaen, Thailand.

[52]   K. Sagoe-Crentsil and B. Trevor, "Some key materials and process parameters governing geopolymer binder performance," in *International Conference on Pozzolan, Concrete and Geopolymer*, 2006, Khon Kaen, Thailand.

[53]   J. G. S. Van Jaarsveld, J. S. J. Van Deventer, and L. Lorenzen, "Factors affecting the immobilization of metals in geopolymerized fly ash," *Metallurgical and Material Transactions B*, vol. 29B, no. 1, pp. 283-291, 1998.

[54]   A. Teixeira-Pinto, P. Fernandes, and S. Jalali, "Geopolymer manufacture and application - Main problems when using concrete technology," in *International Conference on Geopolymers*, 2002, Melbourne, Australia.

[55]   C. Defazio, M. D. Arafa, P. N. Balaguru, "Geopolymer column wrapping," Center for Advanced Infrastructure & Transportation (CAIT), Rutgers, The State University of New Jersey, Piscataway, NJ, Internal Report, 2006.

[56]   A. Palomo, A. Fernandez-Jimenez, C. Lopez-Hombrados, and J. L. Lleyda, "Precast elements made of alkali-activated fly ash concrete," in *Eighth CANMET/ACI International Conference on Fly Ash, Silica Fume, Slag, and Natural Pozzolans in Concrete*, 2004, Las Vegas, USA.

[57] B. V. Rangan, D. Sumajow, S. Wallah, and D. Hardjito, "Studies on reinforced low calcium fly ash based geopolymer beams and columns," Curtin University of Technology, Perth, Australia, Internal Report, 2006.

[58] Q. Zhao, B. Nair, T. Rahimian, and P. Balaguru, "Novel geopolymer based composites with enhanced ductility," *Journal of Materials Science*, vol. 42, pp. 3131-3137, 2007.

[59] C. E. Bakis, L. C. Bank, V. L. Brown, E. Cosenza, J. F. Davalos, J. J. Lesko, A. Machida, S. H. Rizkalla, and T. C. Triantafillou, "Fiber-reinforced polymer composites for construction—State-of-the-Art Review," *Journal of Composites for Construction*, pp. 73-87, 2002.

[60] R. V. Balendran, T. M. Rana, T. Maqsood,W. C. Tang, "Application of FRP bars as reinforcement in civil engineering structures," *Structural Survey*, vol. 20, no. 2, pp. 62-72, 2002.

[61] N. Banthia, and A. J. Boyd, "Sprayed fiber-reinforced polymers for repairs," *Canadian Journal of Civil Engineering*, vol. 27, pp. 907-915, 2000.

[62] T. Uomoto, H. Mutsuyoshi, F. Katsuki, and S. Misra, "Use of fiber reinforced polymer composites as reinforcing material for concrete," *Journal of Materials in Civil Engineering*, vol. 14, pp. 191-209, 2002.

[63] C. Pu-Woei and D. D. L. Chung, "Carbon fiber reinforced concrete as an electrical contact material for smart structures," *Smart Mater. Struct.*, vol. 2, pp. 181-188, 1993.

[64] X. Fu, and D. D. L. Chung, "Self monitoring of fatigue damage in carbon fiber reinforced cement," *Cement and Concrete Research*, vol. 26, no. 1, pp. 15-20, 1996.

[65] S. Zang-Qiang, and D. D. L. Chung, "Carbon fiber-reinforced concrete for traffic monitoring and weighing in motion," *Cement and Concrete Research*, vol. 29, pp. 435-439, 1999.

[66] D. D. L. Chung, "Cement-matrix composites for smart structures", *Smart Materials and Structures*, vol. 9, pp. 389-401, 2000.

[67] C. Bing, K. Wu b, Y. Wu, "Conductivity of carbon fiber reinforced cement-based composites," *Cement & Concrete Composites*, vol. 26, pp. 291–297, 2004.

[68] R. Farhad, B. B. Gordon, A. Y. Jerry and S. L. Jong, "Resistance changes during compression of carbon fiber cement composites," *Journal of Materials in Civil Engineering*, vol. 15, no. 5, pp. 476-483, 2003.

[69] C. Manuela, and Z. Raffaele, "Electrical conductivity of self-monitoring CFRC," *Cement & Concrete Composites*, vol. 27, pp. 463–469, 2005.

[70] N. Banthia, S. Djeridane, and M. Pigeon, "Electrical resistivity of carbon and steel micro-fiber reinforced cements," *Cement and Concrete Research*, vol. 22, pp. 804-814, 1992.

[71] T. O. Mason, M. A. Campo, A. D. Hixson, and L. Y. Woo, "Impedance spectroscopy of fiber-reinforced cement composites," *Cement & Concrete Composites*, vol. 24, pp. 457–465, 2002.

[72] J. M. Torrents, T. O. Mason, A. Peled, S. P. Shah, and E. J. Garboczi, "Analysis of the impedance spectra of short conductive fiber-reinforced composites," *Journal of Materials Science*, vol. 36, pp. 4003–4012, 2001.

[73] W. Xiufeng, W. Yonglan, and J. Zhihao, "Electrical conductivity characterization and variation of carbon fiber reinforced cement composite", *Journal of Materials Science*, vol. 37, pp. 223-227, 2002.

[74] S. Mingqing, L. Qingping, L. Zhuoqiu, and H. Yaozu, "A study of piezoelectric properties of carbon fiber reinforced concrete and plain cement paste during dynamic loading," *Cement and Concrete Research*, vol. 30, pp. 1593-1595, 2000.

[75] P. E. Jongh, D. Vanmaekelbergh, and J. Kelly, "Cu_2O: Electrodeposition and Characterization," *Chemistry of Materials Journal*, vol. 11, pp. 3512- 3517, 1999.